

Summer 2008

A simulation of the neural action potential under the influence of acetylcholinesterase inhibitors modeled in the neuromuscular junction

Frank Jenkins
Louisiana Tech University

Follow this and additional works at: <https://digitalcommons.latech.edu/dissertations>



Part of the [Biomedical Engineering and Bioengineering Commons](#), and the [Chemical Engineering Commons](#)

Recommended Citation

Jenkins, Frank, "" (2008). *Dissertation*. 464.
<https://digitalcommons.latech.edu/dissertations/464>

This Dissertation is brought to you for free and open access by the Graduate School at Louisiana Tech Digital Commons. It has been accepted for inclusion in Doctoral Dissertations by an authorized administrator of Louisiana Tech Digital Commons. For more information, please contact digitalcommons@latech.edu.

A SIMULATION OF THE NEURAL ACTION POTENTIAL UNDER THE
INFLUENCE OF ACETYLCHOLINESTERASE INHIBITORS MODELED IN THE
NEUROMUSCULAR JUNCTION

by

Frank Jenkins

A Dissertation Presented in Partial Fulfillment
of the Requirements for the Degree of
Ph.D in Engineering

COLLEGE OF ENGINEERING AND SCIENCE
LOUISIANA TECH UNIVERSITY

August 2008

UMI Number: 3318927

INFORMATION TO USERS

The quality of this reproduction is dependent upon the quality of the copy submitted. Broken or indistinct print, colored or poor quality illustrations and photographs, print bleed-through, substandard margins, and improper alignment can adversely affect reproduction.

In the unlikely event that the author did not send a complete manuscript and there are missing pages, these will be noted. Also, if unauthorized copyright material had to be removed, a note will indicate the deletion.

UMI[®]

UMI Microform 3318927

Copyright 2008 by ProQuest LLC.

All rights reserved. This microform edition is protected against unauthorized copying under Title 17, United States Code.

ProQuest LLC
789 E. Eisenhower Parkway
PO Box 1346
Ann Arbor, MI 48106-1346

LOUISIANA TECH UNIVERSITY

THE GRADUATE SCHOOL

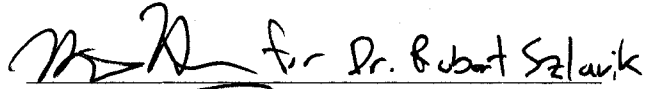
16 July 2008

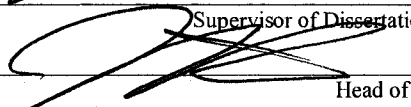
Date

We hereby recommend that the dissertation prepared under our supervision
by Frank Alexander Jenkins

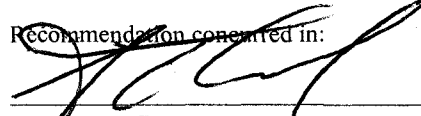
entitled A Simulation of the Neural Action Potential Under the
Influence of Acetylcholinesterase Inhibitors Modeled in the
Neuromuscular Junction


be accepted in partial fulfillment of the requirements for the Degree of
Doctor of Philosophy in Engineering



Supervisor of Dissertation Research


Head of Department
College of Engineering and Science
Department

Recommendation concurred in:




Paul Harts

John Brown

Advisory Committee

Approved:


Director of Graduate Studies

Approved:


Dean of the Graduate School



Dean of the College

ABSTRACT

The rise of terrorism has created an interest in better ways to detect when humans are exposed to neurotoxins, especially nerve gases developed for military use, most of which are acetylcholinesterase inhibitors. Many current methods of detection are based on mass spectrometry, a method that is cumbersome and not particularly robust when used as an early warning method. The detection of acetylcholinesterase inhibitors would benefit from a combined model of the processes occurring in the neuromuscular junction between the presynaptic action potential and the motor end-plate action potential that includes the kinetics of acetylcholine and acetylcholinesterase in the synaptic cleft. The ability to simulate the impact of different amounts of neurotoxin on the physiological processes needed for the generation of an action potential and subsequent muscle contraction would allow better estimates on the physiological toxicity of a nerve agent and its impact on an organism.

The goal of this research was to assist the future development of a unified model and simulation of the chemical kinetics and electrical dynamics occurring in the synaptic cleft during acetylcholinesterase inhibition by neurotoxins. The first objective towards the goal of this research was to develop an accurate and useful model of the kinetics of acetylcholinesterase inhibition that can be simulated and coupled to the voltage and current signals generated by a neuron. A one dimensional diffusion model was used which took advantage of geometric symmetry to focus on the dominant transport effects.

It will be shown that the simulation herein can reproduce the work of earlier research in depicting the time and spatial course of a normal action potential, and the time and spatial course of action potentials influenced by different degrees of acetylcholinesterase inhibition. This is the first simulation to achieve a model of acetylcholinesterase inhibition during the diffusion of a neuro-toxic inhibitor into the neuromuscular junction, and show the altered subsequent action potentials. Also illustrated will be how this simulation could detect the time and space dynamics of moving concentration gradients in the neuromuscular junction under suitable conditions. In addition, an in vivo simulation of inhibited acetylcholinesterase being returned to the active state through the kinetics of pralidoxime therapy will be shown. The mathematical method used in these simulations easily generalizes to a complete three dimensional transport model of the diffusion-reaction processes occurring in the neuromuscular junction.

APPROVAL FOR SCHOLARLY DISSEMINATION

The author grants to the Prescott Memorial Library of Louisiana Tech University the right to reproduce, by appropriate methods, upon request, any or all portions of this Dissertation. It is understood that "proper request" consists of the agreement, on the part of the requesting party, that said reproduction is for his personal use and that subsequent reproduction will not occur without written approval of the author of this Dissertation. Further, any portions of the Dissertation used in books, papers, and other works must be appropriately referenced to this Dissertation.

Finally, the author of this Dissertation reserves the right to publish freely, in the literature, at any time, any or all portions of this Dissertation.

Author Frank A Jenkins

Date 16 JULY 2008

TABLE OF CONTENTS

ABSTRACT.....	iii
LIST OF FIGURES.....	vi
CHAPTER 1 INTRODUCTION.....	1
CHAPTER 2 ENZYME KINETICS FUNDAMENTALS.....	14
CHAPTER 3 MODEL DEVELOPMENT.....	35
CHAPTER 4 MEASUREMENTS AND MODELS OF PRIOR INVESTIGATIONS....	86
CHAPTER 5 RESULTS AND DISCUSSION	93
CHAPTER 6 FUTURE WORK.....	125
APPENDIX A.....	130
APPENDIX B.....	168
REFERENCES.....	171

LIST OF FIGURES

Figure 1.1. Electron micrograph cross-section of the neuromuscular junction [26].....	4
Figure 1.2. A global view of the neuromuscular junction. (1) Neuron, (2) Motor end-plate, (3) Muscle fiber, (4) Myofibril [27].....	4
Figure 1.3. Detailed view of the neuromuscular junction. (1) neuron, (2) Sarcolemma, (3) Synaptic vesicles, (4) Acetylcholine receptor, (5) Mitochondrion, the mitochondria supply the energy needed for all cellular processes [28].....	6
Figure 1.4. The structure and function of the acetylcholine receptor, while embedded in the cellular plasma membrane [34].....	10
Figure 1.5. The structure of acetylcholinesterase, showing the conformations of the primary and secondary structure, and the location of the active site [40].....	13
Figure 2.1. The <i>lock and key</i> theory of enzyme function. The synthesis reaction creates a larger molecule from smaller molecules. The breakdown reaction breaks a large molecule into smaller parts. Both reaction types are equally common in biology [44].....	16
Figure 3.1. A schematic diagram of the neuromuscular junction geometry used in the model. The dimension of width is exaggerated for clarity.....	37
Figure 3.2. The shape and diffusion of the acetylcholine pulse, and the relative location of the acetylcholine receptors in the neuromuscular junction model.....	39

Figure 3.3. The transport model of the acetylcholine, inhibitor, and oxime species in the neuromuscular junction.....	40
Figure 3.4. The relation between each annulus index and the corresponding location on the cleft radius.....	56
Figure 4.1. Post-synaptic potentiation: interaction between quanta of acetylcholine at the skeletal neuromuscular synapse [9].....	87
Figure 4.2. Post-synaptic potentiation: interaction between quanta of acetylcholine at the skeletal neuromuscular synapse [9].....	88
Figure 4.3. Computer averaged end-plate currents showing the increasing decay time with increasing exposure to acetylcholinesterase inhibitors [10].....	89
Figure 4.4. The number of open receptors per acetylcholine quantum from Friboulet's simulation [57].....	90
Figure 4.5. The number of open receptors per acetylcholine quantum from Naka's simulation [52].....	91
Figure 5.1. An illustration of the dynamically coupled enzyme and neurotoxin concentrations in the neuromuscular junction during the diffusion-reaction process.....	94
Figure 5.2. The Number of open receptors per acetylcholine quantum from the Jenkins-Szlavik simulation.....	95
Figure 5.3. A comparison of the Jenkins-Szlavik and Friboulet models of the time course of open receptors in the neuromuscular junction with time. The Friboulet model is approximated as a set of exponential decay processes.....	96
Figure 5.4. The relative error between the Jenkins-Szlavik model and the Friboulet model for different levels of enzyme inhibition.....	97

Figure 5.5. A comparison of the Jenkins-Szlavik and Naka models of the time course of open receptors in the neuromuscular junction with time. The Naka model is approximated as a set of exponential decay processes.....	98
Figure 5.6. The relative error between the Jenkins-Szlavik model and the Naka model for different levels of enzyme inhibition.....	98
Figure 5.7. The idealized “step” concentration distribution	102
Figure 5.8. The idealized “step” concentration gradient	103
Figure 5.9. The idealized relative “step” concentration distribution.....	105
Figure 5.10. The idealized relative “step” concentration gradient.....	106
Figure 5.11. A hypothetical venous injection of inhibitor.....	107
Figure 5.12. The simulated concentration distribution of inhibitor in the neuromuscular junction during diffusion.....	108
Figure 5.13. The simulated concentration gradient of inhibitor during diffusion into the neuromuscular junction	111
Figure 5.14. The inhibitor concentration distributions in the cleft, where $D_1 = 9.0 \cdot 10^{-10} \text{ cm}^2/\text{ms}$, over a time period of 10 seconds.....	112
Figure 5.15. The inhibitor concentration gradients in the cleft, where $D_1 = 9.0 \cdot 10^{-10} \text{ cm}^2/\text{ms}$, over a time period of 10 seconds.....	113
Figure 5.16. The normalized inhibitor concentration distributions in the cleft, where $D_1 = 9.0 \cdot 10^{-10} \text{ cm}^2/\text{ms}$, over a time period of 10 seconds.....	114
Figure. 5.17. The normalized inhibitor concentration distributions in the cleft, where $D_1 = 9.0 \cdot 10^{-11} \text{ cm}^2/\text{ms}$, over a time period of 20 seconds.....	116

Figure. 5.18. The normalized inhibitor concentration distributions in the cleft, where $D_I = 9.0 \cdot 10^{-12} \text{ cm}^2/\text{ms}$, over a time period of 20 seconds.....	117
Figure 5.19. The normalized inhibitor concentration distributions in the cleft, where $D_I = 9.0 \cdot 10^{-13} \text{ cm}^2/\text{ms}$, over a time period of 30 seconds.....	118
Figure 5.20. The average amount of inactive acetylcholinesterase in the cleft during oxime therapy.....	122
Figure 5.21. The average amount of active acetylcholinesterase in the cleft during oxime therapy.....	123
Figure 5.22. The average concentration of oxime in the cleft during oxime therapy.....	124
Figure 6.1. An electron micrograph image of transmitter vesicle release at the neuromuscular junction [30].....	126
Figure 6.2. An example of a three dimensional discretization of the neuromuscular junction composed of three levels, nine annuli, and seventy-two sectors.....	127

CHAPTER 1

INTRODUCTION

The rise of terrorism has created an interest in better ways to detect when humans are exposed to neurotoxins, especially nerve gases developed for military use, most of which are *acetylcholinesterase* inhibitors [1], [2]. Military *acetylcholinesterase* inhibitors are usually organophosphorus-type (OP) compounds. Many current methods of detection are based on mass spectrometry, a method that is cumbersome and not particularly robust when used as an early warning method. The ability to detect *acetylcholinesterase* inhibitors would benefit from a combined model of the processes occurring in the neuromuscular junction between the presynaptic action potential and the motor end-plate action potential that includes the kinetics of acetylcholine and *acetylcholinesterase* in the synaptic cleft. The ability to simulate the impact of different amounts of neurotoxin on the physiological processes needed for the generation of an action potential, and subsequent muscle contraction would better estimate the physiological toxicity of a nerve agent and its impact on an organism.

Chemical warfare agents, particularly nerve gases, present a potential threat to military personnel in theater and a definite threat to civilian populations at home. While considerable concern for this threat exists, the early detection of nerve agents and determination of their effects when present in the environment in differing quantities is problematic at this time.

Determining the physiological effects of specific quantities of neural-toxin on the generation of an action potential and the subsequent muscle contraction requires the development of an integrated model that encompasses both the chemical kinetics within the gap between the synaptic terminal and the motor end-plate; and the electrical dynamics of the excitable motor nerve fiber and the excitable muscle fiber. This combined modeling and simulation approach is what has been lacking so far. There has been extensive research associated with developing models of the activity of excitable neuron and muscle cells [3]-[9], and the kinetics associated with the inhibiting effects of the neural toxins on acetylcholinesterase in the synaptic gap [10]-[17]. However, no work has been published that presents a combination of those processes. The goal of this research is to develop a unified model and simulation of the chemical kinetics and electrical dynamics occurring in the synaptic cleft during acetylcholinesterase inhibition by neurotoxins.

Several research teams have modeled the electro-chemical processes in the neuromuscular junction during a normal action potential event [18]-[20], and they have also examined how the activity of uniformly inhibited acetylcholinesterase affects the length of the action potential and end-plate currents [21]-[25]. The simulation herein is the first to model or address:

- The effects of acetylcholinesterase inhibitors diffusing into the junction during the action potential while the action potential occurs.
- The effects of non-uniformly inhibited acetylcholinesterase in time and space on the duration of the overall action potential.

- The space and time distribution of each state of the acetylcholine receptors in the neuromuscular cleft.
- The potential efficacy of the regeneration of deactivated acetylcholinesterase in the neuromuscular junction via oxime reaction kinetics as a method of therapeutic recovery from OP exposure.

The point where activity is transmitted from one cell to another cell is called a *synapse*. The general components of any biological synapse are called the *presynaptic terminal*, the *postsynaptic terminal*, and the *synaptic gap* (or *cleft*), which separates them. Nerve cells can be a part of two types of synapses, in one case a neuron connects to another neuron, and in the other a motor-neuron connects to a muscle-cell. This work concerns the case of a neuron connecting to a muscle-cell, called the *neuromuscular junction*, and it is in this region that a neuron signals a muscle fiber to contract. The neuromuscular junction consists of three main portions: the neuron (presynaptic terminal), the portion of the muscle's outer membrane (*sarcolemma*) where the neuron is connected, called the *motor end-plate* (postsynaptic terminal), and the cleft separating them where the chemistry of muscle movement is initiated. An electron micrograph image of a cross-section of the neuromuscular junction is shown in Figure 1.1 which depicts the major structures comprising this organ. The section taken is normal to the plane of the cleft and shows the relative size of the junctional folds compared to the width of the cleft. A global illustration of the neuromuscular junction is shown in Figure 1.2, where a neuron is attached to a muscle fiber at the motor end-plate. Figure 1.3 follows with a more detailed view of the junction. At the neuromuscular junction, the motor-nerve fiber (presynaptic membrane) loses its fatty *myelin* sheath and branches into fine terminals. Each terminal

lies in a shallow gutter-like depression on the surface of the muscle cell (postsynaptic membrane) [14], [15].

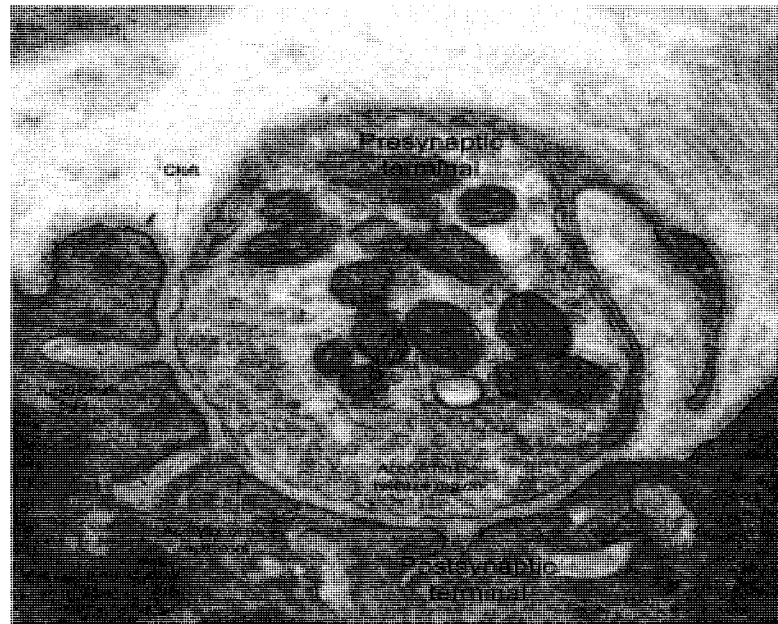


Figure 1.1. Electron micrograph cross-section of the neuromuscular junction [26].

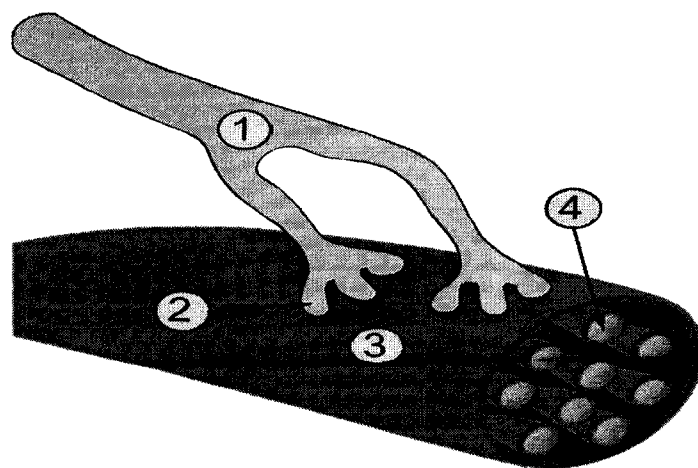


Figure 1.2. A global view of the neuromuscular junction. (1) Neuron, (2) Motor end-plate, (3) Muscle fiber, (4) Myofibril [27].

At the nerve-muscle synapse, the membranes of the nerve terminal and the muscle cell are separated by a fluid filled cleft approximately 50 nanometers (nm) wide. About every micrometer along the nerve terminal there are specialized areas which are associated with clusters of tiny *vesicles*, each containing on the order of 10,000 molecules of the neurotransmitter *acetylcholine* ($C_7H_{16}NO_2$). In the muscle membrane, directly opposite from the vesicle clusters, are deep invaginations called *junctional folds*. At the crests of these folds and part of the way down into them are the acetylcholine *receptors*. These receptors are specialized protein molecules embedded in the membrane of the motor end-plate and can be found anywhere on the surface of a muscle cell [17], [18]. The receptors are tightly packed in these regions, and their density falls off by a factor of at least 100 only a few micrometers from the crest of the fold [3], [22]. Qualitatively, this means that the receptors are densely packed and concentrated along the ridges of the motor end-plate surface, and are very sparse in the junctional fold troughs. That placement makes sense because the acetylcholine receptors are localized in the regions of high acetylcholine concentration.

An impulse arriving at the presynaptic nerve terminal causes an influx of calcium (Ca^{+2}) ions across its membrane. This induces several hundred of the synaptic vesicles to fuse with the presynaptic membrane at specialized regions called *active zones*, liberating the vesicles' content of acetylcholine molecules into the synaptic cleft [14]. The transmitter diffuses rapidly across the cleft to the muscle cell membrane, where it combines with the embedded receptor molecules. Each receptor can bind two acetylcholine molecules, and the acetylcholine molecules stay attached for about 1 millisecond (ms) [17], [23].

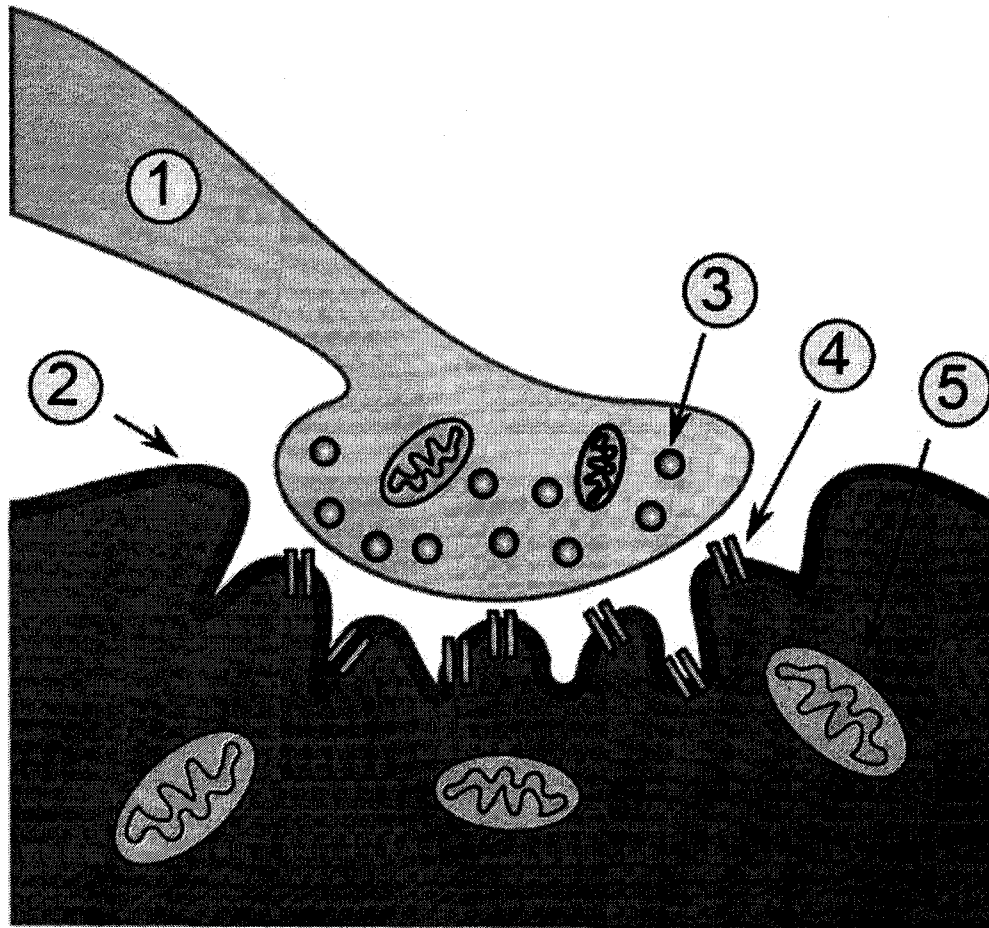


Figure 1.3. Detailed view of the neuromuscular junction. (1) neuron, (2) Sarcolemma, (3) Synaptic vesicles, (4) Acetylcholine receptor, (5) Mitochondrion, the mitochondria supply the energy needed for all cellular processes [28].

Within 0.3 milliseconds after each acetylcholine packet or vesicle load is released, it causes approximately 2,000 receptors in the muscle-cell membrane to change their conformation into an open state. In this open state, the receptors are channels which can pass both sodium (Na^+) and potassium (K^+) ions through the membrane. This flow of ions (Na^+ into the muscle, and K^+ out) gives rise to a net electric current that short-circuits the

normal potential of -90 millivolts (mV) across the resting cell membrane [15]. This brief depolarization is known as the *end-plate potential* or the *excitatory postsynaptic potential*. Under normal conditions, the end-plate potential exceeds the threshold value for initiating an impulse that spreads through the entire muscle-cell membrane and causes the muscle-cell to contract. Other protein structures in the membrane powered by *adenosine triphosphate* (ATP), called *protein pumps*, actively transport Na^+ and K^+ ions continuously through the membrane in their opposite directions, respectively. This simultaneous process consumes energy and restores the depolarized membrane back to its normal resting potential when the open receptors return to their closed state [29], [30]. Acetylcholine molecules would linger in the synaptic cleft, diffusing from one receptor to another on the post-synaptic membrane and opening additional channels, if it were not for the enzyme acetylcholinesterase, which catalytically breaks acetylcholine down into acetate and choline molecules. The molecules of this enzyme are not embedded in the muscle cell membrane like the acetylcholine receptors; instead, they are immobilized within a loose matrix of collagen and mucopolysaccharide fibers that extend throughout the synaptic cleft and deep into the junctional folds [5], [6], [23]. Acetylcholinesterase destroys about a third of the acetylcholine molecules before they even reach the receptors and then rapidly cleaves those remaining as they detach from the receptors. The speed with which acetylcholine is bound to the receptors and inactivated makes it possible for the entire process of neuromuscular transmission to be repeated up to several hundred times per second [22].

The acetylcholine receptor belongs to a family of cell membrane embedded proteins called *ligand-gated ion channels*, where ligand refers to an effector molecule

when it binds to a specific site on a target protein [31]. The receptor, which binds the effector(s), and the ion channel are part of the same nanomolecular protein complex. The ion channel is embedded in the membrane, and the receptor protrudes above the membrane. The best known members of this group respond to the extracellular neurotransmitters acetylcholine, glycine, γ -aminobutyric acid (GABA), and glutamate, and mediate rapid synaptic transmission in the central and peripheral nervous systems. Many of these ligand-gated ion channels share a common structure whose subunits have homologous protein sequences [30]. Most acetylcholine receptors used in experimental research are obtained from the electricity generating organs of the marine ray *Torpedo marmorata* and the famous Amazonian electric eel (*Electrophorus electricus*). These fish use their electric organs for electrogenesis and electroreception during the activities of hunting, navigation, and defense, but the details of the electroreception mechanisms are not yet well understood [30], [31]. The electric organs are built up from charge generating cells called *electrocytes*, or *electroplaxes* (an older term). Electrocytes are flat disk-shaped cells that are stacked in sequence in a similar manner to a battery. The electric organ consists of vertical stacks of several thousand electrocytes that are innervated by a cholinergic nerve on one surface. Stimulation of the nerve causes depolarization of the innervated face of each electrocyte, producing a potential difference between the two sides of the cell. The potentials across the cells in each column add to produce a large electric discharge. The cells function by pumping Na^+ and K^+ ions out of the cell with ATP powered transport proteins to build up a resting potential, and acetylcholine is secreted to open the receptors and equilibrate the ionic concentration with the environment outside the cell. Postsynaptically, electrocytes work much like

muscle cells, but an electric charge is emitted instead of a kinetic contraction. The membranes of electrocytes are packed with acetylcholine receptors. These receptors can be purified from electrocyte membranes for protein sequence and cloning experiments, or the entire membrane with the embedded receptors intact can be used for receptor function experiments [31], [32], [33].

The acetylcholine receptor is comprised of five subunits; three are designated as β , δ , and γ , and two with identical structure designated as α . Each α -unit can bind one acetylcholine molecule at a special acetylcholine binding site. These receptors are normally closed in the absence of ligand binding, and can open within approximately 20 microseconds of an appropriate ligand binding event. The receptor subsequently closes after dissociation of at least one ligand from the receptor. Figure 1.4 below shows the general structure of the acetylcholine receptor. The protein structure and sequence of ligand-gated ion channels is a broad and complex discipline with many good references available [33], [35], [36].

The response of the acetylcholine receptor can be separated into two steps. Each receptor, which is normally in the closed state, binds two acetylcholine molecules, one to each subunit α , to form what is called a *ligand-receptor* complex. After binding, this complex undergoes a conformation transition which opens a pore into the muscle membrane that is permeable to Na^+ , K^+ , and Ca^{+2} . The binding and unbinding steps are relatively slow; transitions to and from the open state of the pore are, in contrast, relatively rapid. Thus, channel openings occur in short bursts which can last several milliseconds, and which represent the lifetime of the ligand-receptor complex. During the burst, the channel flickers open and shut [29], [32], [33].

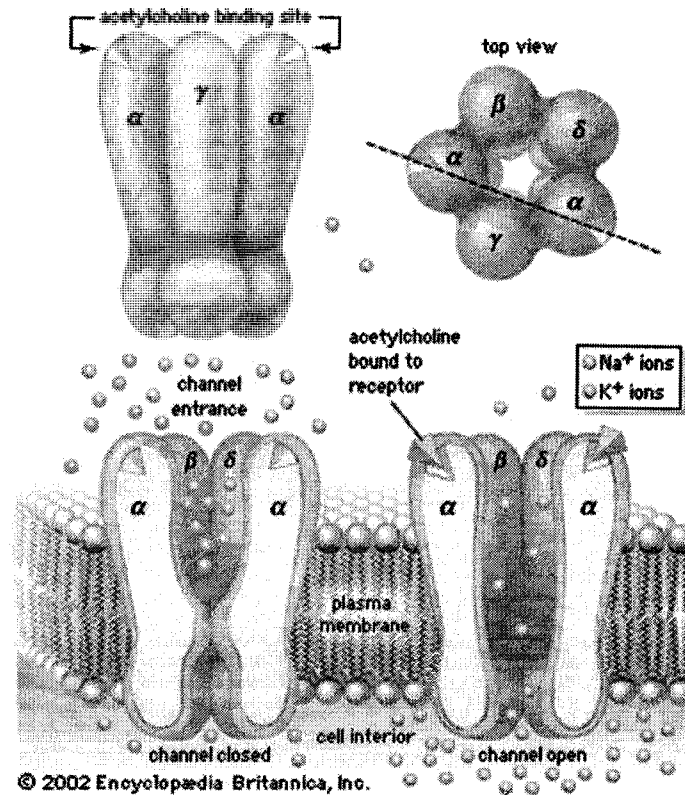


Figure 1.4. The structure and function of the acetylcholine receptor, while embedded in the cellular plasma membrane [34].

If the receptor is exposed to acetylcholine or other molecules which mimic the function of acetylcholine (*agonists*) for a period of seconds or minutes, then the receptor becomes *desensitized* or unresponsive [32], [33]. Conversion of the ligand-receptor complex to the desensitized state occurs at a rate that is influenced by the extracellular concentration of Ca^{+2} and other factors. Receptor desensitization is responsible for the paralyzing effect of anti-cholinesterase drugs which, by inhibiting acetylcholinesterase, prolong the lifetime of acetylcholine in the synaptic cleft [31], [33].

The rapid depolarization and re-polarization events which constitute the many-times-per-second neuromuscular transmission process are possible, in part, because of the activity of the cholinesterase protein. There are at least two kinds of cholinesterases

found in humans: acetylcholinesterase, and *butyrylcholinesterase*. The difference between them is that each has a preference to react with its root-named effector molecule (the *substrate*), acetylcholine and butyrylcholine, respectively [36]. Acetylcholine and butyrylcholine are both transmitter-type molecules with similar chemistry, and each cholinesterase can react with the other's substrate as well, though not preferentially. Acetylcholinesterase is found primarily in the blood and neural synapses, while butyrylcholinesterase is located primarily in the liver [36], [37].

While the consensus in the research literature agrees that acetylcholine is hydrolyzed by cholinesterases, none of them have determined exactly how many cholinesterases exist in the body and their quantity, or their precise distribution [37]. For most purposes, distinguishing between acetylcholinesterase and butyrylcholinesterase is sufficient. Current evidence suggests that in lower animal forms butyrylcholinesterase predominates, gradually giving way to acetylcholinesterase with evolution. Although their molecular forms are similar, the two enzymes are distinct entities, encoded by specific genes. An interesting criterion for differentiating these enzymes is the substrate concentration versus activity relationship which will be described in Chapter 3, where the fundamentals of enzyme chemistry and kinetics will be discussed [37].

As stated earlier, the function of acetylcholinesterase is to deactivate acetylcholine. This is accomplished via a *hydrolysis* (water using) reaction that cleaves acetylcholine into the molecules choline ($C_5H_{14}NO$) and acetic acid (CH_3COOH). The molecular weight of acetylcholinesterase is approximately 7,500,000 grams per mole [37]. Like most enzymes, acetylcholinesterase is a large polymer where the conformation, and inter-molecular and intra-molecular forces of its structure play important roles in its

function. Because of these conditions, the portion of this molecule where its chemical activity is located may be significantly smaller than the body of the entire molecule (in other cases, the entire molecular body may be used to build the active region). In addition, the molecule could have multiple active regions. Consequently, descriptions of the chemical kinetics of enzymes usually focus on their *active sites*: their characterization and number rather than quantifying the properties of individual enzyme molecules [38], [39].

The structure of acetylcholinesterase is shown in Figure 1.5. This illustration is intended to give the reader a general idea of the relative size and complexity of protein enzymes. The position of the active site is indicated by the cluster of spheres in the center. In this dissertation, the function of acetylcholinesterase is the focus rather than issues related to the protein's structure and conformation. The interested reader is invited to examine the following references for more information on protein structure: [41], [42], [43].

The activity of acetylcholinesterase is extremely high. Each active site of this enzyme is able to hydrolyze approximately 14,000 acetylcholine molecules per second at normal body temperature [39], which is also close to the theoretical number of molecular collisions at that same temperature [41]. Typical chemical reactions depend on the number of collisions between molecules and their orientation relative to each other. Some orientations result in a reaction and some do not. Thus, most feasible reactions depend on a high number of collisions to proceed at a rate that scientists would have a reason to find interesting.



Figure 1.5. The structure of acetylcholinesterase, showing the conformations of the primary and secondary structure, and the location of the active site [40].

For acetylcholinesterase, this high activity means that essentially every collision between acetylcholinesterase and acetylcholine molecules results in a reaction, and enzymes with that property are termed *diffusion limited*. Qualitatively, this means the reaction speed of acetylcholinesterase is controlled only by how quickly acetylcholine molecules can reach the active sites. Some enzymes are thought to accelerate catalysis to this limit by using dipolar electric fields to pre-orient their substrate to the optimal position as it is drawn in to the enzyme's active site [39], [41]. The ability to catalyze a reaction with every substrate collision also makes acetylcholine a very reliable enzyme, and reliability is a useful and important attribute for an enzyme whose function is such an integral part of movement and cognition.

CHAPTER 2

ENZYME KINETICS FUNDAMENTALS

A chemical reaction is a process where a substance (or substances) is changed into one or more new substances. A chemical equation is the method used to represent a chemical reaction in a standard way, and it uses symbols to show what happens during a chemical reaction. In a chemical equation, the reactants are conventionally written on the left and the products on the right of the reaction arrow. A more general definition is to say that the arrow points away from the reactants and towards the products.

Any chemical reaction can be represented by the general equation

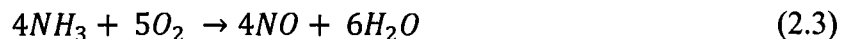


This equation tells that during the course of a reaction, reactants are consumed while products are formed. As a result, the progress of a reaction can be followed by monitoring either the decrease in concentration of the reactants or the increase in concentration of the products.

Chemical equations are almost always written in a way that conserves the total number of atoms which are depicted on the reactant and product sides of the reaction arrow, referred to as a *balanced* stoichiometric equation. A stoichiometric equation can be very simple with two species in one reaction:



Or several reactant species and product species in one reaction:

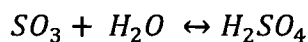
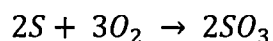


In general, a balanced stoichiometric reaction equation can be represented in the following form:



Where the upper case letters A , B , C , and D represent the molecular formula of each chemical species participating in the reaction, and the lower case letters a , b , c , and d are called the *stoichiometric coefficients*, and represent the number of molecules of each participating species. Any subscript numbers which might appear in a molecular formula represent the number of atoms of each different atomic species in that molecule which is represented by the formula.

If a number of reactants and products are involved in several different reactions which are combined in a stoichiometric reaction network, then there exists a *coupled* system like the following:



Biological processes are well known (notorious even) for the complexity and size of their chemical reaction networks. Chemical networks which describe metabolism may easily contain several hundred species, many of which are enzymes.

Enzymes are proteins which function as catalysts in chemical reactions. A catalyst is a substance which can increase the speed and yield of a chemical reaction without being a reactant or product in the reaction. Because enzymes are proteins, they are

typically involved in cellular reactions and are of primary importance in metabolic pathways. Ordinarily, these metabolic reaction cascades would need large amounts of energy (heat) to proceed. Enzymes allow these reactions to take place at rapid rates and lower temperatures. Enzymes are also known to be highly specific for both substrate and reaction type. The basic *lock and key* theory describes this process as illustrated in Figure 2.1. It assumes that the structure of the enzyme and substrate molecules explain the specificity and inhibition features observed in enzymatic reactions. In particular, an enzyme joins with its substrate and lowers the energy requirements for activation of the reaction, then the reaction occurs, after which the enzyme is then released unchanged and used again.

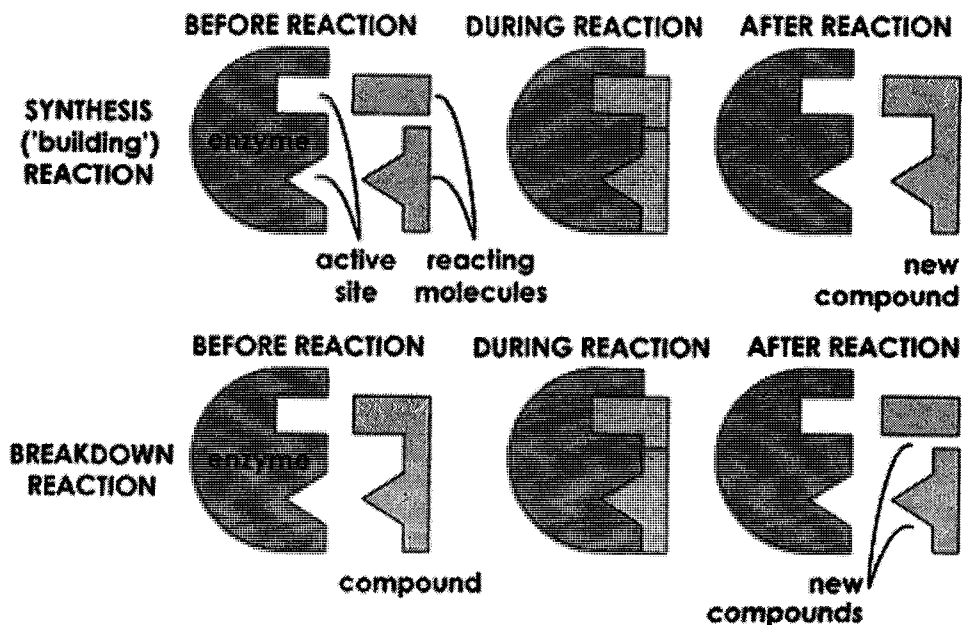
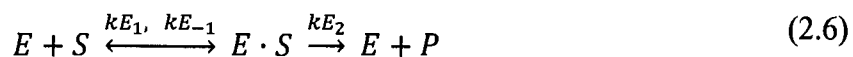


Figure. 2.1. The *lock and key* theory of enzyme function. The synthesis reaction creates a larger molecule from smaller molecules. The breakdown reaction breaks a large molecule into smaller parts. Both reaction types are equally common in biology [44].

While this model explains enzymes' specificity, it fails to explain the stabilization of the transition state that enzymes achieve. Daniel Koshland [45] suggested a modification to the lock and key model. Since enzymes are rather flexible structures, the active site can be reshaped by interactions with the substrate as the substrate interacts with the enzyme. As a result, the amino acids which make up the active site are molded into the precise positions that enable the enzyme to perform its catalytic function. In some cases, such as glycosidases, the substrate molecule also changes shape slightly as it enters the active site.

Consider a single enzyme-plus-substrate-to-product reaction:



where it is assumed that an intermediate substrate-enzyme complex $E \cdot S$ is formed. Further, the reaction $E \cdot S \rightarrow E + P$ is assumed irreversible. While multiple active site enzymes occur and have a developed kinetic theory, the typical enzyme reaction involves 1:1 stoichiometry: one active site per enzyme molecule and one molecule substrate creates one molecule product. Some other important kinetic assumptions are:

- (1) Only initial reaction rates are considered. These rates decrease with time due to the decline in substrate concentration. However, this effect can be ignored with the proper experimental technique.
- (2) There is an excess of substrate concentration in the reaction with the enzyme. The rate constant k_{E+2} is small compared to k_{E-1} and thus the reaction $E + S \leftrightarrow E \cdot S$ reaches equilibrium quickly and maintains this equilibrium throughout the overall reaction.

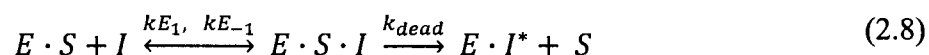
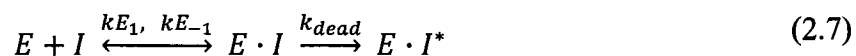
After a negligible time, the rate of formation and dissociation of the complex $E \cdot S$ becomes and remains very small compared to the rate of changes for S and P , which is the “quasi-steady state” assumption. The Michaelis-Menten derivation [42] uses these assumptions to apply mathematical techniques that simplify the kinetic equations for the system. Because of the computing power presently available, it will not be required to apply these simplifications to the model proposed herein.

While enzymes have evolved to react specifically with a particular (or small set of) substrate(s), there also exist molecules which can bind with an enzyme and decrease or increase its activity. Molecules which decrease an enzyme’s activity are called inhibitors, and those which increase its activity are called activators. Enzyme inhibitors are more common than the activators.

The inhibitor binding process can obstruct the substrate reaching the enzyme’s active site and/or impede the enzyme catalysis reaction. Inhibitor binding is defined as either reversible or irreversible, though the distinction between these terms is not absolute and may be difficult to make if the inhibitor-enzyme complex is highly stable. If the effect of an inhibitor can be changed by varying the concentration of the inhibitor, then the inhibition is said to be reversible because of the invocation of LeChatier’s principle [42]. There are three main classes of reversible inhibition: competitive, non-competitive, and mixed. The classification is correlated according to the type of effect on the enzyme kinetics when the inhibitor’s concentration is varied. This investigation will focus on irreversible inhibition. Several researchers have described the fundamental kinetics of reversible inhibition, and unless specifically stated otherwise, their work will form the

framework for this area throughout the remainder of this dissertation, [39], [42], [46], [47].

Irreversible inhibitors usually covalently modify an enzyme. Thus, the inhibition cannot be reversed with concentration changes and equilibrium. Two typical stoichiometric equations involving irreversible inhibitors are shown below (with chemical symbol definitions offered in the text following):



Irreversible inhibitors are also different from irreversible *inactivators*. For example, in extreme concentrations the hydroxide ion (OH^-) functions as an irreversible inactivator because it can permanently destroy (*denature*) the entire structure of many enzymes; however, this effect is non-specific and is not connected to the special structure of any particular enzyme. An irreversible inhibitor, however, is usually specific for one class of enzyme and inhibits by altering only the active site of its target. Irreversible inhibitors form a reversible non-covalent complex with the enzyme species ($E \cdot I$) or with the enzyme-substrate species ($E \cdot S \cdot I$), which then reacts to produce the covalently bonded “dead” or “poisoned” complex, $E \cdot I^*$. The rate at which the dead complex forms is called the inactivation rate, or k_{dead} . Since formation of $E \cdot I$ may compete with $E \cdot S$, binding of irreversible inhibitors can be prevented by competition either with substrate or with a second, reversible inhibitor. This protection effect is good evidence of a specific reaction of the irreversible inhibitor with the active site [42].

In the past, highly toxic organophosphorous compounds have been developed for use as pesticides and chemical warfare agents. The toxic effects of these organophosphorous compounds are mainly due to the increased quantity of inhibited acetylcholinesterase in the neuromuscular junction. Organophosphorous compounds inhibit acetylcholinesterase by reacting with and altering the *amino acid* units that comprise the protein sequences used to build up the enzyme's active site. In this case, the amino acid serine is phosphorylated by the phosphorus atom of the organophosphorous compound. The inability of poisoned enzyme to hydrolyze acetylcholine results in the accumulation of that transmitter and the subsequent over-stimulation of the cholinergic receptors, which is followed by the breakdown of transmission in all synapses that use the acetylcholine/cholinergic receptor system. Organophosphorous compounds are not irreversible inactivators of acetylcholinesterase because they chemically modify only the active site of the enzyme, and therefore, other chemical reactions are able to retro-modify the active site and restore functionality to the enzyme. Restoration reactions with *oxime* compounds are the most effective and best understood in biological systems [48], [49]. Oxime compounds can reactivate acetylcholinesterase by attaching to the phosphorus atom and forming an oxime-phosphonate which then splits away from the acetylcholinesterase protein molecule. Oximes have the general stoichiometric formula of R_1R_2CNOH , where R_1 and R_2 are un-reactive organic side chains consisting only of carbon and hydrogen atoms. Some of the most effective oxime nerve-agent antidotes are obidoxime, pralidoxime, and methoxime. However, the effectiveness of the oxime treatment depends on the particular nerve agent used to inhibit the acetylcholinesterase [50], [51]. Chapters 4 and 5 will explore the chemistry and kinetics of oximes more fully.

A stoichiometric equation makes a statement about the species population at the beginning of a reaction and at the end, but may omit information about intermediate kinetic steps in a complicated reaction. By itself the stoichiometric equation also says nothing about how to follow the progress of the reaction with time, or the rates of species population change. Chemical kinetics is the area of chemistry concerned with the speeds, or rates, at which a chemical reaction occurs. The word “kinetic” suggests movement or change; here, kinetics refers to the rate of a reaction, or the reaction rate, which is the change in the concentration of a reactant or product with time.

There are many reasons for studying the rate of a reaction. To begin with, there is intrinsic curiosity about why reactions have such vastly different rates. Some processes, such as the initial steps in vision and photosynthesis and nuclear chain reactions, take place on a time scale as short as 10^{-12} to 10^{-6} seconds. Others, like the curing of cement and the conversion of graphite to diamond, take years, or millions of years to complete. On a practical level, knowledge of reaction rates is useful in drug design, in pollution control, and in food processing. Industrial chemists often place more emphasis on speeding up the rate of a reaction rather than maximizing its yield. What follows is a description of fundamental chemical kinetics and some rules which allow derivation of kinetic rate equations from a known stoichiometric reaction or reaction network.

The equation below depicts a simple reaction in which a molecules of species A are converted to b molecules of species B:



In general, it is more convenient to express the reaction rate in terms of the change in concentration with time. Thus, the simple reaction $aA \rightarrow bB$ can be rate expressed as

$$\text{rate} = -\frac{1}{a} \frac{\Delta[A]}{\Delta t} \text{ or } \text{rate} = \frac{1}{b} \frac{\Delta[B]}{\Delta t} \quad (2.10)$$

where $\Delta[A]$ and $\Delta[B]$ are the changes in concentration (mole/liter) over time period Δt . Because the concentration of A decreases during Δt , $\Delta[A]$ is a negative quantity. The rate of a reaction is a positive quantity, so a minus sign is needed in the rate expression to make the rate positive. On the other hand, the rate of product formation does not require a minus sign because $\Delta[B]$ is a positive quantity (the concentration of B increases with time). These rates are *average rates* because they are averaged over a certain time period Δt [52].

The rate law or rate equation for a chemical reaction is an equation which links the reaction rate with concentrations or pressures of reactants and constant parameters (normally rate coefficients and partial reaction orders), and is derived from the *law of mass action*. In chemistry, the law of mass action has two aspects: 1) the equilibrium aspect, concerning the composition of a reaction mixture at equilibrium, and 2) the kinetic aspect concerning the rate equations for elementary reactions.

Taken as a statement about kinetics, the rate law states that the rate of an elementary reaction (a reaction that proceeds through only one transition state, that is, one mechanistic step) is proportional to the product of the concentrations of the participating molecules. In modern chemistry, this is derived using statistical mechanics [53].

The hypothesis that reaction rate is proportional to reactant concentrations is, strictly speaking, only true for elementary reactions (reactions with a single mechanistic step). In general, many reactions occur with the formation of reactive intermediates, and/or through parallel reaction pathways. However, all reactions can be represented as a

series of elementary reactions and, if the mechanism is known in detail, the rate equation for each individual step is given by a particular rate expression so that the overall rate equation can be derived from the individual steps. In biochemistry, there has been significant interest in deducing the rate laws for chemical reactions occurring in the intracellular medium. Although deviations of the law of mass action have been reported, it has been shown that the law of mass action can be valid in intracellular environments under certain conditions [54].

To determine the rate equation for a particular system, one combines the reaction rate with a mass balance for the system. For a generic reaction $A + B \rightarrow C$, the simple rate equation (as opposed to the much more common complicated rate equations) is of the notationally simplified form:

$$\frac{d[X]}{dt} = \sum k(T) [A]^m [B]^n \quad (2.11)$$

This rate equation is a differential equation, and as such it can be integrated to obtain the integrated rate equation that links concentrations of reactants or products with time [55]. In this equation, $[X]$ expresses the concentration of a given species X , and $k(T)$ is known as the *reaction rate coefficient* or *rate constant*. Under the imposed experimental conditions used to study chemical kinetics, this rate constant can be treated as constant. In reality, the rate coefficient depends on many things that affect the reaction rate besides the species concentrations. It is mainly a function of temperature, and also ionic strength, surface area of the adsorbent and light irradiation.

The exponents m and n are called *reaction orders* and depend on the reaction mechanism. The stoichiometric coefficients and reaction orders are equal only in simple,

one step reactions. Usually, the reaction orders are determined via experimental measurement, and can be any real number value.

In the more general case, given a known reaction or reaction network, the rate equation for each species in the reaction(s) can be expressed as:

$$\frac{d[X_i]}{dt} = \sum_{j=1}^r \left\{ k_{i,j}(T) \prod_{h=1}^c [X_h]^{f_{j,h}} \right\} \quad (2.12)$$

This form is structurally very rich and general, because for the real number $f_{j,h}$, the system can represent any multinomial, and thus a multidimensional Taylor series approximation, to any continuous and differentiable rate law. In the general case, the stoichiometric coefficients do not explicitly appear in the rate equation and are absorbed into the rate constant. For these purposes, Equation (2.12) shows that the total rate derivative of some particular species i is equal to the sum of the individual reaction rate terms of that species in the reactions where it is a participant. By convention, each reaction rate term is expressed as a function only of the reactant species participating in that particular reaction. As a consequence, chemical species which are purely products will not appear in their own differential rate expressions.

It should also be mentioned here that when species X_i is mobile, and can diffuse throughout the geometry of the system in a way that produces concentration gradients, then (2.12) is modified to the form below:

$$\frac{\partial [X_i]}{\partial t} = \nabla \cdot (D_A \nabla [X_i]) + \sum_{j=1}^r \left\{ k_{i,j}(T) \prod_{h=1}^c [X_h]^{f_{j,h}} \right\} \quad (2.13)$$

The additional term in (2.13) represents the description of the transport of species X_i in the system. Equation (2.13) describes a reaction-diffusion system, and treatment of these systems will be more developed in Chapter 3 [56].

The rules for deriving rate expressions from stoichiometric equations are best illustrated by the following examples. For instructional purposes, the reaction kinetics of these examples are assumed to be one step; thus, the stoichiometric coefficients of each species will be explicitly included in the kinetic expressions.

Example 1:



The stoichiometric equation depicts one kinetic reaction comprised of three chemical species. Description of this system will require the development of three kinetic rate equations: $d[CO]/dt$, $d[O_2]/dt$, and $d[CO_2]/dt$.

Species CO participates in one reaction designated by rate constant k_1 , therefore the kinetic rate equation for species CO will consist of one term. In reaction k_1 , species CO is a reactant, and so that term will be negative and expressed as a multiplicative product of its stoichiometric coefficient, the rate constant k_1 , and all the reactant species concentrations which participate in reaction k_1 , each raised to the power of their respective stoichiometric coefficient. More explicitly, the term will be negative $2k_1$, times $[CO]^2$, times $[O_2]$, thus: $-2k_1[CO]^2[O_2]$. The complete kinetic rate equation for species CO is shown below as:

$$\frac{d[CO]}{dt} = -2k_1[CO]^2[O_2] \quad (2.15)$$

Species O_2 participates in one reaction designated by rate constant k_1 ; therefore, the kinetic rate equation for species O_2 will consist of one term. In reaction k_1 , species O_2 is a reactant, and so that term will be negative and expressed as a multiplicative product of its stoichiometric coefficient, the rate constant k_1 and all the reactant species concentrations which participate in reaction k_1 , each raised to the power of their respective stoichiometric coefficient. More explicitly, the term will be negative k_1 , times $[CO]^2$, times $[O_2]$, thus: $-k_1[CO]^2[O_2]$. The complete kinetic rate equation for species O_2 is shown below as:

$$\frac{d[O_2]}{dt} = -k_1[CO]^2[O_2] \quad (2.16)$$

Species CO_2 participates in one reaction designated by rate constant k_1 ; therefore, the kinetic rate equation for species CO_2 will consist of one term. In reaction k_1 , species CO_2 is a product, and so that term will be positive and expressed as a multiplicative product of its stoichiometric coefficient, the rate constant k_1 and all the reactant species concentrations which participate in reaction k_1 , each raised to the power of their respective stoichiometric coefficient. More explicitly, the term will be positive $2k_1$, times $[CO]^2$, times $[O_2]$, thus: $2k_1[CO]^2[O_2]$. The complete kinetic rate equation for species CO_2 is shown below as:

$$\frac{d[CO_2]}{dt} = 2k_1[CO]^2[O_2] \quad (2.17)$$

Taken all together, the stoichiometric reaction equation, and the kinetic reaction rate equations with their associated initial conditions are shown in (2.18):



Kinetic reaction rate equations	Initial conditions
$\frac{d[CO]}{dt} = -2k_1[CO]^2[O_2]$	$[CO](0) = [CO]_0$
$\frac{d[O_2]}{dt} = -k_1[CO]^2[O_2]$	$[O_2](0) = [O_2]_0$
$\frac{d[CO_2]}{dt} = 2k_1[CO]^2[O_2]$	$[CO_2](0) = [CO_2]_0$

Example 2:



The stoichiometric equation depicts two kinetic reactions (one forward, one backward) comprised of three chemical species. Description of this system will require the development of three kinetic rate equations: $d[NO_2]/dt$, $d[O_2]/dt$, and $d[N_2O_5]/dt$.

Species NO_2 participates in two reactions, designated by the rate constants k_1 and k_{-1} ; therefore, the kinetic rate expression for species NO_2 will be a sum of two terms. For the reaction controlled by k_1 , species NO_2 is a reactant, and the first term is expressed as a negative multiplicative product of its stoichiometric coefficient, the rate constant k_1 , and all the reactant species concentrations which participate in reaction k_1 , each raised to the power of their respective stoichiometric coefficient, written as: $-4k_1[NO_2]^4[O_2]$.

For the reaction controlled by k_{-1} , species NO_2 is a product, and the second term is expressed as a positive multiplicative product of its stoichiometric coefficient, the rate constant k_{-1} , and all the reactant species concentrations which participate in reaction k_{-1} , each raised to the power of their respective stoichiometric coefficient, written thus: $4k_{-1}[N_2O_5]^2$. The complete kinetic rate equation for species NO_2 is shown below as:

$$\frac{d[NO_2]}{dt} = -4k_1[NO_2]^4[O_2] + 4k_{-1}[N_2O_5]^2 \quad (2.20)$$

Species O_2 participates in two reactions designated by the rate constants k_1 and k_{-1} ; therefore, the kinetic rate expression for species O_2 will be a sum of two terms. For the reaction controlled by k_1 , species O_2 is a reactant, and the first term is expressed as a negative multiplicative product of its stoichiometric coefficient, the rate constant k_1 , and all the reactant species concentrations which participate in reaction k_1 , each raised to the power of their respective stoichiometric coefficient, written thus: $-k_1[NO_2]^4[O_2]$. For the reaction controlled by k_{-1} , species O_2 is a product, and the second term is expressed as a positive multiplicative product of its stoichiometric coefficient, the rate constant k_{-1} , and all the reactant species concentrations which participate in reaction k_{-1} , each raised to the power of their respective stoichiometric coefficient, written as: $k_{-1}[N_2O_5]^2$. The complete kinetic rate equation for species O_2 is shown below as:

$$\frac{d[O_2]}{dt} = -k_1[NO_2]^4[O_2] + k_{-1}[N_2O_5]^2 \quad (2.21)$$

Species N_2O_5 participates in two reactions, designated by the rate constants k_1 and k_{-1} ; therefore, the kinetic rate expression for species N_2O_5 will be a sum of two terms. For the reaction controlled by k_1 , species N_2O_5 is a product, and the first term is expressed as a positive multiplicative product of its stoichiometric coefficient, the rate constant k_1 , and all the reactant species concentrations which participate in reaction k_1 , each raised to the power of their respective stoichiometric coefficient; written as: $2k_1[NO_2]^4[O_2]$. For the reaction controlled by k_{-1} , species N_2O_5 is a reactant, and the second term is expressed as a negative multiplicative product of its stoichiometric coefficient, the rate constant k_{-1} , and all the reactant species concentrations which participate in reaction k_{-1} , each raised to

the power of their respective stoichiometric coefficient, written thus: $-2k_{-1}[N_2O_5]^2$. The complete kinetic rate equation for species N_2O_5 is shown below as:

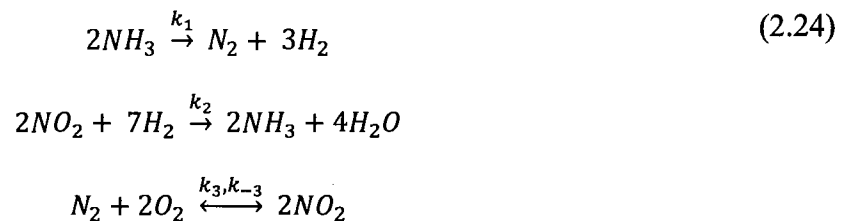
$$\frac{d[N_2O_5]}{dt} = 2k_1[NO_2]^4[O_2] - 2k_{-1}[N_2O_5]^2 \quad (2.22)$$

Taken all together, the stoichiometric reaction equation, the kinetic reaction rate equations, and their associated initial conditions are shown in (2.23):



Kinetic rate equations	Initial conditions
$\frac{d[NO_2]}{dt} = -4k_1[NO_2]^4[O_2] + 4k_{-1}[N_2O_5]^2$	$[NO_2](0) = [NO_2]_0$
$\frac{d[O_2]}{dt} = -k_1[NO_2]^4[O_2] + k_{-1}[N_2O_5]^2$	$[O_2](0) = [O_2]_0$
$\frac{d[N_2O_5]}{dt} = 2k_1[NO_2]^4[O_2] - 2k_{-1}[N_2O_5]^2$	$[N_2O_5](0) = [N_2O_5]_0$

Example 3:



The stoichiometric equation depicts four kinetic reactions (distributed among three equations) comprised of six chemical species. Description of this system will require the development of six kinetic rate equations: $d[NH_3]/dt$, $d[N_2]/dt$, $d[H_2]/dt$, $d[NO_2]/dt$, $d[H_2O]/dt$, and $d[O_2]/dt$.

Species NH_3 participates in two reactions, designated by the rate constants k_1 and k_2 ; therefore, the kinetic rate expression for species NH_3 will be a sum of two terms. For

the reaction controlled by k_1 , species NH_3 is a reactant, and the first term is expressed as a negative multiplicative product of its stoichiometric coefficient, the rate constant k_1 , and all the reactant species concentrations which participate in reaction k_1 , each raised to the power of their respective stoichiometric coefficient, written as: $-2k_1[NH_3]^2$. For the reaction controlled by k_2 , species NH_3 is a product, and the second term is expressed as a positive multiplicative product of its stoichiometric coefficient, the rate constant k_2 , and all the reactant species concentrations which participate in reaction k_2 , each raised to the power of their respective stoichiometric coefficient, written thus: $2k_2[NO_2]^2[H_2]^7$. The complete kinetic rate equation for species NH_3 is shown below as:

$$\frac{d[NH_3]}{dt} = -2k_1[NH_3]^2 + 2k_2[NO_2]^2[H_2]^7 \quad (2.25)$$

Species N_2 participates in three reactions designated by the rate constants k_1 , k_3 and k_{-3} ; therefore, the kinetic rate expression for species N_2 will be a sum of three terms. For the reaction controlled by k_1 , species N_2 is a product, and the first term is expressed as a positive multiplicative product of its stoichiometric coefficient, the rate constant k_1 , and all the reactant species concentrations which participate in reaction k_1 , each raised to the power of their respective stoichiometric coefficient, written as: $k_1[NH_3]^2$. For the reaction controlled by k_3 , species N_2 is a reactant, and the second term is expressed as a negative multiplicative product of its stoichiometric coefficient, the rate constant k_3 and all the reactant species concentrations which participate in reaction k_3 , each raised to the power of their respective stoichiometric coefficient, written thus: $-k_3[N_2][O_2]^2$. For the reaction controlled by k_{-3} species N_2 is a product, and the third term is expressed as a positive multiplicative product of its stoichiometric coefficient, the rate constant k_{-3} , and all the reactant species concentrations which participate in reaction k_{-3} , each raised to the

power of their respective stoichiometric coefficient, written thus: $k_{-3} [NO_2]^2$. The complete kinetic rate equation for species N_2 is shown below as:

$$\frac{d[N_2]}{dt} = k_1[NH_3]^2 - k_3[N_2][O_2]^2 + k_{-3}[NO_2]^2 \quad (2.26)$$

Species H_2 participates in two reactions, designated by the rate constants k_1 and k_2 ; therefore, the kinetic rate expression for species H_2 will be a sum of two terms. For the reaction controlled by k_1 , species H_2 is a product, and the first term is expressed as a positive multiplicative product of their respective stoichiometric coefficient, the rate constant k_1 , and all the reactant species concentrations which participate in reaction k_1 , each raised to the power of its stoichiometric coefficient, written as: $3k_1[NH_3]^2$. For the reaction controlled by k_2 , species H_2 is a reactant, and the second term is expressed as a negative multiplicative product of its stoichiometric coefficient, the rate constant k_2 , and all the reactant species concentrations which participate in reaction k_2 , each raised to the power of their respective stoichiometric coefficient, written as follows: $-7k_2[NO_2]^2[H_2]^7$.

The complete kinetic rate equation for species H_2 is shown below as:

$$\frac{d[H_2]}{dt} = 3k_1[NH_3]^2 - 7k_2[NO_2]^2[H_2]^7 \quad (2.27)$$

Species NO_2 participates in three reactions designated by the rate constants k_2 , k_3 and k_{-3} ; therefore, the kinetic rate expression for species NO_2 will be a sum of three terms. For the reaction controlled by k_2 , species NO_2 is a reactant, and the first term is expressed as a negative multiplicative product of its stoichiometric coefficient, the rate constant k_2 , and all the reactant species concentrations which participate in reaction k_2 , each raised to the power of their respective stoichiometric coefficient, written as: $-2k_2[NO_2]^2[H_2]^7$. For the reaction controlled by k_3 , species NO_2 is a product, and the second term is expressed

as a positive multiplicative product of its stoichiometric coefficient, the rate constant k_3 , and all the reactant species concentrations which participate in reaction k_3 , each raised to the power of their respective stoichiometric coefficient, written thus: $2k_3[N_2][O_2]^2$. For the reaction controlled by k_{-3} species NO_2 is a reactant, and the third term is expressed as a negative multiplicative product of its stoichiometric coefficient, the rate constant k_{-3} , and all the reactant species concentrations which participate in reaction k_{-3} , each raised to the power of their respective stoichiometric coefficient, written thus: $-2k_{-3}[NO_2]^2$. The complete kinetic rate equation for species NO_2 is shown below as:

$$\frac{d[NO_2]}{dt} = -2k_2[NO_2]^2[H_2]^7 + 2k_3[N_2][O_2]^2 - 2k_{-3}[NO_2]^2 \quad (2.28)$$

Species H_2O participates in one reaction designated by the rate constant k_2 . For the reaction controlled by k_2 , species H_2O is a product, and the first term is expressed as a positive multiplicative product of its stoichiometric coefficient, the rate constant k_2 , and all the reactant species concentrations which participate in reaction k_2 , each raised to the power of their respective stoichiometric coefficient, written thus: $7k_2[NO_2]^2[H_2]^7$. The complete kinetic rate equation for species H_2O is shown below as:

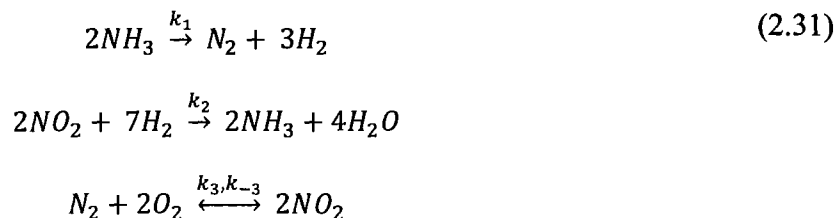
$$\frac{d[H_2O]}{dt} = 7k_2[NO_2]^2[H_2]^7 \quad (2.29)$$

Species O_2 participates in two reactions, designated by the rate constants k_3 and k_{-3} ; therefore, the kinetic rate expression for species O_2 will be a sum of two terms. For the reaction controlled by k_3 , species O_2 is a reactant, and the first term is expressed as a negative multiplicative product of its stoichiometric coefficient, the rate constant k_3 , and all the reactant species concentrations which participate in reaction k_3 , each raised to the power of their respective stoichiometric coefficient, written as: $-2k_3[N_2][O_2]^2$. For the

reaction controlled by k_{-3} , species O_2 is a product, and the second term is expressed as a positive multiplicative product of its stoichiometric coefficient, the rate constant k_{-3} , and all the reactant species concentrations which participate in reaction k_{-3} , each raised to the power of their respective stoichiometric coefficient, written thus: $2k_{-3} [NO_2]^2$. The complete kinetic rate equation for species O_2 is shown below as:

$$\frac{d[O_2]}{dt} = -2k_3[N_2][O_2]^2 + 2k_{-3}[NO_2]^2 \quad (2.30)$$

Taken all together, the stoichiometric reaction equation, and the kinetic reaction rate equations with their associated initial conditions are shown in (2.31):



Kinetic Rate Equations	Initial conditions
$\frac{d[NH_3]}{dt} = -2k_1[NH_3]^2 + 2k_2[NO_2]^2[H_2]^7$	$[NH_3](0) = [NH_3]_0$
$\frac{d[N_2]}{dt} = k_1[NH_3]^2 - k_3[N_2][O_2]^2 + k_{-3}[NO_2]^2$	$[N_2](0) = [N_2]_0$
$\frac{d[H_2]}{dt} = 3k_1[NH_3]^2 - 7k_2[NO_2]^2[H_2]^7$	$[H_2](0) = [H_2]_0$
$\frac{d[NO_2]}{dt} = -2k_2[NO_2]^2[H_2]^7 + 2k_3[N_2][O_2]^2 - 2k_{-3}[NO_2]^2$	$[NO_2](0) = [NO_2]_0$
$\frac{d[H_2O]}{dt} = 7k_2[NO_2]^2[H_2]^7$	$[H_2O](0) = [H_2O]_0$
$\frac{d[O_2]}{dt} = -2k_3[N_2][O_2]^2 + 2k_{-3}[NO_2]^2$	$[O_2](0) = [O_2]_0$

It has been shown that the rules of mass action kinetics can be used to develop model equations of the kinetics of a given stoichiometric reaction network in a straightforward fashion. The stoichiometric reaction coefficients of the chemical species were also shown to correlate to the reaction order (species concentration exponent) in the derived rate equations, and this is true for elementary single step reactions, but not true in general. In balanced stoichiometric equations the stoichiometric coefficients are expressed as the simplest collective set of whole numbers for convenience. In general, stoichiometric coefficients are not necessarily connected to the reaction order. The explicit substitution of the stoichiometric coefficients as concentration exponents and kinetic rate coefficients in the preceding examples was used as a device to clarify the relations between the reaction networks and their coupled differential rate equations. To illustrate, the application of fundamental molecular collision theory to reaction network (2.31) suggests that seven H_2 molecules and two NO_2 molecules coming together simultaneously in the correct proximity and orientation is an unlikely event. This reaction probably occurs in several steps. In practice, the concentration exponents are replaced by additional unknown parameters which must subsequently be determined by experiment, and the stoichiometric coefficients are incorporated into the kinetic rate constant (also determined by experiment). Models based on mass-action kinetics have the advantage of being determined directly from the elemental reactions and their stoichiometry. However, a detriment is the fact that a large number of rate constants and other parameters must be determined in order to implement the model. In many cases, these elemental reactions are not experimentally observable and the parameters would thus be difficult to acquire.

CHAPTER 3

MODEL DEVELOPMENT

The synaptic chemical transmission is an important part of the transport of neuronal signals, and investigation of the molecular events was instrumental in creating neurotransmitter theory. Analysis of such behavior can be best accomplished with the transmission process represented as a reaction-diffusion simulation for the neurotransmitter because experimental analysis is impractical for the molecular processes in the cleft. Unless great care is taken, the tools used to collect the data can disrupt the physical system so badly that it ceases natural function. Several mathematical models for the dynamic behavior of acetylcholine in spontaneous generation of the action potential at the neuromuscular junction have been implemented to analyze the transient process of the synaptic chemical transmission. In the model of Rosenberry [5], the radial diffusion of acetylcholine is treated in two axis-symmetrical compartments with homogeneity in the transverse direction, while Thomas and Friboulet [57] used a model where the transverse coordinate diffusion gradient was discretized and the effects of radial diffusion out of the cleft were described as a uniform sink term. Models where the reaction-diffusion of acetylcholine is developed in a volume consisting of two space variables r and x , representing the radius and axis respectively, and the diffusion is symmetric about the axis, have also been published [5]. A report by Naka and Shiba [58] described a two

dimensional compartment model to examine the effects of transverse and radial diffusion of acetylcholine on the transient behavior of the molecular dynamics of the action potential event. The transmission process is represented as a reaction-diffusion system, in which the acetylcholine concentration varies with time and position in a two dimensional space between the axis-symmetrical discs of the synaptic cleft. The variation in concentration of the open channel form of the receptor in response to the interaction of receptor with incoming acetylcholine corresponds to transient evolution of the action potential. Naka and Shiba [58] did much analytical development and support of simplifying assumptions and modeling techniques which helped unravel the complexities of simulating the neuromuscular action potential event; thus, their work was an integral part of the development of the Jenkins-Szlavik model. This researcher was able to seize a number of concepts and propositions and apply them to the pertinent portions of the model herein which will show simulation of the key issues of the transient neurotransmission process under the influence of acetylcholinesterase inhibitors, and the therapeutic regeneration of inhibited acetylcholinesterase.

Based on an optimal selection of the subdivision numbers and critical radius for their simulation, Naka and Shiba [58] proposed a minimal compartment model which was comprised of three compartments in the transverse direction and ten compartments in the radial direction, in a disc with 500 nm radius and 50 nm in height. Evaluation of varying diffusion coefficients suggested anisotropic diffusion for this model to represent the characteristic behavior of the chemical neurotransmission process. Their proposal of anisotropic diffusion provides a solid case demonstrating that radial diffusion has stronger effects than axial diffusion on the processes occurring in the neuromuscular

junction. For this reason Jenkins chose to ignore axial diffusion in this model, and discretized the cleft volume into 20 annular compartments. Jenkins found that the results of the simulation did not become any smoother at compartment numbers larger than twenty. This choice gave a benefit of simpler computations and still captured the essential character of the dynamics involved in the generation and inhibition of the action potential [58].

Jenkins assumed the neuromuscular junction as a whole to have the general shape of a cylinder where the radius is approximately 10 times that of the height. To illustrate this concept, consider a coin, one face represents the presynaptic membrane, while the other face represents the postsynaptic membrane, as shown in Figure 3.1 below.

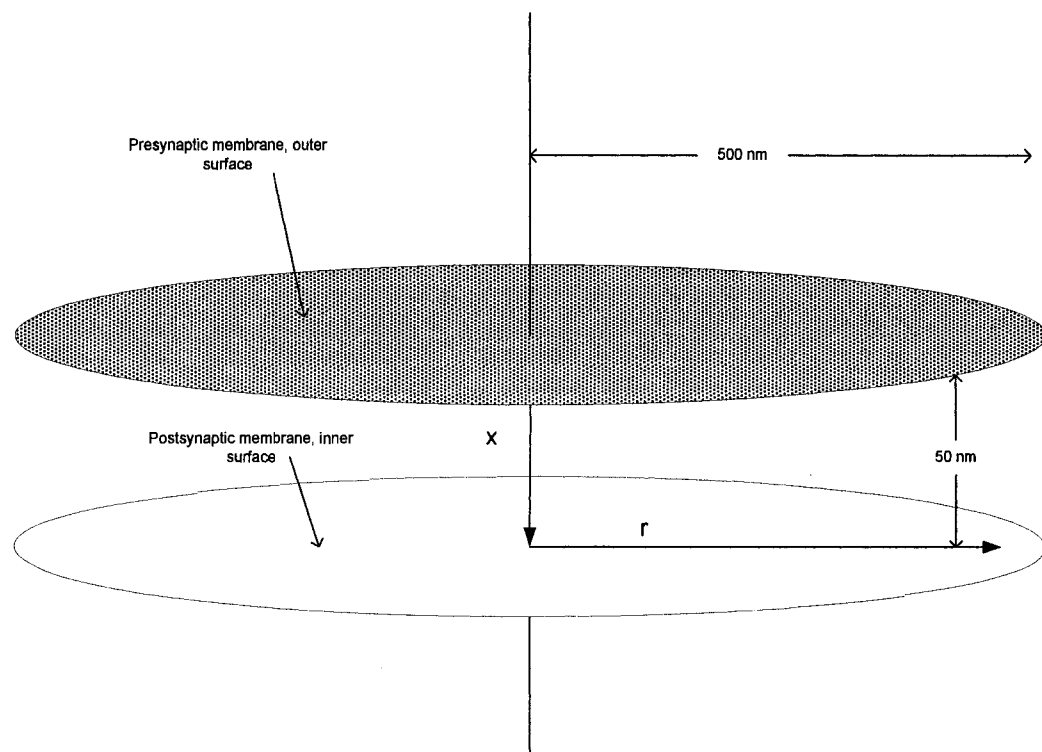


Figure 3.1. A schematic diagram of the neuromuscular junction geometry used in the model. The dimension of width is exaggerated for clarity.

The material between each face has been removed such that the edge of the coin becomes a void which represents the cleft that separates the presynaptic membrane and the postsynaptic membrane (motor end-plate). The result is a model of the cleft as a very thin disk comprised of two circular plates separated by a space of 50 nm, with a radius of 500 nm, and open to the environment along the circumference. The coordinate system is embedded such that a line connecting each membrane through their respective centers represents the direction along the axis, designated by the variable x ; and the direction normal to this axis, along the radius and which terminates at the circumference, is designated by the variable r . As shown in Figure 3.2, acetylcholine vesicles are modeled as a cylindrical shape entering the cleft through the surface of the presynaptic membrane at the center. The pulse of acetylcholine is assumed to enter the cleft, instantaneously diffuse axially across the cleft to the motor end-plate, and then diffuse radially towards the circumference of the membranes and then into the environment. The radial diffusion process is assumed to be angularly symmetric about the axis. It should be mentioned here that in reaction-diffusion systems with anisotropic diffusion, it is important to make a distinction between directions where diffusion occurs at some finite rate, and those directions where the diffusion is modeled as instantaneous. Instantaneous diffusion is often termed *instantaneously well mixed* or *instantaneous uniform concentration*.

The acetylcholine receptors are immobilized in the surface of the postsynaptic. A schematic representation of this transport model is shown in Figure 3.3, as viewed along the axis and normal to the surface of the cleft. The enzyme acetylcholinesterase is assumed to be uniformly distributed and immobilized throughout the volume of the cleft, and reacts with acetylcholine as it diffuses out of the cleft.

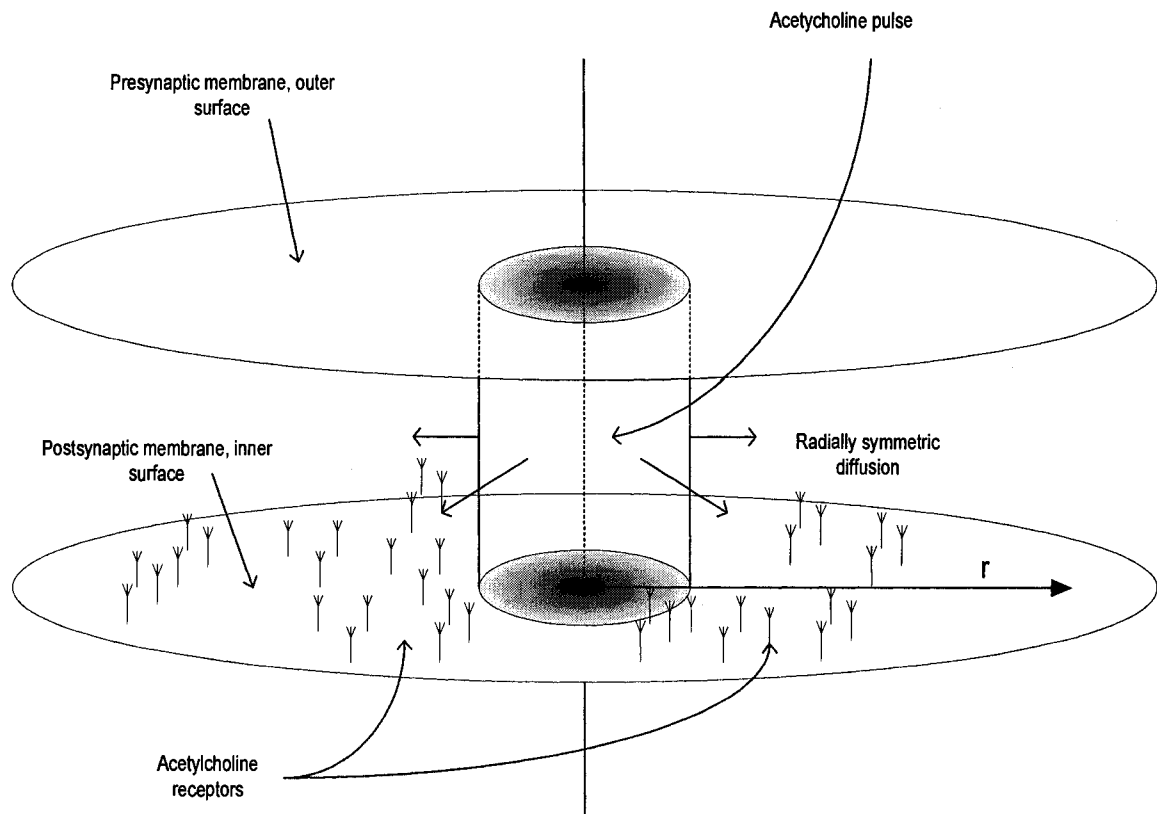


Figure 3.2. The shape and diffusion of the acetylcholine pulse, and the relative location of the acetylcholine receptors in the neuromuscular junction model.

The inhibitor and oxime species are each modeled as diffusing into the cleft from the environment through the edge and towards the center, through the same series of concentric annuli. None of the chemical species in this reaction-diffusion system are allowed to permeate through both the presynaptic and postsynaptic membranes in either the positive axial direction (postsynaptic membrane) or the negative axial direction (presynaptic membrane).

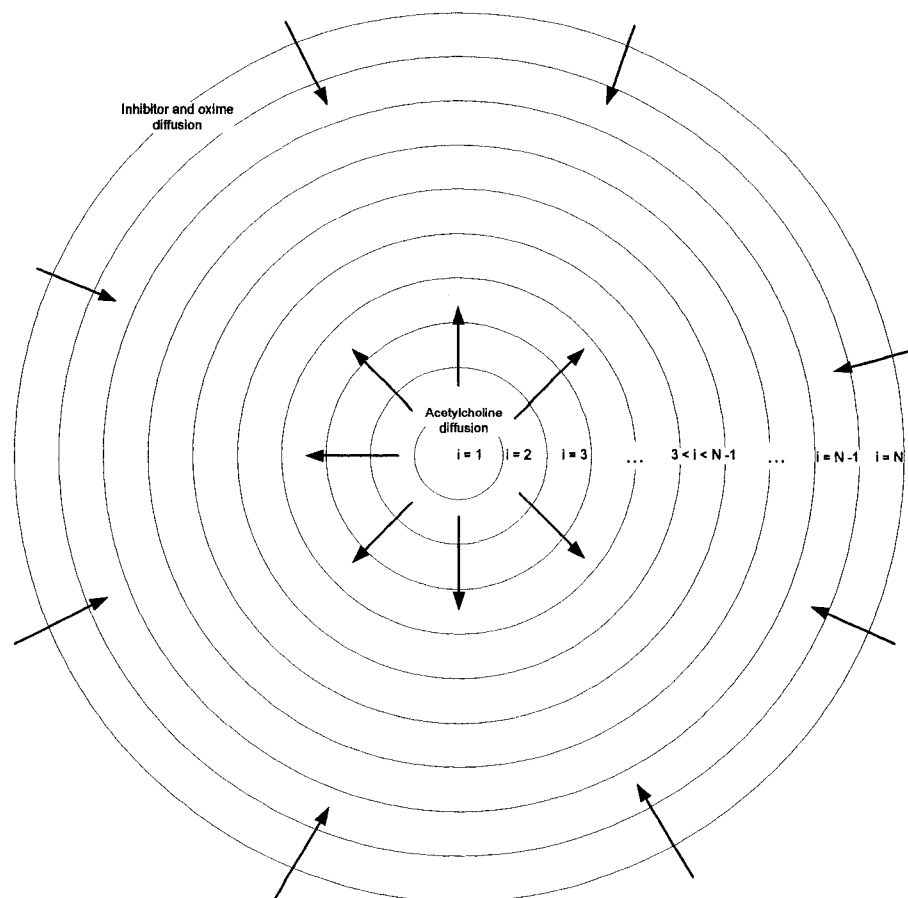
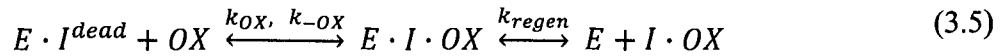
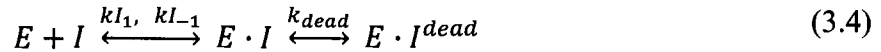
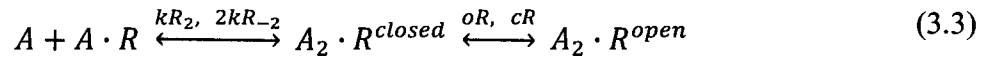
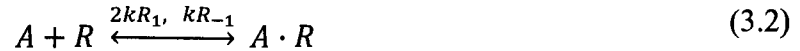
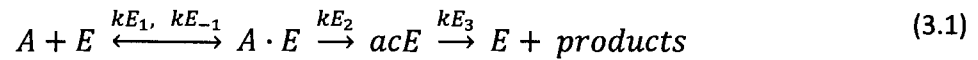


Figure 3.3. The transport model of the acetylcholine, inhibitor, and oxime species in the neuromuscular junction.

The behavior of this reaction-diffusion system is mathematically expressed by a one-dimensional, axially symmetric partial differential diffusion equation with nonlinear reaction terms for acetylcholine, organophosphate inhibitor, and oxime species. These equations are coupled with a set of nonlinear ordinary differential equations that represent the immobilized receptor and enzyme species which are distributed at spatial compartments in the cleft. The spatio-temporal analysis employs computer simulation via discretization of the radial coordinates in the space for the partial differential equations,

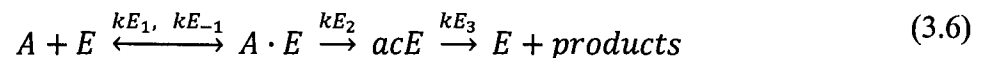
and numerical integration of the governing ordinary differential equations. Simulation of the response of this system to release a discrete packet of acetylcholine into the cleft leads to characterization of the radial diffusion process of acetylcholine in the chemical transmission with reference to their effect on spontaneous generation of the action potential during normal and inhibited conditions.

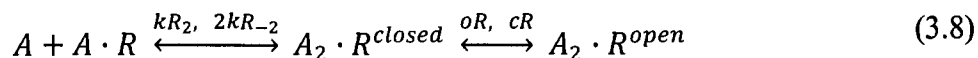
The stoichiometric Equations (3.1) to (3.5) represent the full set of chemical species and their stoichiometric reactions that were modeled in this dissertation. Some of



the stoichiometric equations depict two or more reactions, and these equations can be collected into different groups, depending on which of the three processes in this model are being described: normal cleft reactions, inhibited enzyme cleft reactions, and enzyme regeneration reactions.

To begin, determine all the stoichiometric chemical equations which comprise the reactions in the neuromuscular junction during a normal action potential event. By choosing from the complete set, these equations are:



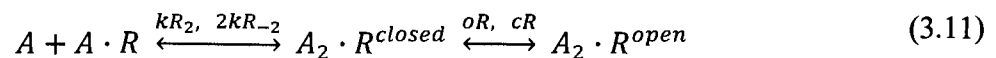
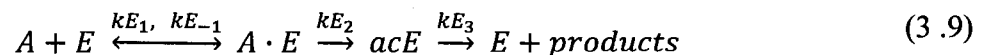


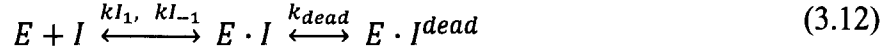
Equation (3.6) represents the full kinetic cycle of acetylcholine initially reacting with acetylcholinesterase and proceeding to the final renewal of the enzyme. The first step shows acetylcholine, A , reacting with acetylcholinesterase, E , reversibly to form the Michaelis complex of $A \cdot E$. The forward reaction, controlled by the rate constant kE_1 , is several orders of magnitude faster than the reverse reaction controlled by kE_{-1} . In the next step, species $A \cdot E$ then irreversibly reacts to form the acylated enzyme intermediate acE , where the reaction rate is controlled by the constant kE_2 . The final step shows how acE then decomposes back to acetylcholinesterase and reaction products, where the rate is controlled by the rate constant kE_3 and one of the reaction products is choline. This final step regenerates the enzyme and is the major resource for acetylcholine replacement because choline is a precursor of acetylcholine. Water is also a reactant in this last step, but in this case, water is treated as an excess solvent, and as such, its concentration does not change and so it is not included in the reaction kinetics.

Equation (3.7) represents the first acetylcholine molecule reversibly binding to the closed receptor. Because there are two sites available for docking, a numerical factor of two is included with the kinetic rate constant $2kR_1$, which controls the forward binding reaction. Because only one acetylcholine molecule can dissociate from the receptor in the reverse reaction, the kinetic rate constant kR_{-1} does not require an additional multiplicative factor.

The two-step process kinetics of acetylcholine receptor function is represented by Equation (3.8). Just as in Equation (3.7), the first step of this equation shows a second acetylcholine molecule binding reversibly to the ligand-receptor complex $A \cdot R$. Only one position for binding exists on the receptor in this case, so the forward kinetic rate constant, kR_2 , does not require a multiplicative factor. In the reverse reaction, either of the two acetylcholine molecules could dissociate from the closed ligand-receptor complex A_2R^{closed} so the numerical factor of two is included with the kinetic rate constant $2kR_{-2}$. The second step of Equation (3.8) shows the closed, double bound, ligand-receptor complex reversibly changing from the closed conformation to the open conformation, A_2R^{open} (forward reaction), and back to the closed conformation (reverse reaction). The forward and backward reactions are controlled by the kinetic rate constants oR and cR , respectively. It is at this step where the redistribution of sodium and potassium ions through this open channel leads to the eventual contraction of the muscle cell. Several experiments, and kinetic-thermodynamic analyses, [8], [23], [41], have shown that the conformational change from A_2R^{closed} to A_2R^{open} is energetically favored, so that a channel which has two molecules of acetylcholine bound to it will spend most of its time of existence in the open condition.

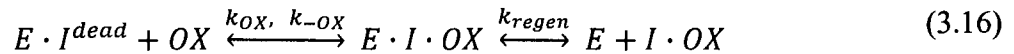
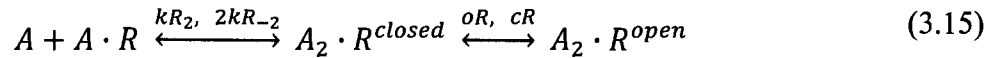
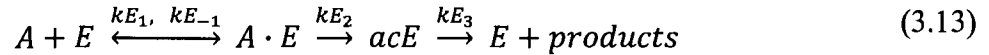
The inhibited enzyme cleft reactions include Equations (3.9) through (3.11) with the addition of Equation (3.12), as shown below:





The qualitative kinetics represented by the stoichiometric Equations (3.9) through (3.11) has been discussed. Equation (3.12) shows the two-step kinetic process of acetylcholinesterase, E , reacting with an inhibiting organophosphorus compound I , where the reaction leads to the non-functional inhibited enzyme $E \cdot I^{dead}$. In the first step, acetylcholinesterase reacts reversibly with the inhibitor to produce the intermediate enzyme-inhibitor complex $E \cdot I$. The forward and reverse reactions of this step are controlled by the respective kinetic rate constants k_{I1} and k_{I-1} . The second step represents the enzyme-inhibitor complex irreversibly reacting to produce the non-functional inhibited enzyme $E \cdot I^{dead}$, and the reaction rate is controlled by the kinetic rate constant k_{dead} .

The reactions which describe the process of acetylcholinesterase regeneration in the neuromuscular junction in this model are given by:



All the reactions of a normal action potential event are included again (Equations (3.13) - (3.15)), and the addition of Equation (3.16). Equation (3.16) shows the two-step kinetic process of regenerating functional acetylcholinesterase from the deactivated enzyme via

the use of an oxime compound. In the first step, the inhibited enzyme, $E \cdot I^{dead}$, reacts reversibly with the oxime compound, OX , to form the intermediate phosphyl-oxime complex $E \cdot I \cdot OX$. The forward and backward reactions are controlled by the reaction rate constants k_{OX} and k_{-OX} , respectively, where k_{OX} is many orders of magnitude larger than k_{-OX} . The second step represents the irreversible dissociation reaction of the phosphyl-oxime complex, controlled by reaction rate constant k_{regen} , to produce the phosphylated oxime residue $I \cdot OX$, and also regenerates functional acetylcholinesterase, E . This completes the qualitative analysis of all the chemical reactions used in the Jenkins-Szlavik model of the neuromuscular junction.

Next, it will be useful to develop a robust and general algorithm to describe how to start with a set of stoichiometric equations, derive their resulting theoretical differential kinetic equations, and finish with the set of coupled numerical equations. The numerical equations can then be used to calculate numerical values that can be compared to measurements obtained from the actual physical system, and the results of that comparison can be used to evaluate the validity of the model. In this system, a key issue is the reaction that occurs between mobile chemical species and immobile chemical species. All the species vary in concentration with time; however, some of the species are mobile, and some are immobile. The mobile species have concentrations that can vary with respect to position in space, as well as time. Most kinetic chemical equations are modeling chemical species which are assumed to be mobile in a uniformly mixed environment, but one's first encounter with describing the kinetics of mobile and immobilized molecules can be non-intuitive. To address this issue, two species which include all of the important characteristics associated with the mobile and immobile

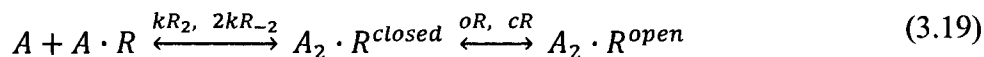
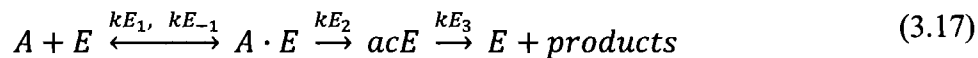
kinetics will be selected, and a general algorithmic procedure that can be applied to all of the other species and reactions will be developed.

The molecules acetylcholine and acetylcholinesterase have been chosen as the species with the important characteristics which are shared by all the other different molecules in this system, and as such are suitable for the detailed algorithmic derivation and development. Collectively, the chemical kinetics of these two species includes mobility, immobilization, reaction with different mobile and immobile species, and reaction with each other. A detailed development of their chemical kinetics starting from the stoichiometric reactions and finishing with the full set of numerical computable equations will allow comparison between similarities and differences. This comparison will lead to the recognition of patterns and establishment of the general principles which describe the complete kinetic behavior of the system in time and space.

Both acetylcholine and acetylcholinesterase vary in concentration with time; however, acetylcholine is mobile, and acetylcholinesterase is immobile. The mobile species have concentrations that can vary with respect to position in space, as well as time. Therefore, these species are modeled with partial differential equations. The immobile chemical species are modeled with ordinary differential equations. The end result is a set of coupled partial and ordinary differential equations that describe how mobile molecular species and immobile molecular species are able to interact with each other.

The stoichiometric equations that describe the normal cleft reactions are a suitable choice for the forthcoming derivation because acetylcholine and acetylcholinesterase are members of these reactions. The differential equation for acetylcholine will be derived

first, and this goal will require knowledge of where acetylcholine occurs in the network of coupled normal cleft reactions, shown as Equations (3.17) to (3.19), which have been included here for easy reference:



Because acetylcholine is known to be a mobile species in this system, it is known that the general form of the kinetic partial differential equation (PDE) is shown below in (3.20) according to the description given in Chapter 2 (page 11) of this dissertation. The details

$$\frac{\partial[A]}{\partial t} = \nabla \cdot (D_A \nabla[A]) + \sum k_{i,j}(T) \left(\prod [X_h]^\omega \right) \quad (3.20)$$

of the rigorous and general enumeration rules of $k_{i,j}$ and X_h are omitted to avoid unnecessary complexity. Recall that this equation is a function of the concentration of acetylcholine, $[A]$, and that the symbol for acetylcholine is given by A . The term on the left-hand-side of (3.20) is the partial derivative of $[A]$ with respect to time, t . The first term on the right-hand-side of (3.20) describes the diffusion of acetylcholine throughout the cleft, and the second term on the LHS relate to the reactions of acetylcholine with other species in the cleft. At this point, it will be more instructive to show the fully developed theoretical form of (3.20) and explain the rules used for its derivation while

the reader can easily refer to it and the equations of the stoichiometric reaction network that contains acetylcholine.

Equation (3.21) shows the full theoretical kinetic rate equation for the reaction of acetylcholine in the neuromuscular junction. Recall that the neuromuscular junction

$$\begin{aligned} \frac{\partial[A(r, t)]}{\partial t} = & D_A \frac{\partial^2[A(r, t)]}{\partial r^2} + D_A \frac{1}{r} \frac{\partial[A(r, t)]}{\partial r} - 2kR_1[A(r, t)][R] + kR_{-1}[A \cdot R] \\ & - kR_2[A(r, t)][A \cdot R] + kR_{-2}[A_2 \cdot R^{closed}] - kE_1[A(r, t)][E] + kE_{-1}[A \cdot E] \end{aligned} \quad (3.21)$$

geometry is modeled as a thin coin, in cylindrical coordinates, with acetylcholine entering the coin between the plates at the center, and diffusing and reacting from the center to the outer edge. Acetylcholine, chemical species A , is mobile, and is transported throughout the cleft by diffusion where it reacts with some of the other species it encounters. This reaction-diffusion process is described by Equation (3.21), and is known as a *reaction-diffusion equation*. A qualitative description of the terms on each side of (3.21) now follows.

The first term on the left-hand side of the equal sign is of course the partial derivative of acetylcholine concentration with respect to time. The first two terms on the RHS of the equal sign account for the transport of acetylcholine in the cleft. These two terms are the result of implementing the gradient and divergence operators on the concentration of species A , embedded in cylindrical coordinates. The first term describes transport by diffusion, and the second term accounts for the increased radial dispersion effects caused by the geometry of the model. The rest of the terms in (3.21) relate to the reaction of acetylcholine where it appears in each of the stoichiometric equations shown

in (3.17) to (3.19), and these terms result from applying the same rules developed in Chapter 2 (page 11) for deriving differential rate expressions from a given stoichiometric network. Referring to those coupled stoichiometric equations, it is easy to see that acetylcholine participates in six reactions, designated by the rate constants kE_1 , kE_{-1} , $2kR_1$, kR_{-1} , kR_2 , and $2kR_{-2}$. These six reactions explain why (3.21) has six kinetic rate terms for species A , each comprised of a multiplicative product of the particular rate constant and all the reactant species concentrations participating in that reaction, where each species concentration is raised to the power of its stoichiometric coefficient.

The derivation of the complete reaction-diffusion equation for acetylcholine is not yet accomplished, but at this point it seems useful to walk through the derivation rules of the kinetic reaction equation for the other representative species, acetylcholinesterase. In the Jenkins-Szlavik model of the neuromuscular cleft system, the species acetylcholinesterase, E , is known to be immobilized and assumed uniformly distributed. As an immobile species, the concentration of acetylcholinesterase depends only on time, t . This means the kinetic reaction equation for acetylcholinesterase is an ordinary differential equation (ODE), not another diffusion-reaction equation. As such, this reaction equation will be less complicated than (3.21) and familiar to readers with some experience with chemical kinetics. As was done with acetylcholine, the full theoretical kinetic equation for acetylcholinesterase will be given in (3.22), and the rules of its derivation will follow.

$$\frac{d[E]}{dt} = -kE_1[A(r, t)][E] + kE_{-1}[A \cdot E] + kE_3[acE] \quad (3.22)$$

Equation (3.22) shows the full theoretical kinetic rate equation for the reaction of acetylcholinesterase in the neuromuscular junction with the same conditions and geometry of Equation (3.21). The first term on the left hand side is the derivative of the concentration of species E , $[E]$, with respect to time, t . Since species E is immobile in the cleft, there are no transport terms appearing on the right hand side of (3.22). This means all the right hand side terms are related to the reaction of species E where it appears in the coupled stoichiometric reaction network depicted in Equations (3.17) to (3.19). Referring to those coupled stoichiometric equations, the reader will note that species E participates in three reactions, designated by the rate constants kE_1 , kE_{-1} , and kE_3 . These three reactions explain why (3.22) has three kinetic rate terms for species E , each comprised of a multiplicative product of the particular rate constant and all the reactant species concentrations participating in that reaction, where each species concentration is raised to the power of its stoichiometric coefficient.

The full theoretical kinetic reaction rate equations for the representative mobile species acetylcholine and immobile species acetylcholinesterase have now been derived. All types of differential equations must have their initial and boundary conditions specified before they can be solved, and the determination of these conditions for (3.21) and (3.22) follow next.

Equation (3.23), the PDE which governs the reaction-diffusion of acetylcholine in the neuromuscular junction, now needs to have the initial and boundary conditions

$$\frac{\partial[A(r, t)]}{\partial t} = D_A \frac{\partial^2[A(r, t)]}{\partial r^2} + D_A \frac{1}{r} \frac{\partial[A(r, t)]}{\partial r} - 2kR_1[A(r, t)][R] + kR_{-1}[A \cdot R] \quad (3.23)$$

$$-kR_2[A(r, t)][A \cdot R] + kR_{-2}[A_2 \cdot R^{closed}] - kE_1[A(r, t)][E] + kE_{-1}[A \cdot E]$$

determined. These conditions are imposed by the geometry and physio-chemical parameters of the system. The determination of those conditions will now require a focus on the partial derivative terms in Equation (3.23). Recall that the physical system is modeled as the volume bounded by the two sides of a very thin coin, the two side surfaces are impermeable, and the circumference edge is open to the environment. Acetylcholine enters the cleft in the center of that volume and diffuses radially (outward) towards the edge, reacting with other molecular species along the way. Because PDE (3.23) contains a second derivative with respect to the radius, determining the solution will require known information about the concentration of species A at two points in the domain of r that is simultaneously true for all points in the domain of t . Intuitively, one should suspect the best candidates would be the extreme values of r in its domain: $r = 0$ and $r = 500$ nm; i.e., those values of r designate the physical boundaries. The known information about the concentration of acetylcholine at these points specifies the boundary conditions. At the maximum value of r , the edge of the cleft and beyond, the reader knows the concentration of species A is essentially zero for all time. Therefore, this boundary condition is easy to understand and state mathematically:

$$[A(500, t)] = 0, \forall t \geq 0 \quad (3.24)$$

The physical interpretation is that acetylcholine diffuses from inside the cleft into a region outside the cleft where its concentration is maintained at zero. At the center of the

cleft where $r = 0$, intuition is of less help and it is beneficial to explain the situation in more detail. There does not exist a known relationship describing the concentration of acetylcholine at $r = 0$ as a function of all time, so seeking a boundary condition explicitly in terms of $[A(r,t)]$ is not useful. The next candidate is to examine what is known about the first partial derivative of $[A(r,t)]$ with respect to r at $r = 0$. By the use of symmetry, it is possible to model diffusion in a two-dimensional space with a one-dimensional direction. However, the diffusion process in this two-dimensional space is identical to a particular one-dimensional problem where diffusion occurs in the x -direction. Imagine a linear tube of length L , where $0 \leq x \leq L$. At $x = 0$ the tube is closed, and at $x = L$ the tube is open to the environment. Particles of species A are inserted into this system at $x = 0$ and allowed to diffuse along the tube. In this case, because the tube is closed at $x = 0$ for all values of time, the reader would determine the boundary condition there as

$$\frac{\partial[A(0,t)]}{\partial x} = 0, \forall t \geq 0 \quad (3.25)$$

This is known as a Neumann boundary condition, and it shows the mathematical expression of describing how a quantity is not allowed to leave the system at some identified location. Now imagine this one-dimensional problem is mathematically rotated 2π radians about the axis at $x = 0$. This will produce the symmetric two-dimensional space, one-dimensional direction diffusion system, where x is now defined to be r and the boundary condition at $r = 0$ is still the same Neumann condition. In this case, it is expressed as:

$$\frac{\partial[A(0, t)]}{\partial r} = 0, \quad \forall t \geq 0 \quad (3.26)$$

The physical interpretation means that acetylcholine cannot leave the cleft at its center. Two thought experiments are described here to aid the reader's intuition in understanding this condition at $r = 0$. First, imagine a perfectly frictionless and hemispherical surface (concave down) at rest in a uniform gravitational field. By nature of the non-friction surface, no object could be placed on it without sliding off, unless it was balanced exactly at the top and center point, the "pole". Balanced at that point, all the forces acting on the object would resolve to zero, and it would stay in place if not disturbed, regardless of the lack of friction at the surface. Finally, imagine a traveler moving north along a longitudinal. When the geographic North Pole is reached, the direction "North" no longer exists. Every direction from that point is south.

The initial condition for acetylcholine is

$$[A(r, 0)] = \begin{cases} 0.17 \text{ mmole/cm}^3 & 0 \leq r \leq 25\text{nm} \\ 0 & \text{otherwise} \end{cases} \quad (3.28)$$

The physical interpretation is that the vesicle of acetylcholine which instantaneously enters the cleft centered at $r = 0$ has a radius of 25 nm, and no acetylcholine initially exists anywhere else in the cleft.

Equation (3.29), the ODE which governs the reaction-diffusion of acetylcholine in the neuromuscular junction, only needs to have the initial condition on the concentration

$$\frac{d[E]}{dt} = -kE_1[A(r, t)][E] + kE_{-1}[A \cdot E] + kE_3[acE] \quad (3.29)$$

of species E specified. The concentration of acetylcholinesterase in the neuromuscular junction is known to be 0.845 mmole/cm^3 ([5], [57], [58]), which means that when $t = 0$

$$[E](0) = 0.845 \text{ mmole/cm}^3 \quad (3.30)$$

With the boundary and initial conditions of (3.23) and (3.29) determined, these equations are now ready for numerical development. No general method for the analytic solution of coupled nonlinear PDE/ODE systems yet exists. As a rule, transport-reaction equations are “well behaved”, albeit stiff (the variables can exhibit a wide distribution of rates of change), and thus can be reliably approximated with numerical techniques. For systems involving PDEs, the two usual numerical methods of choice are the finite difference method (FDM) and the finite element method (FEM). The FEM can model a broad array of physical systems and is better able to handle complex shapes and boundaries. However, because the FEM approximates the solution of the PDE instead of the actual PDE, implementing this method can be very abstract for the non-specialist in numerical techniques. In contrast, finite difference methods approximate the original equations that describe the physical model, and so the less experienced investigator has a larger opportunity to use physical intuition during the implementation. Jenkins modeled the neuromuscular junction as a cylinder because that shape captured the relevant dynamics along with a simple geometry and boundaries [58], and so the finite difference method was the natural choice.

Several classes of finite difference methods exist, of which one is the method of lines (MOL). The MOL is well suited for equations developed from transport-reaction processes, and is typically the first method of choice [59]-[65]. This technique involves discretizing one or more PDEs in all but one dimension, and then integrating the semi-

discrete problem as a system of ODEs. The advantage is that the methods for numerically solving coupled ODE systems are well understood and mature. If the original PDEs are well posed as an initial value problem, then there are many algorithms that provide an efficient and robust method of solution. This model's descriptive equations were numerically solved with the method of lines and the Matlab ODE solver algorithm ode15s [59].

To begin, one needs to have the coordinate system chosen and the applicable equations derived, as per the description in this chapter beginning on page 3. The first step in applying the MOL is to divide the system volume into a group of sub-volumes, where the shape of the sub-volumes is influenced by the chosen coordinate system, as shown below in Figure 3.4. A Cartesian system would be divided into squares or cubes, and a spherical system would be partitioned into thin concentric shells. The model of this dissertation uses a polar coordinate system with angular symmetry; therefore a series of concentric circles was a natural choice. The neuromuscular cleft was modeled as a cylinder with an axial length of L , and a radius of R . Further, the cleft was subdivided into 20 concentric volumes, arranged such that the origin of the radial coordinate r was at the center of the annuli, and the width of each annular volume r_i was centered at radial coordinate $(R/20)*(i - 1/2)$, for $i = 2, 3, \dots, 20$ (The centermost sub-volume at $i = 1$ is a disk, not an annulus). Recall that twenty volumes was the optimal volume number for accuracy and mitigation of computational labor, and this number was derived from the analysis of the model developed by Naka. A change of variables will now be required because of the large number of different chemical species in these equations.

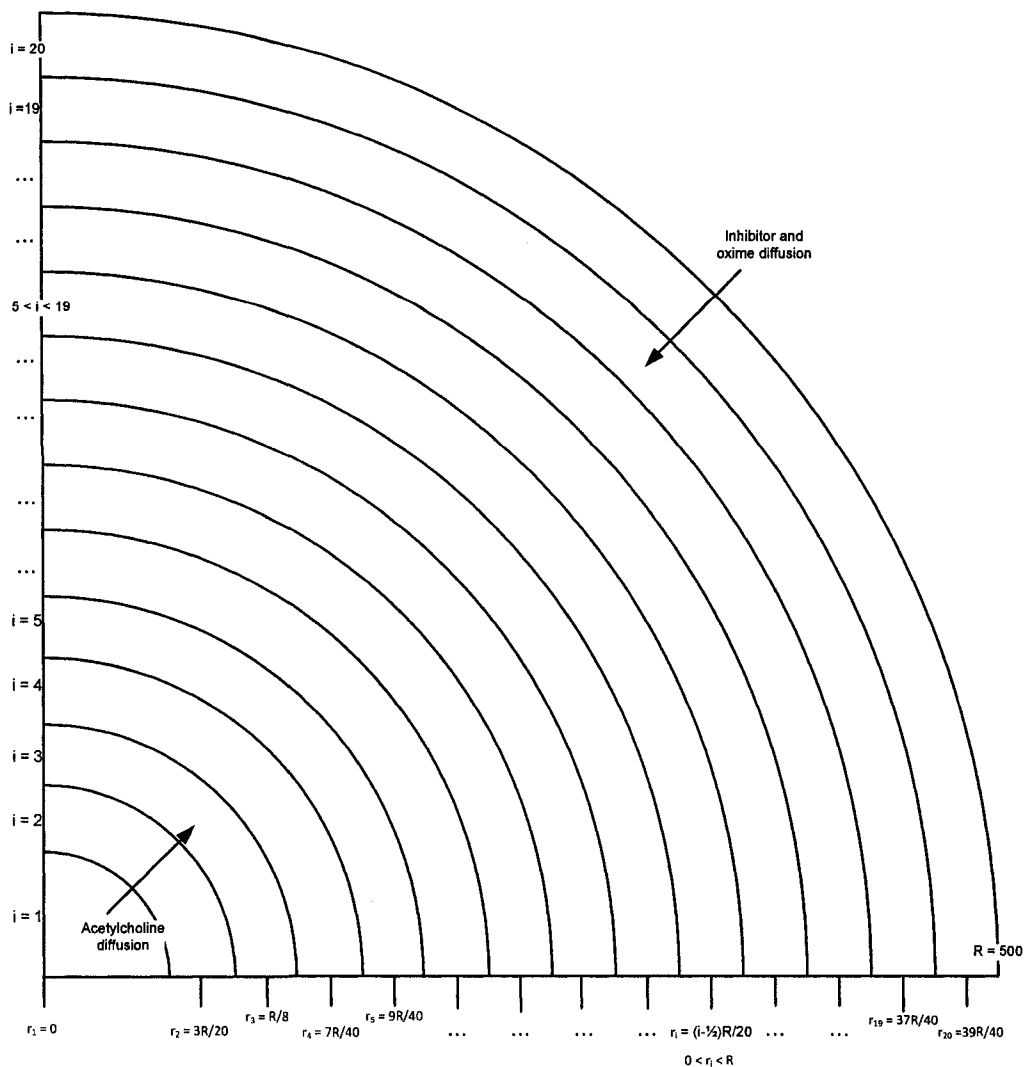


Figure 3.4. The relation between each annulus index and the corresponding location on the cleft radius.

The complexity of the symbols used for the chemical species would obscure the steps taken to transform the analytic equations into their respective numerical approximations, so the variables will be re-expressed in a more standard notation that is used in numerical calculations. The closer-to-standard notation should also provide a better interface between the numerical equations and conceptualizing the computer code that must be developed to compute those equations. The analytic PDE for the diffusion-

reaction of acetylcholine and the associated initial and boundary conditions is shown by Equation (3.31):

$$\frac{\partial[A(r,t)]}{\partial t} = D_A \frac{\partial^2[A(r,t)]}{\partial r^2} + D_A \frac{1}{r} \frac{\partial[A(r,t)]}{\partial r} - 2kR_1[A(r,t)][R] + kR_{-1}[A \cdot R] \quad (3.31)$$

$$-kR_2[A(r,t)][A \cdot R] + kR_{-2}[A_2 \cdot R^{closed}] - kE_1[A(r,t)][E] + kE_{-1}[A \cdot E]$$

$$[A(500,t)] = 0, \quad \forall t \geq 0$$

$$\frac{\partial[A(0,t)]}{\partial r} = 0, \quad \forall t \geq 0$$

$$[A(r,0)] = \begin{cases} 0.17 \text{ mmole/cm}^3 & 0 \leq r \leq 25nm \\ 0 & \text{otherwise} \end{cases}$$

Next, make the variable substitutions defined in (3.32)

$$\begin{aligned} [A(r,t)] &= U_1 & [A \cdot R] &= U_4 \\ [E] &= U_2 & [A_2 \cdot R^{closed}] &= U_5 \\ [R] &= U_3 & [A \cdot E] &= U_6 \end{aligned} \quad (3.32)$$

After substitution, Equation (3.30) now becomes Equation (3.33)

$$\frac{\partial U_1}{\partial t} = D_A \frac{\partial^2 U_1}{\partial r^2} + D_A \frac{1}{r} \frac{\partial U_1}{\partial r} - 2kR_1 U_1 U_3 + kR_{-1} U_4 - kR_2 U_1 U_4 + kR_{-2} U_5 \quad (3.33)$$

$$-kE_1 U_1 U_2 + kE_{-1} U_6$$

$$U_1(500,t) = 0, \quad \forall t \geq 0$$

$$\frac{\partial}{\partial r} U_1(0,t) = 0, \quad \forall t \geq 0$$

$$U_1(r,0) = \begin{cases} 0.17 \text{ mmole/cm}^3 & 0 \leq r \leq 25nm \\ 0 & \text{otherwise} \end{cases}$$

Now discretize Equation (3.33) via application of a standard central difference approximation to both the first and second partial derivative with respect to r . The result

is that the original PDE (3.33) is transformed into the general form of its numerical approximation, shown in Equation (3.34) below. This discretization “absorbs” the boundary conditions of (3.33) and they are processed when the index i is given numeric

$$\begin{aligned} \frac{d(U_1)_i}{dt} = & \frac{D_A}{(\Delta r)^2} [(U_1)_{i+1} - 2(U_1)_i + (U_1)_{i-1}] + \frac{D_A}{r_i(\Delta r)} [(U_1)_{i+1} - (U_1)_{i-1}] \quad (3.34) \\ & -2kR_1(U_1)_i(U_3)_i + kR_{-1}(U_4)_i - kR_2(U_1)_i(U_4)_i + kR_{-2}(U_5)_i \\ & -kE_1(U_1)_i(U_2)_i + kE_{-1}(U_6)_i \\ (U_1)_i(0) = & \begin{cases} 0.17 \frac{\text{mmole}}{\text{cm}^3} & i = 1 \\ 0 & i > 1 \end{cases} \end{aligned}$$

values. Discretizing the initial conditions of (3.33) requires applying the knowledge about the initial distribution of acetylcholine in the cleft with respect to position. The above equation represents the general expression a coupled system of ODEs that approximate the behavior of analytic Equation (3.33), where each i -subscript represents one of the enumerated sub-volumes. Each i -specific equation may differ from all the others depending on the boundary, mobility, location, and time-dependence of each species in the equation. For the system considered in this study, the ODEs in (3.34) are well behaved initial value equations. However, in the general case, the resulting coupled ODE system may contain boundary value equations, which do not use the same numerical solution algorithms as initial value equations. The particular equation associated with each index from $i = 1$, to $i = 20$ must now be determined.

The sub-volume at $i = 1$ represents the system being modeled at the system boundary at $r = 0$, and is the location where species A enters the cleft. Substitution of $i = 1$ into (3.34) gives the result:

$$\frac{d(U_1)_1}{dt} = \theta_A[(U_1)_2 - 2(U_1)_1 + (U_1)_0] + \frac{D_A}{r_1(\Delta r)} [(U_1)_2 - (U_1)_0] \quad (3.35)$$

$$-2kR_1(U_1)_1(U_3)_1 + kR_{-1}(U_4)_1 - kR_2(U_1)_1(U_4)_1 + kR_{-2}(U_5)_1$$

$$-kE_1(U_1)_1(U_2)_1 + kE_{-1}(U_6)_1$$

$$(U_1)_1(0) = 0.17 \frac{\text{mmole}}{\text{cm}^3}$$

$$\theta_A = \frac{D_A}{(\Delta r)^2}$$

As written, this equation presents two difficulties which may be unfamiliar to the non-specialist, and a detailed explanation of their resolution is beneficial. First, the term $\frac{D_A}{r_1(\Delta r)} [(U_1)_2 - (U_1)_0]$ contains an index where $i = 0$, when i was previously defined as strictly $1 \leq i \leq 20$. However, that term is an approximation of $\frac{\partial U_1}{\partial r}$ at $r = 0$, and the boundary condition in (3.33) stated that $\frac{\partial U_1}{\partial r} = 0$ at $r = 0$, thus $\frac{D_A}{r_1(\Delta r)} [(U_1)_2 - (U_1)_0] = 0$. Second, notice that the term $\theta_A[(U_1)_2 - 2(U_1)_1 + (U_1)_0]$ also contains an index where $i = 0$, but is not as easily resolved as the earlier, similar index. This index is an artifact of the numerical solution method, and is defined as a *ghost point*. The ghost point is resolved by using the boundary conditions to get a relationship between $(U_1)_0$ and the valid points in the system's physical domain. This can be done by using the given boundary condition and applying a central difference approximation about $i = 1$. To begin, relate the analytic boundary expression to its general central difference numerical analog:

$$\frac{\partial[A(r, t)]}{\partial r} \Big|_{r=0} = \frac{\partial(U_1)_i}{\partial r} \approx \frac{(U_1)_{i+1} - (U_1)_{i-1}}{2(\Delta r)} = 0 \quad (3.36)$$

Next, use algebra to relate the ghost point to a valid point in the physical domain of the system when $i = 1$:

$$\frac{(U_1)_2 - (U_1)_0}{2(\Delta r)} = 0 \quad (3.37)$$

$$(U_1)_2 - (U_1)_0 = 0 \quad (3.38)$$

$$(U_1)_0 = (U_1)_2 \quad (3.39)$$

The ghost point is now resolved. After substitution and algebraic manipulations, this leads to the computable specific equation for species A in sub-volume $i = 1$, given by (3.40):

$$\begin{aligned} \frac{d(U_1)_1}{dt} = & 2\theta_A[(U_1)_2 - (U_1)_1] - 2kR_1(U_1)_1(U_3)_1 + kR_{-1}(U_4)_1 \\ & - kR_2(U_1)_1(U_4)_1 + kR_{-2}(U_5)_1 - kE_1(U_1)_1(U_2)_1 + kE_{-1}(U_6)_1 \end{aligned} \quad (3.40)$$

$$(U_1)_1(0) = 0.17 \frac{\text{mmole}}{\text{cm}^3}$$

In the annular volumes $i = 2$ through $i = 19$, species A is transported into and out of each annulus and reacts with other chemical species. These volume elements are all mathematically similar and differ only by virtue of their index value, i . Therefore, for $i = 2, \dots, 19$, we represent for each of $d(U_1)_2/dt, d(U_1)_3/dt, \dots, d(U_1)_{19}/dt$, the entire set of equations and their associated initial conditions as follows:

$$\begin{aligned} \frac{d(U_1)_i}{dt} = & \theta_A[(U_1)_{i+1} - 2(U_1)_i + (U_1)_{i-1}] + \frac{D_A}{r_2(\Delta r)} [(U_1)_{i+1} - (U_1)_{i-1}] \quad (3.41) \\ & - 2kR_1(U_1)_i(U_3)_i + kR_{-1}(U_4)_i - kR_2(U_1)_i(U_4)_i + kR_{-2}(U_5)_i \\ & - kE_1(U_1)_i(U_2)_i + kE_{-1}(U_6)_i \end{aligned}$$

$$(U_1)_i(0) = 0$$

The sub-volume at $i = 20$ represents the system being modeled at the system boundary at $r = 25$ nm, and is the location where species A exits the cleft. Substitution of $i = 20$ into (3.41) gives the result:

$$\begin{aligned} \frac{d(U_1)_{20}}{dt} = & \theta_A[(U_1)_{21} - 2(U_1)_{20} + (U_1)_{19}] + \frac{D_A}{r_{20}(\Delta r)} [(U_1)_{21} - (U_1)_{19}] \\ & - 2kR_1(U_1)_{20}(U_3)_{20} + kR_{-1}(U_4)_{20} - kR_2(U_1)_{20}(U_4)_{20} + kR_{-2}(U_5)_{20} \\ & - kE_1(U_1)_{20}(U_2)_{20} + kE_{-1}(U_6)_{20} \\ (U_1)_{20}(0) = & 0 \end{aligned} \quad (3.42)$$

Another ghost point, $(U_1)_{21}$, appears twice in this equation. In this case, $(U_1)_{21}$ represents the concentration of species A outside the cleft and this quantity has been defined in the boundary condition of (3.33) as equal to zero. Since other molecular species can be outside the cleft and may have constant (or time dependent) concentrations other than zero, it will be useful to define a new symbol to represent a molecular species concentration in the environment outside the neuromuscular junction. Consequently, it is not complicated to attach a label, “inf”, to indicate some species concentration outside the cleft. Following this logic, define $(U_1)_{21} = A_{inf}$, where A_{inf} represents the concentration of species A outside the cleft. That ghost point is now resolved. The substitution of A_{inf} into (3.42) leads to the computable specific equation for species A in sub-volume $i = 20$, given by (3.43):

$$\begin{aligned} \frac{d(U_1)_{20}}{dt} = & \theta_A[A_{inf} - 2(U_1)_{20} + (U_1)_{19}] + \frac{D_A}{r_{20}(\Delta r)} [A_{inf} - (U_1)_{19}] \\ & - 2kR_1(U_1)_{20}(U_3)_{20} + kR_{-1}(U_4)_{20} - kR_2(U_1)_{20}(U_4)_{20} + kR_{-2}(U_5)_{20} \\ & - kE_1(U_1)_{20}(U_2)_{20} + kE_{-1}(U_6)_{20} \end{aligned} \quad (3.43)$$

$$(U_1)_{20}(0) = 0$$

This completes the derivation of the numerical equations that describe the diffusion-reaction of acetylcholine in the neuromuscular junction under normal conditions.

The analytic ODE for the reaction of acetylcholinesterase and the associated initial condition is shown by Equation (3.44):

$$\frac{d[E]}{dt} = -kE_1[A(r, t)][E] + kE_{-1}[A \cdot E] + kE_3[acE] \quad (3.44)$$

$$[E](0) = 0.845 \text{ mmole/cm}^3$$

Next, make the variable substitutions defined in (3.45)

$$\begin{aligned} [A(r, t)] &= U_1 & [E] &= U_2 \\ [A \cdot E] &= U_3 & [acE] &= U_7 \end{aligned} \quad (3.45)$$

After substitution, Equation (3.44) now becomes Equation (3.46)

$$\frac{dU_2}{dt} = -kE_1U_1U_2 + kE_{-1}U_6 + kE_3U_7 \quad (3.46)$$

$$U_2(0) = 0.845 \text{ mmole/cm}^3$$

Now prepare to discretize Equation (3.46) with respect to the space variable. This discretization process will require knowledge about the functional relation between the initial concentration of acetylcholinesterase and its position in the in the cleft neuromuscular junction. In other words, the relation $[E] = f(r)$ when $t = 0$ must be known, and this relation would then be applied to the discretized initial condition. Since the distribution of acetylcholinesterase in the junctional cleft is assumed to be uniform, then the discretization result is that the theoretical ODE and the initial condition merely become notationally compatible with the system of equations defined in (3.34) with no other changes, as shown below in (3.47):

$$\frac{d(U_2)_i}{dt} = -kE_1(U_1)_i(U_2)_i + kE_{-1}(U_6)_i + kE_3(U_7)_i \quad (3.47)$$

$$(U_2)_i(0) = 0.845 \text{ mmole/cm}^3$$

The above equation represents the general expression of a coupled system of ODEs that approximate the behavior of analytic Equation (3.46), where each i -subscript represents one of the enumerated sub-volumes. Acetylcholinesterase is known to be immobilized and distributed uniformly throughout the cleft; consequently, the volume elements designated by indices $i = 1$ through $i = 20$ are all mathematically similar and differ only by virtue of their index value, i . Therefore, for $i = 1, \dots, 20$, we represent for each of $d(U_2)_1/dt, d(U_2)_3/dt, \dots, d(U_2)_{20}/dt$, the entire set of equations and their associated initial conditions as follows:

$$\frac{d(U_2)_i}{dt} = -kE_1(U_1)_i(U_2)_i + kE_{-1}(U_6)_i + kE_3(U_7)_i \quad (3.48)$$

$$(U_2)_i(0) = 0.845 \text{ mmole/cm}^3$$

This finishes the derivation of the numerical equations which describe the reaction of acetylcholinesterase in the neuromuscular junction under normal conditions for the two representative species acetylcholine and acetylcholinesterase. Only two chemical species were derived in detail, but the same process could be used to develop the numerical equations for the remaining molecular species in the normal action potential reaction network.

To derive the reaction equations associated with the inhibited enzyme regime, and the enzyme regeneration regime, one would apply these same techniques and rules to every chemical species in the stoichiometric reaction network of each of those reaction regimes. For completeness, the stoichiometric reaction network, theoretical reaction

equations, and numerical reaction equations for all the chemical species in each reaction regime will be presented.

Normal action potential reaction regime:

Description:

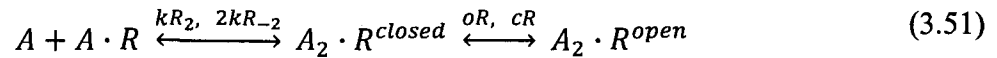
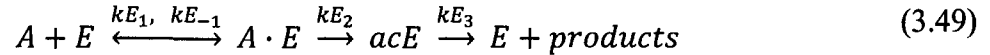
This regime consists of 20 sub-volume elements, 8 chemical species, and 10 separate kinetic reactions.

Mobile species: A

Immobile species: $E, A \cdot E, acE, R, A \cdot R, A_2 \cdot R^{closed}, A_2 \cdot R^{open}$

The initial concentration of A in the cleft is 0.17 mmole/cm^3 for $r \leq 25 \text{ nm}$, and the concentration of A outside the cleft is A_{inf} for all $t \geq 0$. Species E and R are uniformly distributed throughout the cleft with initial concentrations of 0.845 mmole/cm^3 and $0.000664 \text{ mmole/cm}^3$, respectively. All other species have initial concentrations of zero.

Stoichiometric reaction network:



Theoretical reaction equations:

$$\begin{aligned} \frac{\partial[A(r, t)]}{\partial t} = & D_A \frac{\partial^2[A(r, t)]}{\partial r^2} + D_A \frac{1}{r} \frac{\partial[A(r, t)]}{\partial r} - 2k_{R1}[A(r, t)][R] \\ & + k_{R-1}[A \cdot R] - k_{R2}[A(r, t)][A \cdot R] + k_{R-2}[A_2 \cdot R^{closed}] - k_{E1}[A(r, t)][E] \\ & + k_{E-1}[A \cdot E] \end{aligned} \quad (3.52)$$

$$[A(500, t)] = 0, \quad \forall t \geq 0$$

$$\frac{\partial[A(0, t)]}{\partial r} = 0, \quad \forall t \geq 0$$

$$[A(r, 0)] = \begin{cases} 0.17 \text{ mmole/cm}^3 & 0 \leq r \leq 25\text{nm} \\ 0 & \text{otherwise} \end{cases}$$

$$\frac{d[E]}{dt} = -kE_1[A(r, t)][E] + kE_{-1}[A \cdot E] + kE_3[acE] \quad (3.53)$$

$$[E](0) = 0.845 \text{ mmole/cm}^3$$

$$\frac{d[R]}{dt} = -2kR_1[A(r, t)][R] + kR_{-1}[A \cdot R] \quad (3.54)$$

$$[R](0) = 0.000664 \text{ mmole/cm}^3$$

$$\frac{d[A \cdot R]}{dt} = 2kR_1[A(r, t)][R] - kR_{-1}[A \cdot R] - kR_2[A(r, t)][A \cdot R] \quad (3.55)$$

$$+ 2kR_{-2}[A_2 \cdot R^{closed}]$$

$$[A \cdot R](0) = 0$$

$$\frac{d[A_2 \cdot R^{closed}]}{dt} = kR_2[A(r, t)][A \cdot R] - 2kR_{-2}[A_2 \cdot R^{closed}] \quad (3.56)$$

$$-oR[A_2 \cdot R^{closed}] + cR[A_2 \cdot R^{open}]$$

$$[A_2 \cdot R^{closed}](0) = 0$$

$$\frac{d[A \cdot E]}{dt} = kE_1[A(r, t)][E] - kE_{-1}[A \cdot E] - kE_2[A \cdot E] \quad (3.57)$$

$$[A \cdot E](0) = 0$$

$$\frac{d[acE]}{dt} = kE_2[A \cdot E] - kE_3[acE] \quad (3.58)$$

$$[acE](0) = 0$$

$$\frac{d[A_2 \cdot R^{open}]}{dt} = oR[A_2 \cdot R^{closed}] - cR[A_2 \cdot R^{open}] \quad (3.59)$$

$$[A_2 \cdot R^{open}](0) = 0$$

Change of variable definitions:

$$[A(r,t)] = U_1 \quad [A_2R^{closed}] = U_5 \quad (3.60)$$

$$[E] = U_2 \quad [A \cdot E] = U_6$$

$$[R] = U_3 \quad [acE] = U_7$$

$$[A \cdot R] = U_4 \quad [A_2 \cdot R^{open}] = U_8$$

Numerical reaction equations:

$$\frac{d(U_1)_1}{dt} = 2\theta_A[(U_1)_2 - (U_1)_1] - 2kR_1(U_1)_1(U_3)_1 + kR_{-1}(U_4)_1 \quad (3.61)$$

$$-kR_2(U_1)_1(U_4)_1 + kR_{-2}(U_5)_1 - kE_1(U_1)_1(U_2)_1 + kE_{-1}(U_6)_1$$

$$(U_1)_1(0) = 0.17 \frac{\text{mmole}}{\text{cm}^3}$$

For $i = 2, 3, 4, \dots, 19$

$$\frac{d(U_1)_i}{dt} = \theta_A[(U_1)_{i+1} - 2(U_1)_i + (U_1)_{i-1}] + \frac{D_A}{r_i(\Delta r)} [(U_1)_{i+1} - (U_1)_{i-1}] \quad (3.62)$$

$$\begin{aligned}
& -2kR_1(U_1)_i(U_3)_i + kR_{-1}(U_4)_i - kR_2(U_1)_i(U_4)_i + kR_{-2}(U_5)_i \\
& \quad -kE_1(U_1)_i(U_2)_i + kE_{-1}(U_6)_i \\
& \quad (U_1)_i(0) = 0
\end{aligned}$$

$$\frac{d(U_1)_{20}}{dt} = \theta_A [A_{inf} - 2(U_1)_{20} + (U_1)_{19}] + \frac{D_A}{r_{20}(\Delta r)} [A_{inf} - (U_1)_{19}] \quad (3.63)$$

$$\begin{aligned}
& -2kR_1(U_1)_{20}(U_3)_{20} + kR_{-1}(U_4)_{20} - kR_2(U_1)_{20}(U_4)_{20} + kR_{-2}(U_5)_{20} \\
& \quad -kE_1(U_1)_{20}(U_2)_{20} + kE_{-1}(U_6)_{20} \\
& \quad (U_1)_{20}(0) = 0
\end{aligned}$$

$$\frac{d(U_2)_i}{dt} = -kE_1(U_1)_i(U_2)_i + kE_{-1}(U_6)_i + kE_3(U_7)_i \quad (3.64)$$

$$(U_2)_i(0) = 0.845 \text{ mmole/cm}^3$$

For $i = 1, 2, 3, \dots, 20$

$$\frac{d(U_3)_1}{dt} = -2kR_1(U_1)_1(U_3)_1 + kR_{-1}(U_4)_1 \quad (3.65)$$

$$(U_3)_1(0) = 0.000664 \text{ mmole/cm}^3$$

For $i = 1, 2, 3, \dots, 20$

$$\frac{d(U_4)_1}{dt} = 2kR_1(U_1)_1(U_3)_1 - kR_{-1}(U_4)_1 - kR_2(U_1)_1(U_4)_1 - 2kR_{-2}(U_5)_1 \quad (3.66)$$

$$(U_4)_1(0) = 0$$

For $i = 1, 2, 3, \dots, 20$

$$\frac{d(U_5)_1}{dt} = kR_2(U_1)_1(U_4)_1 - 2kR_{-2}(U_5)_1 - oR(U_5)_1 + cR(U_8)_1 \quad (3.67)$$

$$(U_5)_1(0) = 0$$

For $i = 1, 2, 3, \dots, 20$

$$\frac{d(U_6)_1}{dt} = kE_1(U_1)_1(U_2)_1 - kE_{-1}(U_6)_1 - kE_2(U_6)_1 \quad (3.68)$$

$$(U_6)_1(0) = 0$$

For $i = 1, 2, 3, \dots, 20$

$$\frac{d(U_7)_1}{dt} = kE_2(U_6)_1 - kE_3(U_7)_1 \quad (3.69)$$

$$(U_7)_1(0) = 0$$

For $i = 1, 2, 3, \dots, 20$

$$\frac{d(U_8)_1}{dt} = oR(U_5)_1 - cR(U_8)_1 \quad (3.70)$$

$$(U_8)_1(0) = 0$$

The normal reaction regime produces a coupled numerical system comprised of 8 variables distributed among 160 ODEs.

Inhibited enzyme reaction regime:

Description:

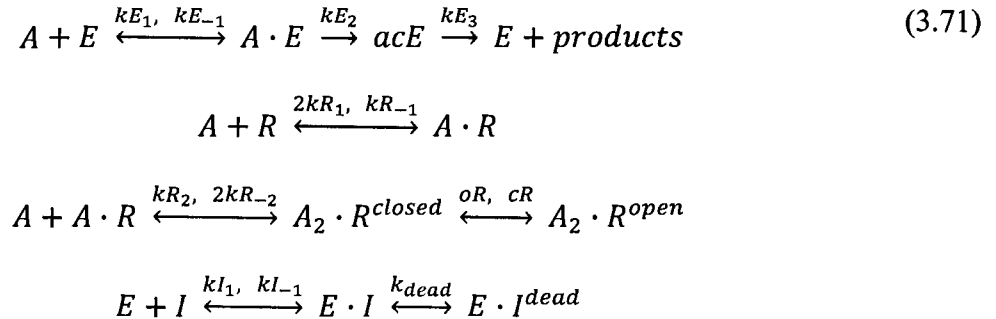
This regime consists of 20 sub-volume elements, 11 chemical species, 13 separate kinetic reactions,

Mobile species: A, I

Immobile species: $E, A \cdot E, acE, R, A \cdot R, A_2 \cdot R^{closed}, A_2 \cdot R^{open}, E \cdot I, E \cdot I^{dead}$

The initial concentration of A in the cleft is 0.17 mmole/cm^3 for $r \leq 25 \text{ nm}$, and the concentration of A outside the cleft is A_{inf} for all $t \geq 0$. Species E and R are uniformly distributed throughout the cleft with initial concentrations of 0.845 mmole/cm^3 and $0.000664 \text{ mmole/cm}^3$, respectively. The initial concentration of I in the cleft is zero, and the concentration of I outside the cleft is I_{inf} for all $t \geq 0$. All other species have initial concentrations of zero.

Stoichiometric reaction network:



Theoretical reaction equations:

$$\frac{\partial[A(r, t)]}{\partial t} = D_A \frac{\partial^2[A(r, t)]}{\partial r^2} + D_A \frac{1}{r} \frac{\partial[A(r, t)]}{\partial r} - 2kR_1[A(r, t)][R] \quad (3.72)$$

$$+kR_{-1}[A \cdot R] - kR_2[A(r, t)][A \cdot R] + kR_{-2}[A_2 \cdot R^{closed}] - kE_1[A(r, t)][E] \\ + kE_{-1}[A \cdot E]$$

$$[A(500, t)] = 0, \quad \forall t \geq 0$$

$$\frac{\partial[A(0, t)]}{\partial r} = 0, \quad \forall t \geq 0$$

$$[A(r, 0)] = \begin{cases} 0.17 \text{ mmole/cm}^3 & 0 \leq r \leq 25\text{nm} \\ 0 & \text{otherwise} \end{cases}$$

$$\frac{d[E]}{dt} = -kE_1[A(r, t)][E] + kE_{-1}[A \cdot E] + kE_3[acE] \quad (3.73)$$

$$[E](0) = 0.845 \text{ mmole/cm}^3$$

$$\frac{d[A \cdot E]}{dt} = kE_1[A(r, t)][E] - kE_{-1}[A \cdot E] - kE_2[A \cdot E] \quad (3.74)$$

$$[A \cdot E](0) = 0$$

$$\frac{d[acE]}{dt} = kE_2[A \cdot E] - kE_3[acE] \quad (3.75)$$

$$[acE](0) = 0$$

$$\frac{d[R]}{dt} = -2kR_1[A(r, t)][R] + kR_{-1}[A \cdot R] \quad (3.76)$$

$$[R](0) = 0.000664 \text{ mmole/cm}^3$$

$$\frac{d[A \cdot R]}{dt} = 2kR_1[A(r, t)][R] - kR_{-1}[A \cdot R] - kR_2[A(r, t)][A \cdot R] \quad (3.77)$$

$$+ 2kR_{-2}[A_2 \cdot R^{closed}]$$

$$[A \cdot R](0) = 0$$

$$\frac{d[A_2 \cdot R^{closed}]}{dt} = kR_2[A(r, t)][A \cdot R] - 2kR_{-2}[A_2 \cdot R^{closed}] \quad (3.78)$$

$$- oR[A_2 \cdot R^{closed}] + cR[A_2 \cdot R^{open}]$$

$$[A_2 \cdot R^{closed}](0) = 0$$

$$\frac{d[A_2 \cdot R^{open}]}{dt} = oR[A_2 \cdot R^{closed}] - cR[A_2 \cdot R^{open}] \quad (3.79)$$

$$[A_2 \cdot R^{open}](0) = 0$$

$$\frac{\partial[I(r, t)]}{\partial t} = D_I \frac{\partial^2[I(r, t)]}{\partial r^2} + D_I \frac{1}{r} \frac{\partial[I(r, t)]}{\partial r} - kI_1[E][I(r, t)] + kI_{-1}[E \cdot I] \quad (3.80)$$

$$[I(500, t)] = I_{inf}, \quad \forall t \geq 0$$

$$\frac{\partial[I(0, t)]}{\partial r} = 0, \quad \forall t \geq 0$$

$$[I(r, 0)] = \begin{cases} I_{inf} & r = 500 \text{ nm} \\ 0 & \text{otherwise} \end{cases}$$

$$\frac{d[E \cdot I]}{dt} = kI_1[E][I(r, t)] - kI_{-1}[E \cdot I] - k_{dead}[E \cdot I] \quad (3.81)$$

$$[E \cdot I](0) = 0$$

$$\frac{d[E \cdot I^{dead}]}{dt} = k_{dead}[E \cdot I] \quad (3.82)$$

$$[E \cdot I^{dead}](0) = 0$$

Change of variable definitions:

$$[A(r,t)] = U_1 \quad [E] = U_2 \quad (3.82)$$

$$[A \cdot E] = U_3 \quad [acE] = U_4$$

$$[R] = U_5 \quad [A \cdot R] = U_6$$

$$[A_2 \cdot R^{closed}] = U_7 \quad [A_2 \cdot R^{open}] = U_8$$

$$[I(r,t)] = U_9 \quad [E \cdot I] = U_{10}$$

$$[E \cdot I^{dead}] = U_{11}$$

Numerical reaction equations:

$$\frac{d(U_1)_1}{dt} = 2\theta_A[(U_1)_2 - (U_1)_1] - 2kR_1(U_1)_1(U_3)_1 + kR_{-1}(U_4)_1 \quad (3.83)$$

$$-kR_2(U_1)_1(U_4)_1 + kR_{-2}(U_5)_1 - kE_1(U_1)_1(U_2)_1 + kE_{-1}(U_6)_1$$

$$(U_1)_1(0) = 0.17 \frac{\text{mmole}}{\text{cm}^3}$$

For $i = 2, 3, 4, \dots, 19$

$$\frac{d(U_1)_i}{dt} = \theta_A[(U_1)_{i+1} - 2(U_1)_i + (U_1)_{i-1}] + \frac{D_A}{r_i(\Delta r)} [(U_1)_{i+1} - (U_1)_{i-1}] \quad (3.84)$$

$$-2kR_1(U_1)_i(U_3)_i + kR_{-1}(U_4)_i - kR_2(U_1)_i(U_4)_i + kR_{-2}(U_5)_i$$

$$-kE_1(U_1)_i(U_2)_i + kE_{-1}(U_6)_i$$

$$(U_1)_i(0) = 0$$

$$\begin{aligned} \frac{d(U_1)_{20}}{dt} &= \theta_A [A_{inf} - 2(U_1)_{20} + (U_1)_{19}] + \frac{D_A}{r_{20}(\Delta r)} [A_{inf} - (U_1)_{19}] \\ &\quad - 2kR_1(U_1)_{20}(U_3)_{20} + kR_{-1}(U_4)_{20} - kR_2(U_1)_{20}(U_4)_{20} \\ &\quad + kR_{-2}(U_5)_{20} - kE_1(U_1)_{20}(U_2)_{20} + kE_{-1}(U_6)_{20} \\ (U_1)_{20}(0) &= 0 \end{aligned} \quad (3.85)$$

For $i = 1, 2, 3, \dots, 20$

$$\begin{aligned} \frac{d(U_2)_i}{dt} &= -kE_1(U_1)_i(U_2)_i + kE_{-1}(U_6)_i + kE_3(U_7)_i \\ (U_2)_i(0) &= 0.845 \text{ mmole/cm}^3 \end{aligned} \quad (3.86)$$

For $i = 1, 2, 3, \dots, 20$

$$\begin{aligned} \frac{d(U_3)_i}{dt} &= kE_1(U_1)_i(U_2)_i - kE_{-1}(U_3)_i - kE_2(U_3)_i \\ (U_3)_i(0) &= 0 \end{aligned} \quad (3.87)$$

For $i = 1, 2, 3, \dots, 20$

$$\begin{aligned} \frac{d(U_4)_i}{dt} &= kE_2(U_3)_i - kE_3(U_4)_i \\ (U_4)_i(0) &= 0 \end{aligned} \quad (3.88)$$

For $i = 1, 2, 3, \dots, 20$

$$\frac{d(U_5)_i}{dt} = -2kR_1(U_1)_i(U_5)_i + kR_{-1}(U_6)_i \quad (3.89)$$

$$(U_5)_i(0) = 0.000664 \text{ mmole/cm}^3$$

For $i = 1, 2, 3, \dots, 20$

$$\frac{d(U_6)_i}{dt} = 2kR_1(U_1)_i(U_5)_i - kR_{-1}(U_6)_i - kR_2(U_1)_i(U_6)_i - 2kR_{-2}(U_7)_i \quad (3.90)$$

$$(U_6)_i(0) = 0$$

For $i = 1, 2, 3, \dots, 20$

$$\frac{d(U_7)_i}{dt} = kR_2(U_1)_i(U_6)_i - 2kR_{-2}(U_7)_i - oR(U_7)_i + cR(U_8)_i \quad (3.91)$$

$$(U_7)_i(0) = 0$$

For $i = 1, 2, 3, \dots, 20$

$$\frac{d(U_8)_i}{dt} = oR(U_7)_i - cR(U_8)_i \quad (3.92)$$

$$(U_8)_i(0) = 0$$

$$\frac{d(U_9)_1}{dt} = 2\theta_I[(U_9)_2 - (U_9)_1] - kI_1(U_2)_1(U_9)_1 + kI_{-1}(U_{10})_1 \quad (3.93)$$

$$(U_9)_1(0) = 0$$

For $i = 2, 3, 4, \dots, 19$

$$\frac{d(U_9)_i}{dt} = \theta_I[(U_9)_{i+1} - 2(U_9)_i + (U_9)_{i-1}] + \frac{D_I}{r_i(\Delta r)} [(U_9)_{i+1} - (U_9)_{i-1}] \quad (3.94)$$

$$-kI_1(U_2)_i(U_9)_i + kI_{-1}(U_{10})_i$$

$$(U_9)_i(0) = 0$$

$$\begin{aligned} \frac{d(U_9)_{20}}{dt} &= \theta_I [I_{inf} - 2(U_9)_{20} + (U_9)_{19}] + \frac{D_I}{r_{20}(\Delta r)} [I_{inf} - (U_9)_{19}] \\ &\quad - k_{I_1}(U_2)_{20}(U_9)_{20} + k_{I_{-1}}(U_{10})_{20} \\ (U_9)_{20}(0) &= 0 \end{aligned} \quad (3.95)$$

For $i = 1, 2, 3, \dots, 20$

$$\begin{aligned} \frac{d(U_{10})_i}{dt} &= k_{I_1}(U_2)_i(U_9)_i - k_{I_{-1}}(U_{10})_i - k_{dead}(U_{10})_i \\ (U_{10})_i(0) &= 0 \end{aligned} \quad (3.96)$$

For $i = 1, 2, 3, \dots, 20$

$$\begin{aligned} \frac{d(U_{11})_i}{dt} &= k_{dead}(U_{10})_i \\ (U_{11})_i(0) &= 0 \end{aligned} \quad (3.97)$$

The inhibited enzyme reaction regime produces a coupled numerical system comprised of 11 variables distributed among 220 ODEs.

Enzyme regeneration reaction regime:

Description:

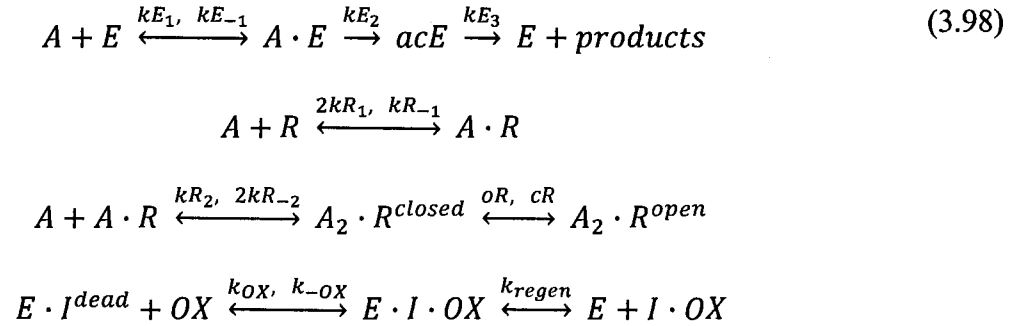
This regime consists of 20 sub-volume elements, 12 chemical species, 13 separate kinetic reactions,

Mobile species: A , OX , $I \cdot OX$

Immobile species: E , $A \cdot E$, acE , R , $A \cdot R$, $A_2 \cdot R^{closed}$, $A_2 \cdot R^{open}$, $E \cdot I$, $E \cdot I^{dead}$

The initial concentration of A in the cleft is 0.17 mmole/cm^3 for $r \leq 25 \text{ nm}$, and the concentration of A outside the cleft is A_{inf} for all $t \geq 0$. Species $E \cdot I^{dead}$ and R are uniformly distributed throughout the cleft with initial concentrations of 0.845 mmole/cm^3 and $0.000664 \text{ mmole/cm}^3$, respectively. The initial concentration of OX and $I \cdot OX$ in the cleft is zero, and the concentration of OX and $I \cdot OX$ outside the cleft is OX_{inf} and $I \cdot OX_{inf}$ for all $t \geq 0$. All other species have initial concentrations of zero.

Stoichiometric reaction network:



Theoretical reaction equations:

$$\begin{aligned}
 \frac{\partial[A(r,t)]}{\partial t} &= D_A \frac{\partial^2[A(r,t)]}{\partial r^2} + D_A \frac{1}{r} \frac{\partial[A(r,t)]}{\partial r} - 2k_{R1}[A(r,t)][R] & (3.99) \\
 &+ k_{R-1}[A \cdot R] - k_{R2}[A(r,t)][A \cdot R] + k_{R-2}[A_2 \cdot R^{closed}]
 \end{aligned}$$

$$-kE_1[A(r,t)][E] + kE_{-1}[A \cdot E]$$

$$[A(500,t)] = 0, \quad \forall t \geq 0$$

$$\frac{\partial[A(0,t)]}{\partial r} = 0, \quad \forall t \geq 0$$

$$[A(r,0)] = \begin{cases} 0.17 \text{ mmole/cm}^3 & 0 \leq r \leq 25\text{nm} \\ 0 & \text{otherwise} \end{cases}$$

$$\frac{d[E]}{dt} = -kE_1[A(r,t)][E] + kE_{-1}[A \cdot E] + kE_3[acE] + k_{regen}[E \cdot I \cdot OX] \quad (3.100)$$

$$[E](0) = 0$$

$$\frac{d[A \cdot E]}{dt} = kE_1[A(r,t)][E] - kE_{-1}[A \cdot E] - kE_2[A \cdot E] \quad (3.101)$$

$$[A \cdot E](0) = 0$$

$$\frac{d[acE]}{dt} = kE_2[A \cdot E] - kE_3[acE] \quad (3.102)$$

$$[acE](0) = 0$$

$$\frac{d[R]}{dt} = -2kR_1[A(r,t)][R] + kR_{-1}[A \cdot R] \quad (3.103)$$

$$[R](0) = 0.000664 \text{ mmole/cm}^3$$

$$\frac{d[A \cdot R]}{dt} = 2kR_1[A(r, t)][R] - kR_{-1}[A \cdot R] - kR_2[A(r, t)][A \cdot R] \quad (3.104)$$

$$+ 2kR_{-2}[A_2 \cdot R^{closed}]$$

$$[A \cdot R](0) = 0$$

$$\frac{d[A_2 \cdot R^{closed}]}{dt} = kR_2[A(r, t)][A \cdot R] - 2kR_{-2}[A_2 \cdot R^{closed}] \quad (3.105)$$

$$-oR[A_2 \cdot R^{closed}] + cR[A_2 \cdot R^{open}]$$

$$[A_2 \cdot R^{closed}](0) = 0$$

$$\frac{d[A_2 \cdot R^{open}]}{dt} = oR[A_2 \cdot R^{closed}] - cR[A_2 \cdot R^{open}] \quad (3.106)$$

$$[A_2 \cdot R^{open}](0) = 0$$

$$\frac{d[E \cdot I^{dead}]}{dt} = -k_{OX}[E \cdot I^{dead}][OX(r, t)] + k_{-OX}[E \cdot I \cdot OX] \quad (3.107)$$

$$[E \cdot I^{dead}](0) = 0.845 \text{ mmole/cm}^3$$

$$\frac{\partial[OX(r, t)]}{\partial t} = D_{ox} \frac{\partial^2[OX(r, t)]}{\partial r^2} + D_{ox} \frac{1}{r} \frac{\partial[OX(r, t)]}{\partial r} \quad (3.108)$$

$$-k_{ox}[E \cdot I^{dead}][OX(r, t)] + k_{-ox}[E \cdot I \cdot OX]$$

$$[OX(500, t)] = OX_{inf}, \quad \forall t \geq 0$$

$$\frac{\partial[OX(0, t)]}{\partial r} = 0, \quad \forall t \geq 0$$

$$[OX(r, 0)] = \begin{cases} OX_{inf} & r = 500 \text{ nm} \\ 0 & \text{otherwise} \end{cases}$$

$$\frac{d[E \cdot I \cdot OX]}{dt} = k_{ox}[E \cdot I^{dead}][OX(r, t)] - k_{-ox}[E \cdot I \cdot OX] \quad (3.109)$$

$$-k_{regen}[E \cdot I \cdot OX]$$

$$[E \cdot I \cdot OX](0) = 0$$

$$\frac{\partial[I \cdot OX(r, t)]}{\partial t} = D_{I \cdot ox} \frac{\partial^2[I \cdot OX(r, t)]}{\partial r^2} + D_{I \cdot ox} \frac{1}{r} \frac{\partial[I \cdot OX(r, t)]}{\partial r} \quad (3.110)$$

$$+k_{regen}[E \cdot I \cdot OX]$$

$$[I \cdot OX(500, t)] = I \cdot OX_{*inf}, \quad \forall t \geq 0$$

$$\frac{\partial[I \cdot OX(0, t)]}{\partial t} = 0, \quad \forall t \geq 0$$

$$[I \cdot OX(r, 0)] = \begin{cases} I \cdot OX_{inf} & r = 500 \text{ nm} \\ 0 & \text{otherwise} \end{cases}$$

Change of variable definitions:

$$\begin{aligned}
 [A(r,t)] &= U_1 & [E] &= U_2 & (3.111) \\
 [A \cdot E] &= U_3 & [acE] &= U_4 \\
 [R] &= U_5 & [A \cdot R] &= U_6 \\
 [A_2 \cdot R^{closed}] &= U_7 & [A_2 \cdot R^{open}] &= U_8 \\
 [E \cdot I^{dead}] &= U_9 & [OX(r,t)] &= U_{10} \\
 [E \cdot I \cdot OX] &= U_{11} & [I \cdot OX(r,t)] &= U_{12}
 \end{aligned}$$

Numerical reaction equations:

$$\begin{aligned}
 \frac{d(U_1)_1}{dt} &= 2\theta_A[(U_1)_2 - (U_1)_1] - 2kR_1(U_1)_1(U_3)_1 + kR_{-1}(U_4)_1 & (3.112) \\
 &- kR_2(U_1)_1(U_4)_1 + kR_{-2}(U_5)_1 - kE_1(U_1)_1(U_2)_1 + kE_{-1}(U_6)_1 \\
 (U_1)_1(0) &= 0.17 \frac{\text{mmole}}{\text{cm}^3}
 \end{aligned}$$

For $i = 2, 3, 4, \dots, 19$

$$\begin{aligned}
 \frac{d(U_1)_i}{dt} &= \theta_A[(U_1)_{i+1} - 2(U_1)_i + (U_1)_{i-1}] + \frac{D_A}{r_i(\Delta r)} [(U_1)_{i+1} - (U_1)_{i-1}] & (3.113) \\
 &- 2kR_1(U_1)_i(U_3)_i + kR_{-1}(U_4)_i - kR_2(U_1)_i(U_4)_i + kR_{-2}(U_5)_i \\
 &- kE_1(U_1)_i(U_2)_i + kE_{-1}(U_6)_i \\
 (U_1)_i(0) &= 0
 \end{aligned}$$

$$\begin{aligned} \frac{d(U_1)_{20}}{dt} &= \theta_A [A_{inf} - 2(U_1)_{20} + (U_1)_{19}] + \frac{D_A}{r_{20}(\Delta r)} [A_{inf} - (U_1)_{19}] \\ &- 2kR_1(U_1)_{20}(U_3)_{20} + kR_{-1}(U_4)_{20} - kR_2(U_1)_{20}(U_4)_{20} + kR_{-2}(U_5)_{20} \\ &- kE_1(U_1)_{20}(U_2)_{20} + kE_{-1}(U_6)_{20} \\ (U_1)_{20}(0) &= 0 \end{aligned} \quad (3.114)$$

For $i = 1, 2, 3, \dots, 20$

$$\begin{aligned} \frac{d(U_2)_i}{dt} &= -kE_1(U_1)_i(U_2)_i + kE_{-1}(U_6)_i + kE_3(U_7)_i + k_{regen}(U_{11})_i \\ (U_2)_i(0) &= 0 \end{aligned} \quad (3.115)$$

For $i = 1, 2, 3, \dots, 20$

$$\begin{aligned} \frac{d(U_3)_i}{dt} &= kE_1(U_1)_i(U_2)_i - kE_{-1}(U_3)_i - kE_2(U_3)_i \\ (U_3)_i(0) &= 0 \end{aligned} \quad (3.116)$$

For $i = 1, 2, 3, \dots, 20$

$$\begin{aligned} \frac{d(U_4)_i}{dt} &= kE_2(U_3)_i - kE_3(U_4)_i \\ (U_4)_i(0) &= 0 \end{aligned} \quad (3.117)$$

For $i = 1, 2, 3, \dots, 20$

$$\begin{aligned} \frac{d(U_5)_i}{dt} &= -2kR_1(U_1)_i(U_5)_i + kR_{-1}(U_6)_i \\ (U_5)_i(0) &= 0.000664 \text{ mmole/cm}^3 \end{aligned} \quad (3.118)$$

For $i = 1, 2, 3, \dots, 20$

$$\frac{d(U_6)_i}{dt} = 2kR_1(U_1)_i(U_5)_i - kR_{-1}(U_6)_i - kR_2(U_1)_i(U_6)_i - 2kR_{-2}(U_7)_i \quad (3.119)$$

$$(U_6)_i(0) = 0$$

For $i = 1, 2, 3, \dots, 20$

$$\frac{d(U_7)_i}{dt} = kR_2(U_1)_i(U_6)_i - 2kR_{-2}(U_7)_i - oR(U_7)_i + cR(U_8)_i \quad (3.120)$$

$$(U_7)_i(0) = 0$$

For $i = 1, 2, 3, \dots, 20$

$$\frac{d(U_8)_i}{dt} = oR(U_7)_i - cR(U_8)_i \quad (3.121)$$

$$(U_8)_i(0) = 0$$

For $i = 1, 2, 3, \dots, 20$

$$\frac{d(U_9)_i}{dt} = -k_{ox}(U_9)_i(U_{10})_i + k_{-ox}(U_{11})_i \quad (3.122)$$

$$(U_9)_i = 0.845 \text{ mmole/cm}^3$$

$$\frac{d(U_{10})_1}{dt} = 2\theta_{ox}[(U_{10})_2 - (U_{10})_1] - k_{ox}(U_9)_1(U_{10})_1 + k_{-ox}(U_{11})_1 \quad (3.123)$$

$$(U_{10})_1(0) = 0$$

For $i = 2, 3, 4, \dots, 19$

$$\begin{aligned} \frac{d(U_{10})_i}{dt} &= \theta_{ox}[(U_{10})_{i+1} - 2(U_{10})_i + (U_{10})_{i-1}] \\ &+ \frac{D_{ox}}{r_i(\Delta r)} [(U_{10})_{i+1} - (U_{10})_{i-1}] - k_{ox}(U_9)_i(U_{10})_i + k_{-ox}(U_{11})_i \\ (U_{10})_i(0) &= 0 \end{aligned} \quad (3.124)$$

$$\begin{aligned} \frac{d(U_{10})_{20}}{dt} &= \theta_{ox}[OX_{inf} - 2(U_{10})_{20} + (U_{10})_{19}] \\ &+ \frac{D_{ox}}{r_{20}(\Delta r)} [OX_{inf} - (U_{10})_{19}] - k_{ox}(U_9)_{20}(U_{10})_{20} + k_{-ox}(U_{11})_{20} \\ (U_{10})_{20}(0) &= 0 \end{aligned} \quad (3.125)$$

For $i = 1, 2, 3, \dots, 20$

$$\begin{aligned} \frac{d(U_{11})_i}{dt} &= k_{ox}(U_9)_i(U_{10})_i - k_{-ox}(U_{11})_i - k_{regen}(U_{11})_i \\ (U_{11})_i(0) &= 0 \end{aligned} \quad (3.126)$$

$$\begin{aligned} \frac{d(U_{12})_1}{dt} &= 2\theta_{1,ox}[(U_{12})_2 - (U_{12})_1] + k_{regen}(U_{11})_1 \\ (U_{12})_1(0) &= 0 \end{aligned} \quad (3.127)$$

For $i = 2, 3, 4, \dots, 19$

$$\begin{aligned} \frac{d(U_{12})_i}{dt} &= \theta_{I \cdot OX} [(U_{12})_{i+1} - 2(U_{12})_i + (U_{12})_{i-1}] \\ &+ \frac{D_{I \cdot OX}}{r_i(\Delta r)} [(U_{12})_{i+1} - (U_{12})_{i-1}] + k_{regen}(U_{11})_i \end{aligned} \quad (3.128)$$

$$(U_{12})_2(0) = 0$$

$$\begin{aligned} \frac{d(U_{12})_{20}}{dt} &= \theta_{I \cdot OX} [I \cdot OX_{inf} - 2(U_{12})_{20} + (U_{12})_{19}] \\ &+ \frac{D_{I \cdot OX}}{r_{20}(\Delta r)} [I \cdot OX_{inf} - (U_{12})_{19}] + k_{regen}(U_{11})_{20} \end{aligned} \quad (3.129)$$

$$(U_{12})_{20}(0) = 0$$

The enzyme regeneration reaction regime produces a coupled numerical system comprised of 12 variables distributed among 240 ODEs.

This completes the derivation of the numerical equations which describe the reaction of all the molecular species in the neuromuscular junction during the three reaction regimes. The same procedure would produce the computable numerical equations for any known or postulated reaction network. Assumption of mass-action dynamics greatly simplifies deriving the differential kinetic equations, and it is a valid first assumption for simple reactions. However, kinetics which does not follow mass-action dynamics is also common, especially with stoichiometrically complex reactions. Therefore, all kinetic expressions should be supported and verified with experimental data. All the kinetic expressions written in this model have been verified by experiment, predominantly *in vitro*. There are also some investigations supported by *in vivo*

experiments ([3], [4], [7], [66]-[68]). That endeavor is presently much more difficult and provides one of the reasons why description of the molecular transport and reaction events occurring in the neuromuscular junction depends heavily on mathematical models.

CHAPTER 4

MEASUREMENTS AND MODELS OF

PRIOR INVESTIGATIONS

There is substantial literature describing and modeling all the chemical reactions in the neuromuscular cleft, along with incorporation of the transport effects [3]-[5], [18]-[21], [57], [58], [66]. While many investigators have examined the reactions of acetylcholine with acetylcholinesterase, acetylcholine with its receptor, and *in vitro* inhibition of acetylcholinesterase and acetylcholine, the Jenkins-Szlavik model is the first attempt to model the simultaneous reaction-diffusion dynamics of acetylcholine, receptor, acetylcholinesterase, and a mobile acetylcholinesterase inhibitor, in an *in vivo* environment. This work shall also demonstrate a novel model of the reaction-diffusion kinetics of *in vivo* reactivation of inhibited acetylcholinesterase via exposure to oxime species diffusing into the cleft. In addition, this model shows that cleft-averaged receptor kinetics is valid at the time scales of interest because the receptors always show uniform conformation states across the entire post-synaptic membrane during the action potential regardless of the degree of enzyme inhibition.

Figure 4.1, from Miledi [9], shows the results of experimentally measured end-plate currents from the frog neuromuscular junction. Part A shows the response when

approximately five acetylcholine quanta were released into the cleft from a Ca^{+2} filled pipette, in a region restricted close to the pipette tip. Part B shows the response for a release of five to eighteen quanta diffusely scattered across the entire end-plate, and part C depicts the result when about 300 quanta are released over the entire end-plate area. The arrow in each picture represents the half-decline time of each event.

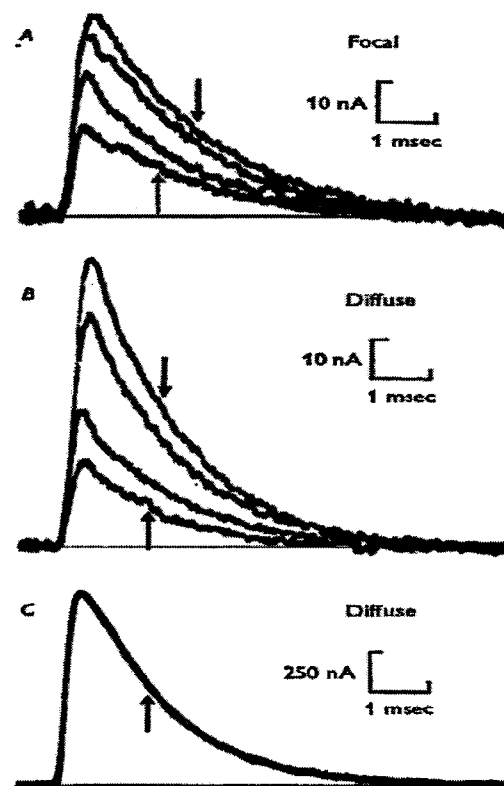


Figure 4.1. Post-synaptic potentiation: interaction between quanta of acetylcholine at the skeletal neuromuscular synapse [9].

Figure 4.2 depicts experimental measurements from the same investigators for the response of increasing doses of acetylcholine applied iontophoretically onto the motor end-plate [9]. A 0.5 ms acetylcholine pulse was varied in amplitude, and the circle on

each falling phase marks the half-decline time. This time is progressively prolonged with increasing peak amplitude because of potentiation. These pictures show the general shape of the amplitude vs. time course of the end-plate current, and that there is little difference in the time course of the end-plate currents generated by one or many acetylcholine quanta under normal physiological conditions [3] - [10]. Since the end-plate current is directly proportional to the conductivity of an acetylcholine receptor, the time course of an end-plate current should have the same shape as the time course of the number of conducting (open) acetylcholine receptors under “clamped” voltage conditions, differing only by some scaling factor. The Jenkins-Szlavik model was concerned with simulating the transport and chemical reaction events in the neuromuscular junction, so the population vs. time course of open receptors was a natural product of the calculations.

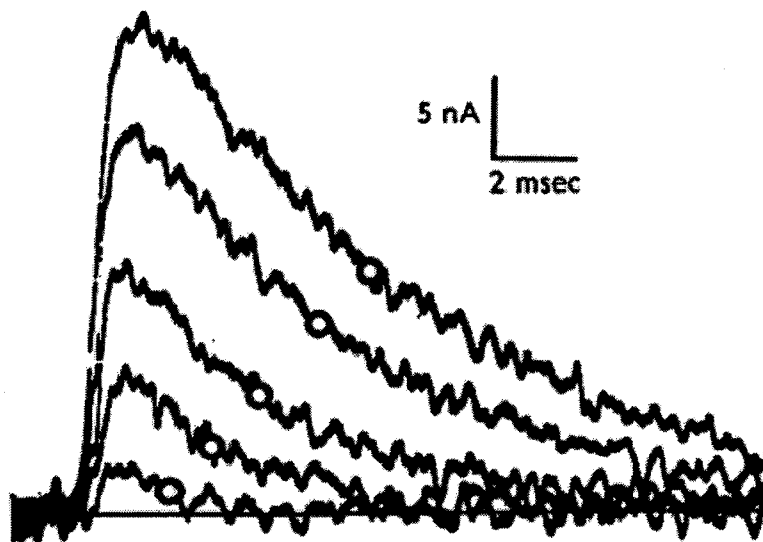


Figure 4.2. Post-synaptic potentiation: interaction between quanta of acetylcholine at the skeletal neuromuscular synapse [9].

The effect of acetylcholinesterase inhibition on the end-plate current is of great importance, and it has been investigated through experiment and simulation by several researchers. Miledi [10], as shown in Figure 4.3, measured the inhibition effect of several enzyme inhibitors during an end-plate current event on skeletal frog muscle.

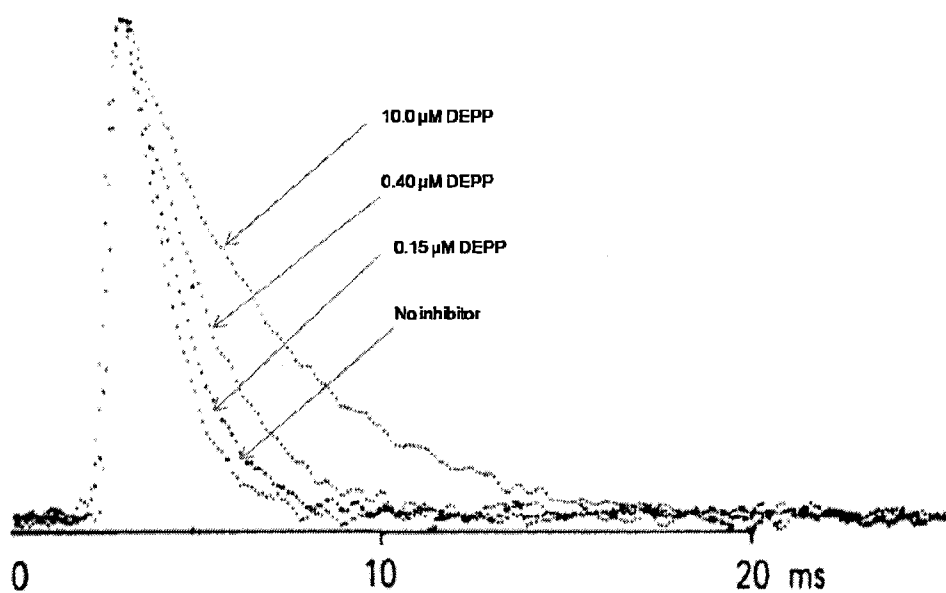


Figure 4.3. Computer averaged end-plate currents showing the increasing decay time with increasing exposure to acetylcholinesterase inhibitors [10].

Friboulet [57] and Naka [58], shown in Figures 4.4 and 4.5, respectively, also simulated the effect of acetylcholinesterase inhibition directly on the population of open receptors with time. These two models are in good agreement with each other and experimental measurements. There have been many such simulations in the last three decades, [3]-[8], [18]-[21], but these are two of the latest and each has excellent clarity. Most of the others have been overtaken by the advancement of experimental technique

and computing resources. For example, Wathey [18] developed a simulation that used sophisticated mathematical and numerical techniques which were implemented to compensate for the low capacity (and expense) of the computer memory available in 1979.

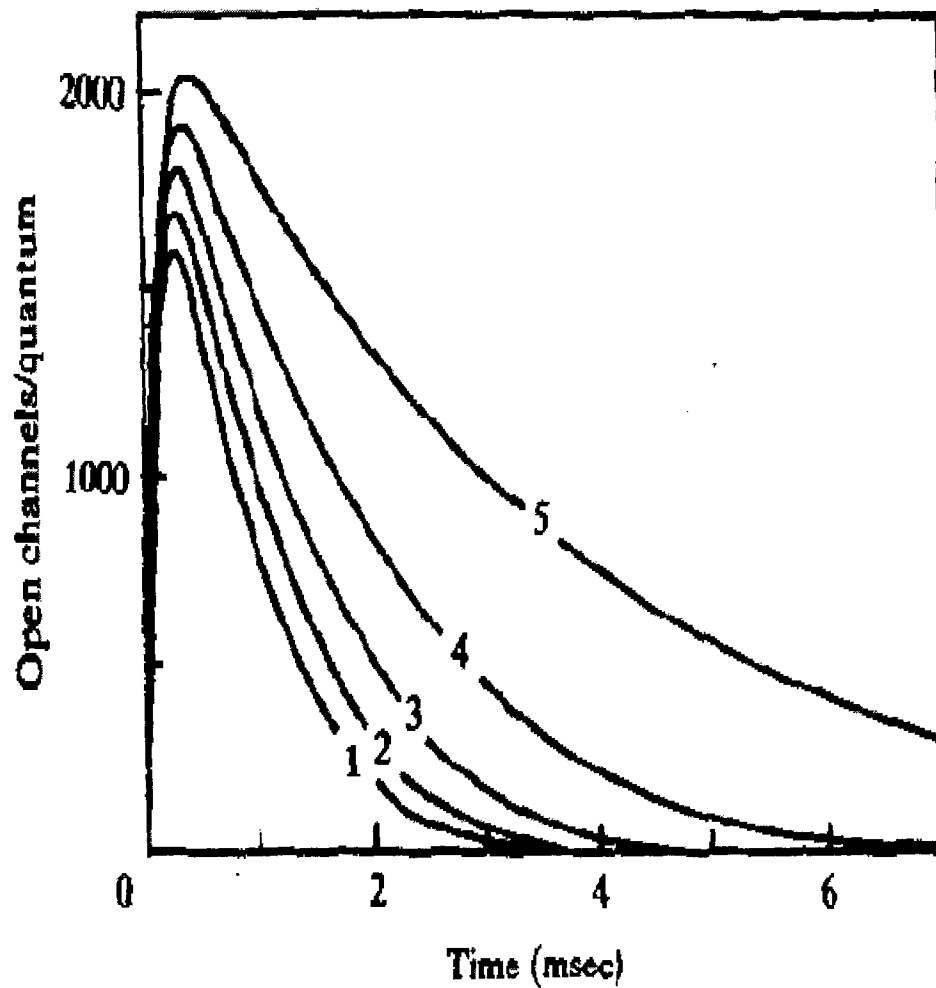


Figure 4.4. The number of open receptors per acetylcholine quantum from Friboulet's simulation [57].

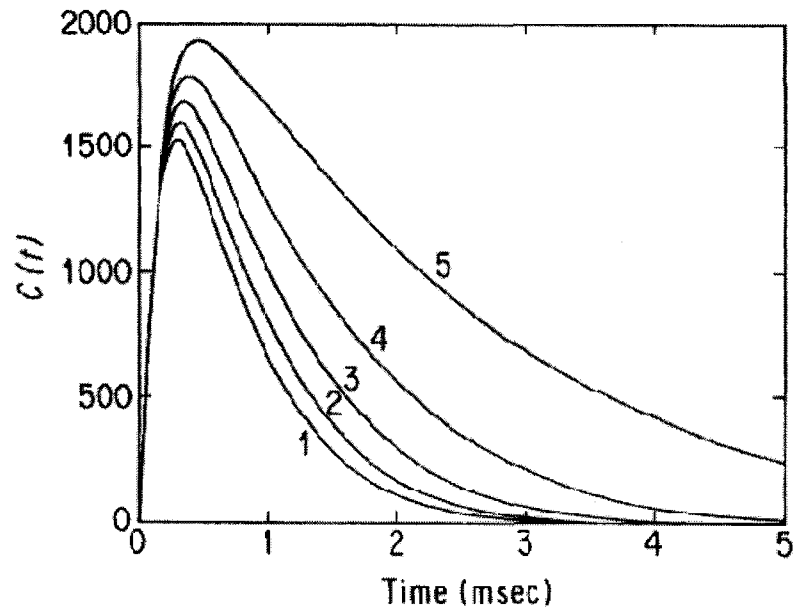


Figure 4.5. The number of open receptors per acetylcholine quantum from Naka's simulation [52].

The diffusion constant of acetylcholine is a critical parameter in every simulation of the neuromuscular junction. Friboulet used a diffusion coefficient of $2.0 \cdot 10^{-9} \text{ cm}^2/\text{ms}$, Naka [58] used diffusion coefficients in the range: $2.5 \cdot 10^{-10} \sim 4.0 \cdot 10^{-9} \text{ (cm}^2/\text{ms)}$ in the development of their model, Wathey [18] used a value of $3.0 \cdot 10^{-9} \text{ cm}^2/\text{ms}$, Madsen [19] used $4.0 \cdot 10^{-9} \text{ cm}^2/\text{ms}$, and the diffusivities used by Tsoukaias [69] were valued at greater than $3.0 \cdot 10^{-9} \text{ cm}^2/\text{ms}$. Diffusion constants in biological tissue are especially difficult to measure quantitatively [48], [69]-[71], so differences in the published values for the diffusion constant is expected.

While the time course of a normal action potential is not sensitive to the amount of acetylcholine present, these data show that the degree of acetylcholinesterase activity can drastically alter the time and magnitude profile of an action potential. Regarding the degree of enzyme activity, note that all of these investigators have addressed

acetylcholinesterase inhibition either with *in vitro* chemical kinetics, or via a “blanket” degree of defined inactivity in cleft simulation calculations [6], [10], [21], [24], [57], [58]. While those methods of enzyme inhibition are serviceable ways to investigate acetylcholine kinetics, they are also artificial and not versatile. A model in which the enzyme inhibition emerged from the coupled kinetics of acetylcholine, neurotoxin, and acetylcholinesterase would provide more insight and greater resolution in simulations of the neuromuscular junction.

CHAPTER 5

RESULTS AND DISCUSSION

For the Jenkins-Szlavik simulation being presented in this dissertation, a model was constructed to represent the chemical transmission and inhibition process of acetylcholine in the neuromuscular junction as a reaction-diffusion system. This system model is a one-dimensional space, radially symmetric about the axis, and the generation of the receptor states that leads to the miniature end plate potential is included in the simulation. The system is comprised of twenty annular compartments in the radial direction which take advantage of the dominance of radial transport over axial transport [58] at the length scales of the neuromuscular junction to reduce the computational requirements. While this model can be considered as something of a synthesis of similar two dimensional models by Naka and Wathey, [57], [18], it simultaneously builds on their work and omits details which were non essential to mitigate the computational load. Despite the omitted details, this model captured the essential temporal and spatial behavior of the reaction-diffusion processes occurring in the neuromuscular junction.

The Jenkins-Szlavik model is the first to quantify the degree of acetylcholinesterase inhibition as a process emerging from the reaction-diffusion kinetics as the neurotoxin diffuses into the neuromuscular cleft. An illustration of this feature is shown in Figure 5.1. This figure depicts the concentration of neurotoxin and active

acetylcholinesterase in the cleft as a function of time as the neurotoxin diffuses into the cleft. The graph is intended for illustrative purposes only, as the diffusion constant of the neurotoxin was assigned an unrealistically low value. This low value allowed the process to spread over a larger portion of time to clarify the illustration. Notice that the two concentration curves are not reflections, where one curve could be derived from knowledge of the other. Instead, they result from genuinely coupled chemical and diffusional kinetics. The known initial amount of enzyme and the known amount of enzyme as a function of some later time (and location) are easily translated into a number which represents degree or percentage of enzyme inhibition.

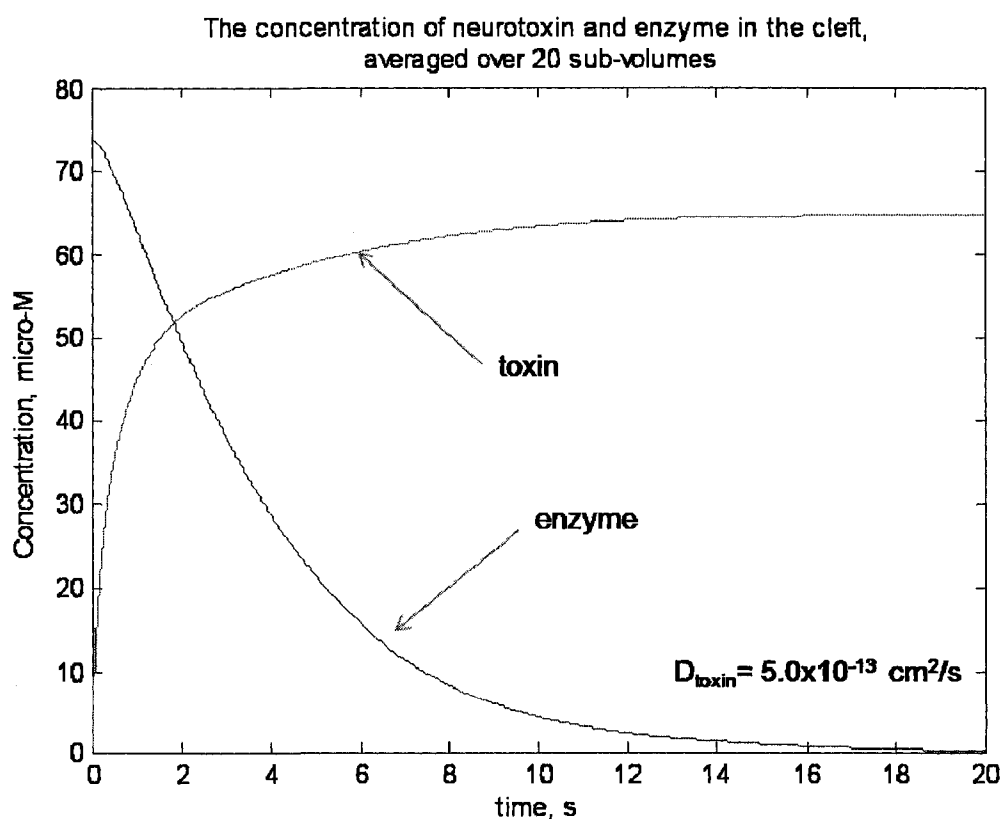


Figure 5.1. An illustration of the dynamically coupled enzyme and neurotoxin concentrations in the neuromuscular junction during the diffusion-reaction process.

The primary function of a simulation of the events in the neuromuscular junction is to measure the state of the acetylcholine receptors during the course of an action potential. The result of the Jenkins-Szlavik model of that process is shown in Figure 5.2. The figure below shows the simulation of different degrees of enzyme inhibition on the time course of open receptors in the cleft under an acetylcholine diffusion constant of $9.0 \cdot 10^{-10} \text{ cm}^2/\text{ms}$. The result visually resembles the same process trends as Friboulet and Naka. This qualitative resemblance is initially reassuring, but some kind of quantitative comparison of the error between the Jenkins-Szlavik model and the Naka and Friboulet models will be needed.

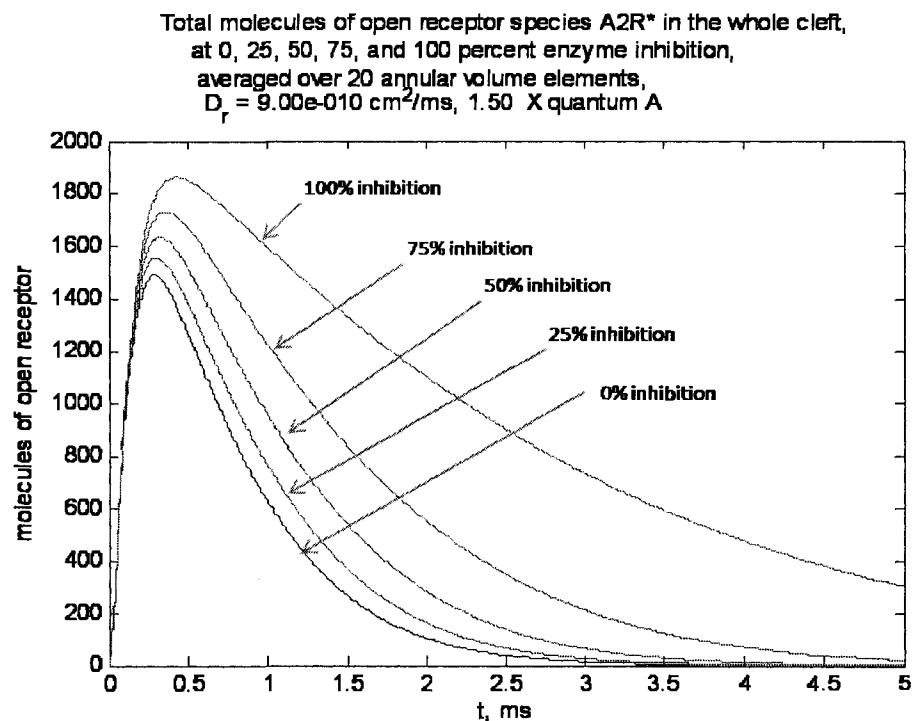


Figure 5.2. The Number of open receptors per acetylcholine quantum from the Jenkins-Szlavik simulation.

Figures 5.3, 5.4, 5.5, and 5.6 show a comparison plot of the Jenkins-Szalvik model with the Friboulet and Naka models, respectively, and show the error between the Jenkins-Szalvik model and the respective Friboulet and Naka models. The results of the Friboulet and Naka simulations were derived from numerical integration of differential equations, so no mathematical expressions for the receptor vs. time curves were available. Therefore, it was decided to approximate the Friboulet and Naka results as two-parameter exponential decay processes: $R^{open}(t) = ae^{-bt}$.

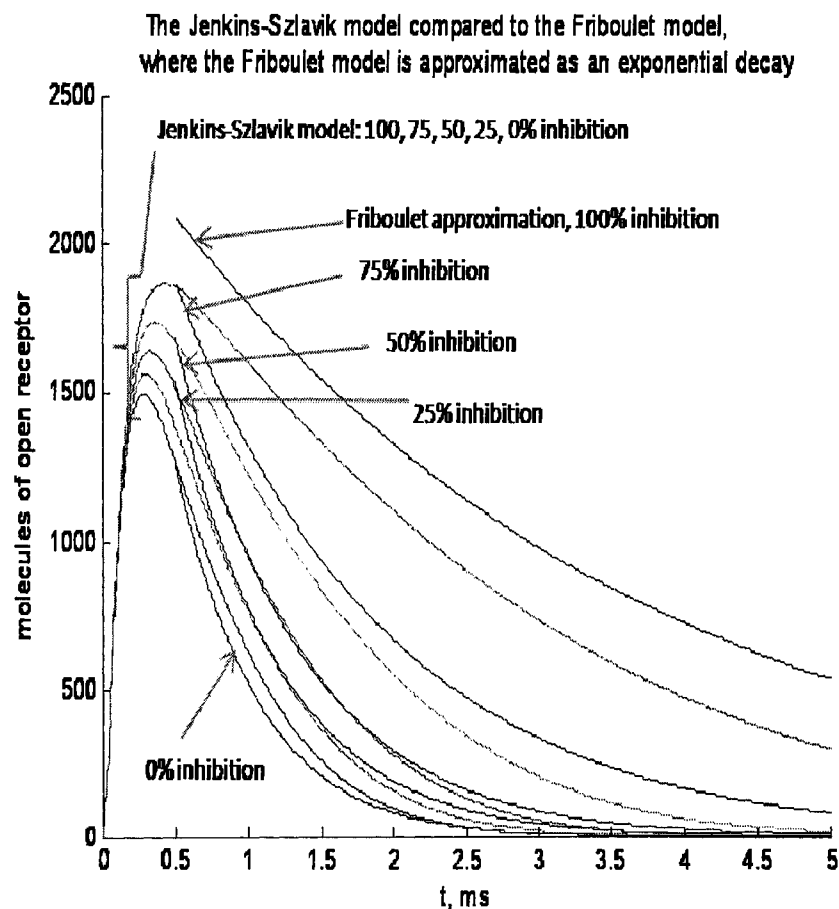


Figure 5.3. A comparison of the Jenkins-Szalvik and Friboulet models of the time course of open receptors in the neuromuscular junction with time. The Friboulet model is approximated as a set of exponential decay processes.

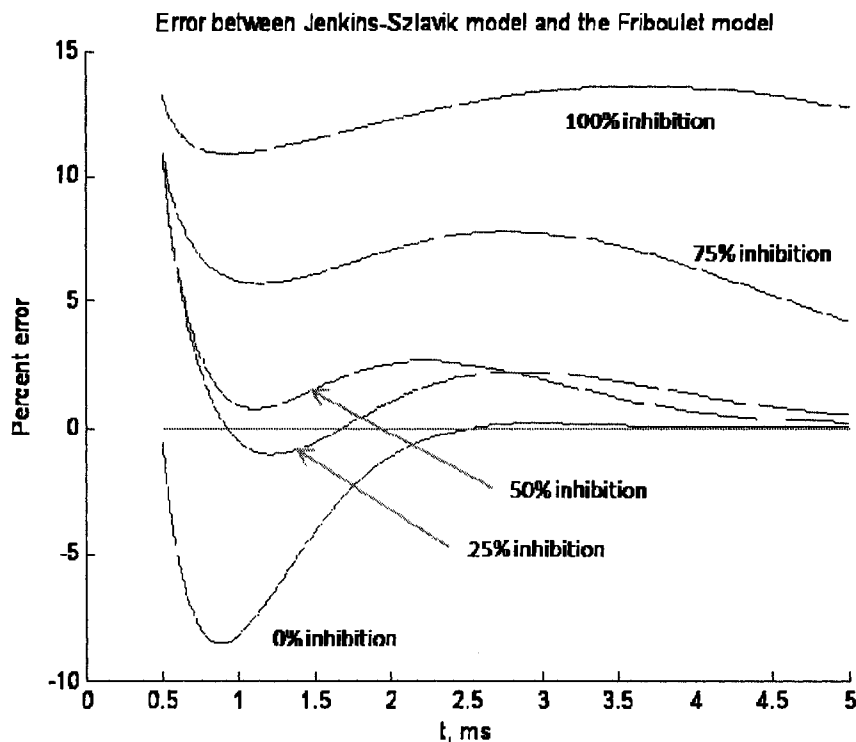


Figure 5.4. The relative error between the Jenkins-Szlavik model and the Friboulet model for different levels of enzyme inhibition.

All the receptor vs. time curves contained an inflection point, which does not occur in a pure exponential decay process, so it was necessary to model the Friboulet and Naka approximations at a time point later than the inflection point for all the curves. The point $t = 0.5$ ms was chosen as the initial point to begin the approximations, which still left 90% of the time domain available for analysis. The measurements used to develop the equations for the approximations had to be taken directly from the graphs of the Friboulet and Naka models, and these measurements contain much uncertainty derived from the thickness of each curve's ink, the interpolation between increments on the axes, the thickness of the increment markers on the ruler, and other sources.

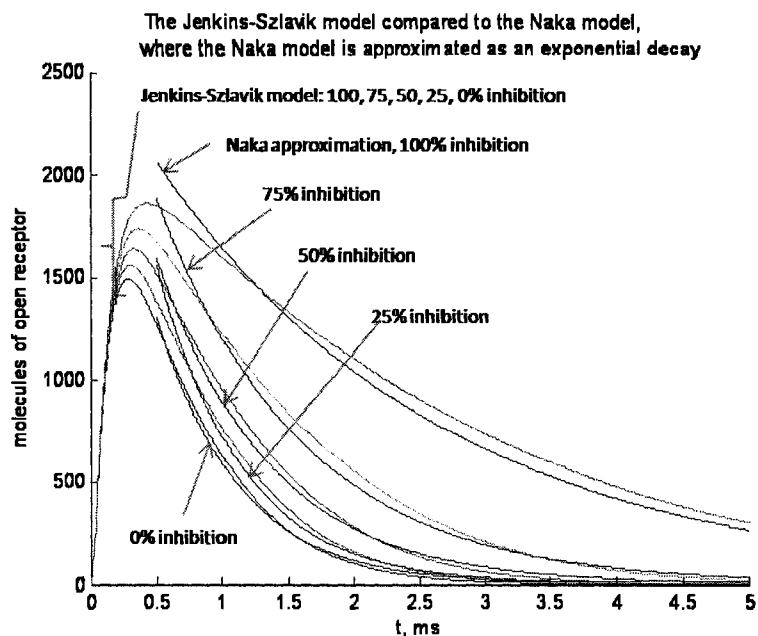


Figure 5.5. A comparison of the Jenkins-Szlavik and Naka models of the time course of open receptors in the neuromuscular junction with time. The Naka model is approximated as a set of exponential decay processes.

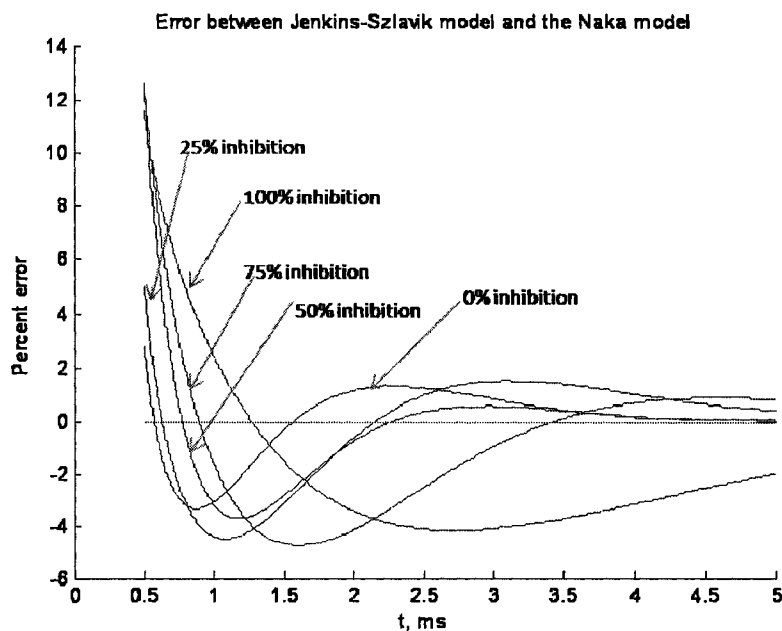


Figure 5.6. The relative error between the Jenkins-Szlavik model and the Naka model for different levels of enzyme inhibition.

From Figures 5.4 and 5.6, which show the error between the Jenkins-Szlavik model and Friboulet and Naka models, respectively, it is seen that over the interval of [0.75, 5.0] milliseconds (85% of the time domain), the error between the models is never greater than $\pm 13\%$, and for most of the curves it is less than $\pm 10\%$. This magnitude is acceptable when all the sources of error and uncertainty are considered [57], [58].

The error comparison figures also show that in general, the Jenkins-Szlavik model agrees better with the Naka model than the Friboulet model, and the error of the Jenkins-Szlavik model increases as the degree in enzyme inhibition increases in both the Friboulet and Naka models. The Friboulet system modeled acetylcholine diffusion in one direction and along the axis, and the process of acetylcholine leaving the cleft was modeled as a uniformly distributed sink in space. The Naka system modeled acetylcholine diffusion along the axis and radially, the process of acetylcholine leaving the cleft was modeled as radial diffusion to the edge of the cleft and into the external environment, and is a process closer to physical reality. Recall that the Jenkins-Szlavik system modeled acetylcholine diffusion in one dimension along the radius, and modeled acetylcholine leaving the cleft in the same manner as Naka. In all three models, increasing the degree of enzyme inhibition caused a greater number of acetylcholine molecules to remain in the system, which in turn causes the effects of acetylcholine diffusion to become more prominent [57], [58].

The investigation of Naka presented evidence which asserted that radial diffusion in the neuromuscular junction is of greater importance than diffusion along the axis. If true, that assertion would explain why the Jenkins-Szlavik model agrees better with the Naka model than the Friboulet model. In addition, since the Jenkins-Szlavik system

models diffusion processes differently from the Friboulet and Naka systems, one would expect the error between the respective models to increase as diffusion begins to predominate, i.e. as the degree of enzyme inhibition increases [57], [58].

The equations (5.1) – (5.3) below, derive the relation between the time course of

$$I_{ep}(t) = E \cdot g_{ep}(t) \quad (5.1)$$

$$I_{ep}(t) = E \cdot \gamma_R \cdot \sum_N R^{open}(t) \quad (5.2)$$

$$I_{ep}(t) = E \cdot \gamma_R \cdot \int \left(\frac{d[A_2R^{open}]}{dt} \right) dt \quad (5.3)$$

the open acetylcholine receptors and the end-plate current. The relation shows that the end-plate current is directly proportional to the number of open receptors in time, and means that the end-plate current differs from the number of open receptors only by a multiplicative constant. This result also gives a method to couple the chemical and diffusional kinetics occurring in the cleft to the current and voltage dynamics which follow in the neurons.

The Jenkins-Szlavik model has been constructed such that it can show the temporal and radial concentration gradients of all the chemical species involved in action potential kinetics, in the normal and inhibited regime. In addition, this model is the first simulation to attempt modeling the kinetics of acetylcholinesterase inhibition with an organophosphorus compound and the effects of this inhibition on the action potential *while the inhibitor diffuses into the neuromuscular cleft*. It would be possible for this model to resolve the position of a moving interface between different chemical species if the process of the inhibitor diffusion could create such an event. Of particular interest

might be the moving boundary between normal and inhibited enzyme, and the state of receptor conformation in the inhibitor-occupied and inhibitor-free zones. While this model should be able to detect the boundaries between different chemical species, subsequent calculations show that under the conditions extant in the neuromuscular junction, these boundaries are not likely to exist. An illustration of this conclusion follows in the next paragraph.

By definition, if the existence of an interface or boundary requires the presence of a type of *gradient*, and the larger the gradient in the interval of its domain; then the greater the distinction of the interface across that same domain. In this case, the gradient would refer to the molar concentration of one or more chemical species as a function of a spatial coordinate. The illustration of an idealized case of this concept would be helpful, and Figure 5.7 below shows a concentration distribution where the inhibitor is diffusing radially into the neuromuscular junction from the blood, under conditions that produce a sudden and large increase in concentration for a small change in the radial position (often called a *step* change in concentration). This sudden concentration increase can be interpreted as the boundary between high and low concentrations of the inhibitor. If this boundary evolves in time and position, then it is called a moving boundary. The gradient of this concentration distribution would measure the relative intensity of the change with position, and would provide a metric of how closely the concentration profile resembles this step increase. Figure 5.8 shows the derivative of the concentration distribution with respect to the cleft radius (called the gradient) of the idealized step function and it resembles the shape of a Gaussian distribution. The larger the magnitude and narrower

the spread of a given gradient, then the closer the associated concentration distribution resembles an ideal step function, which leads to the possibility of resolving and tracking the evolution of a moving interface between different chemical species in the cleft.

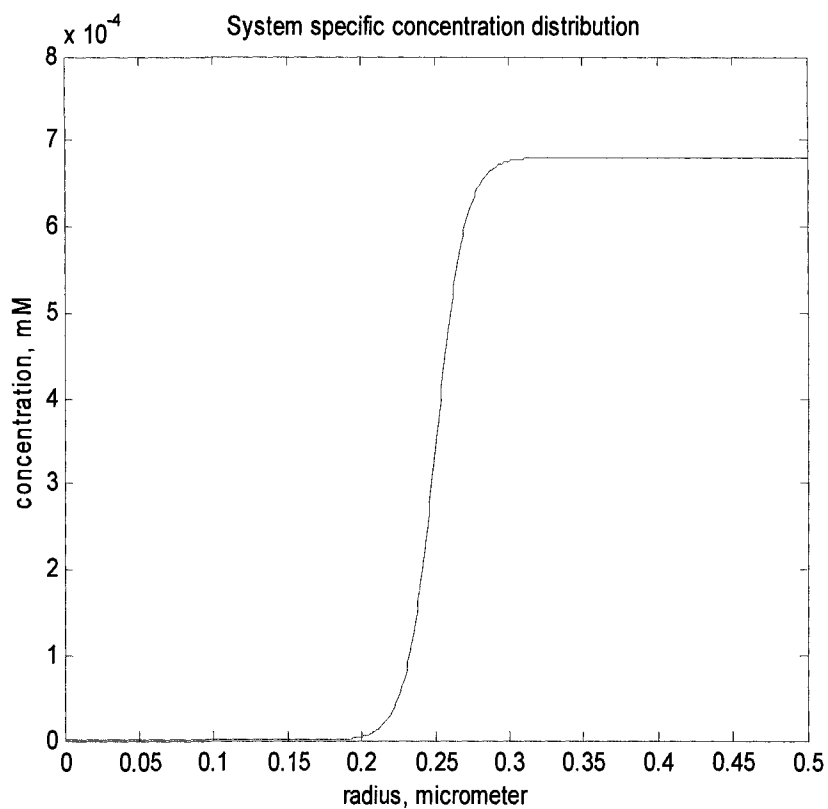


Figure 5.7. The idealized “step” concentration distribution.

Qualitatively describing the shape of a concentration distribution curve or gradient curve as a metric for the intensity of an interface is not sufficient for scientific research: one does not have science until one has numbers. It would be useful to develop a numerical scale for the concentration distribution and concentration gradient whose magnitude would indicate the intensity of the interface across a known distance. It would also be useful to have a numerical description of an interface intensity that was more

generally applicable to a wide range of conditions and parameters, instead of a case-by-case or system-by-system interpretation.

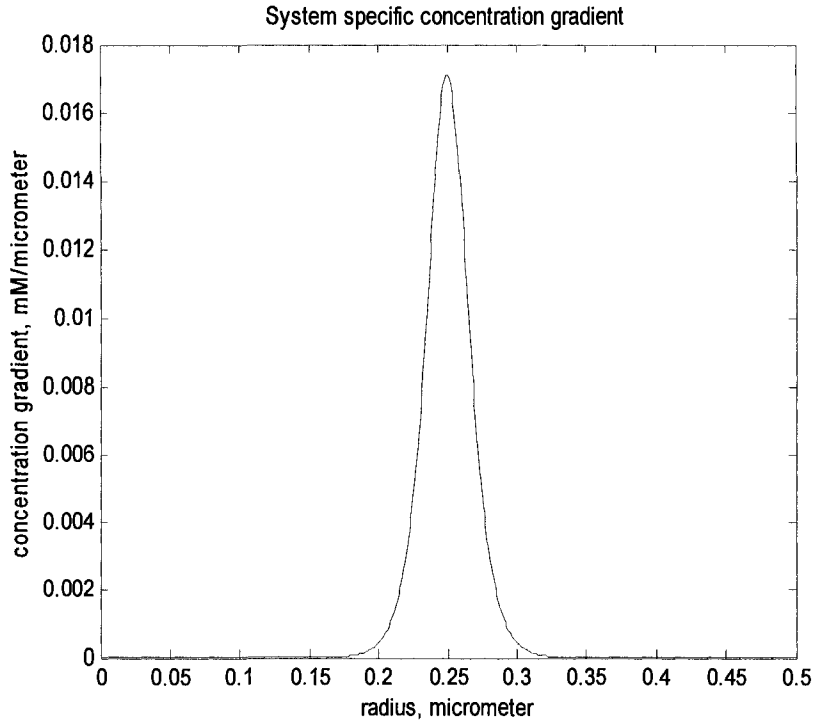


Figure 5.8. The idealized “step” concentration gradient

Towards this goal is the introduction of the *relative length*, and *relative concentration distribution*, given respectively by

$$r_{rel} = \frac{r}{R} \quad 0 \leq r \leq R \quad (5.4)$$

$$C(r)_{rel} = \frac{C(r)}{C_{max}} \quad 0 \leq C(r) \leq C_{max} \quad (5.5)$$

where r is the variable radial distance, R is the maximum radial distance, $C(r)$ is the concentration as a function of the radius, and C_{max} is the maximum concentration

achieved in the cleft volume. The relative length and relative concentration distribution are derived by a simple and common nondimensionalization technique which maps the length and concentration variables onto a dimensionless and universal scale. This scale can be used to express any known concentration distribution in a standard form. When the standard form of an ideal step concentration is known, then the scaled concentration distributions of any other system can be compared to it and the degree of step concentration “membership” of those distributions can be judged, as shown in Equations (5.6) to (5.8) below

$$0 \leq C(r) \leq C_{max} \quad C(r) = f(r) \quad 0 \leq r \leq R \quad (5.6)$$

$$0 \leq C(r)_{rel} \cdot C_{max} \leq C_{max} \quad C(r)_{rel} \cdot C_{max} = f(r_{rel} \cdot R) \quad 0 \leq r_{rel} \cdot R \leq R \quad (5.7)$$

$$0 \leq C(r)_{rel} \leq 1 \quad C(r)_{rel} = \frac{f(r_{rel} \cdot R)}{C_{max}} \quad 0 \leq r_{rel} \leq 1 \quad (5.8)$$

However, applying this same scaling method directly on the gradient of the concentration distribution would restrict those resulting relative gradient values to a domain whose magnitude could never be greater than unity, a condition which is not useful and difficult to interpret. A better way to create a standard scale for the concentration gradient is to take the derivative of the relative concentration distribution, $C(r)_{rel}$, with respect to r_{rel} , thus:

$$\frac{d\{C(r)_{rel}\}}{dr_{rel}} = \frac{1}{C_{max}} \cdot f'(r_{rel} \cdot R) \cdot R \quad (5.9)$$

Equation (5.9) shows that this definition of the relative concentration gradient is primarily another constant scaling factor applied to the concentration gradient function, but this definition does not restrict the gradient to values between zero and unity.

Applying these concepts to the idealized step concentration distribution and step concentration gradient introduced in Figures 5.7 and 5.8 will illustrate their utility. When the ideal step concentration distribution and step concentration gradient are scaled to their relative forms, the results are shown in Figures 5.9 and 5.10.

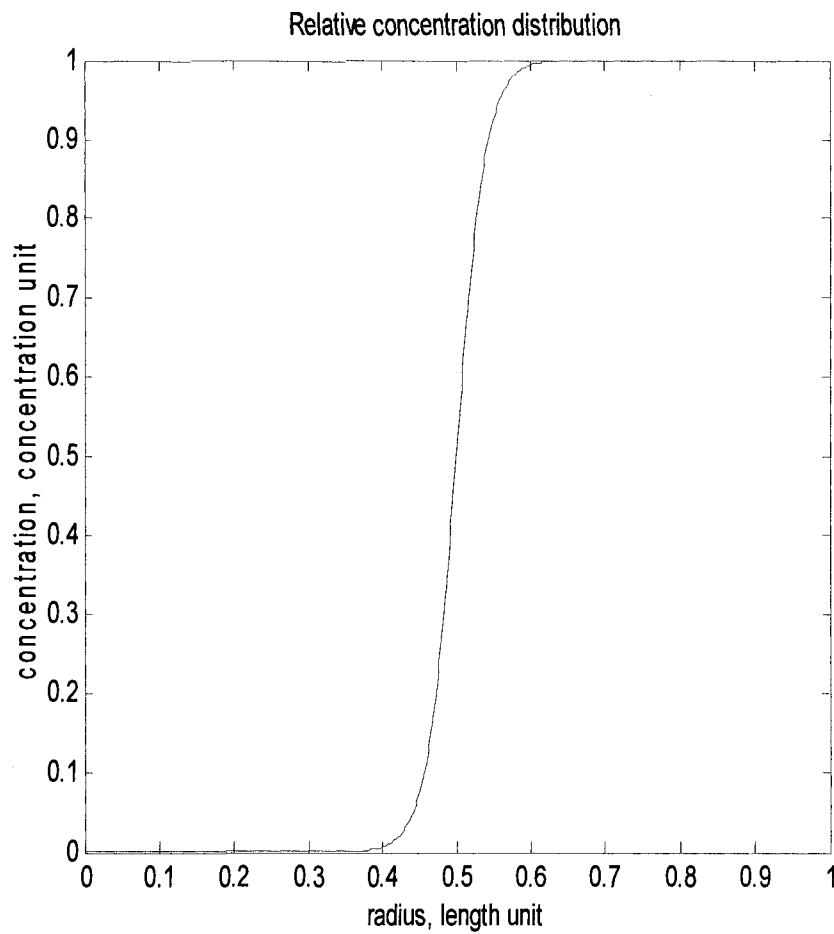


Figure 5.9. The idealized relative “step” concentration distribution.

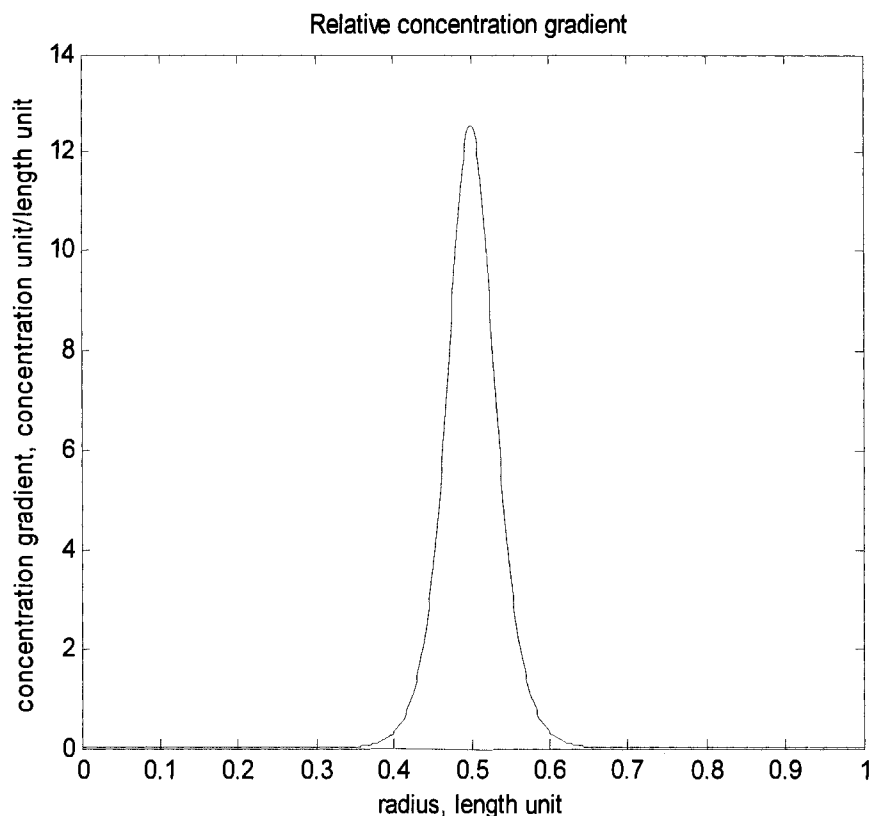


Figure 5.10. The idealized relative “step” concentration gradient.

From these graphs it can be seen that for a concentration distribution to have credible step-like qualities, there should be some continuous interval in the length domain, less than or equal to 0.05 fraction of the total length, where the rate of concentration change is on the order of at least 20 concentration units per length unit across that interval. This method of evaluation can be used with any system of arbitrary size and arbitrary concentration units. Intuitively, one should suspect that the best conditions to detect the presence of a chemical interface within the cleft would be an initially large difference in concentration of a diffusible species between the cleft and the bloodstream. Let us imagine the military neurotoxin *VX* (molecular weight 267.4 g/mole),

one of the fastest and most potent acetylcholinesterase inhibitors, as the neurotoxin diffusing into the neuromuscular junction from the blood. The lethal dose of VX for an average human is about 10 mg VX per kg body mass. An average adult human male has a mass of 86 kg and a blood volume of approximately 5.0 liters. Therefore, the lethal VX blood concentration is 0.68 mM in the blood [72]. Let us assume a venous injection process of VX which produces that particular blood concentration as a logistic function of time over a 5 second period, as shown in Figure 5.11. Further, imagine the process subsequently maintains that concentration indefinitely under conditions where physiological detoxification mechanisms are negligible.

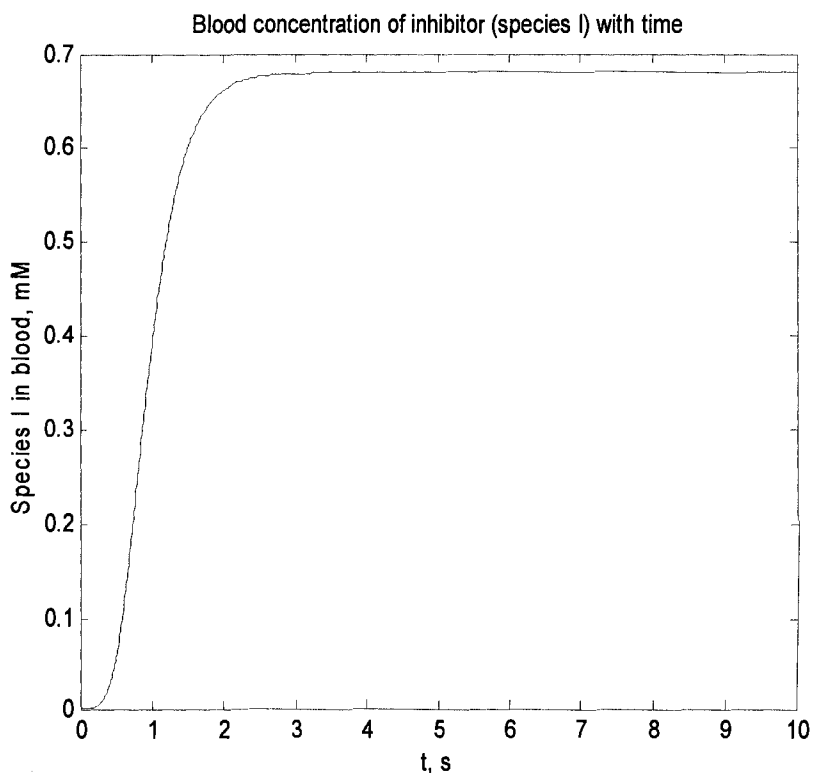


Figure 5.11. A hypothetical venous injection of inhibitor.

The known military grade neurotoxins are all small molecules whose diffusion constant in blood plasma are not precisely known, but are assumed to be not much different from that of acetylcholine diffusing through water. Literature sources of information, [73] - [77], on molecules of a similar size as the military neurotoxins give diffusion coefficient values in the range $2.5 \cdot 10^{-10} - 3.0 \cdot 10^{-8} \text{ cm}^2/\text{ms}$ and the same diffusion constant as that used for acetylcholine in [5], [57], [58], namely $9.0 \cdot 10^{-10} \text{ cm}^2/\text{ms}$ has been assumed for these molecules. A surface plot of the simulated VX concentration, represented by [I], in the cleft as a function of the radial distance and time is shown in Figure 5.12, where the rapid rise and apparently close to uniform concentration along the radius of the inhibitor can be viewed. The cleft reaches saturation of inhibitor in 2.5 seconds.

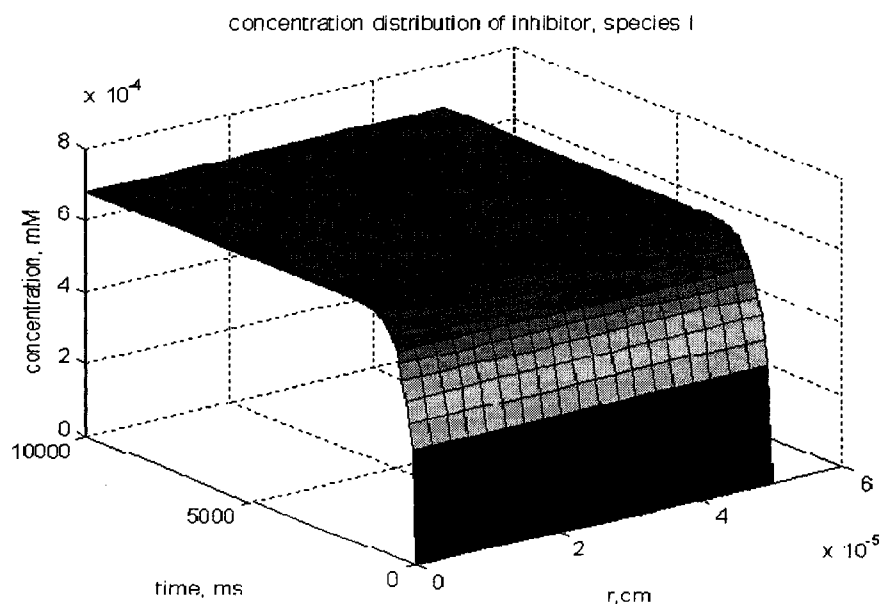


Figure 5.12. The simulated concentration distribution of inhibitor in the neuromuscular junction during diffusion.

The curves shown in Figures 4.4, 4.5, 4.6, and 5.2 depict the concentration of a substance as a function of time in a single, well mixed volume. The curves are naturally smooth over the time domain because several hundred time points are calculated, and separated by a small interval (Δt) between them. The reader should now recall that in this case the cleft of the neuromuscular junction is modeled as a cylinder with a very small height to base ratio, and that cylindrical volume has been sectioned into 20 concentric annular sub-volumes. In Figure 5.12 the simulation data has been arranged to represent a cross-section of all the annular rings in sequence, along with their inhibitor concentration data. Referring to the radius scale in Figure 5.12, 0 micrometers represents the center of the cleft, and 50 micrometers represents the cleft/bloodstream interface. This radial distance has been divided into 20 sections ($\Delta r = 2.5$ micrometers) each of which represents one of the annular volumes, and the concentration in each of these sections as a function of time has been plotted. Because Δr is large compared to the total radial distance, a direct plot of the concentration vs. radius data would not necessarily appear smooth. Therefore, it is more useful to fit a polynomial curve to the data via a regression, and plot the derived polynomial curve.

Figure 5.12 shows multiple concentration vs. radius distributions in the neuromuscular junction during the venous injection of VX process that was shown in Figure 5.11. Figure 5.12 depicts these distributions over a 10 second period, where each curve has been sampled at 200 millisecond intervals in the domains where the concentration was rapidly changing. The maximum concentration of 0.68 mM is reached at between 2 and 3 seconds (see Figure 5.11); however, no significant concentration gradients are obviously visible for any of the distributions. After a period greater than 3

seconds the cleft is saturated with the inhibitor, and the concentration distribution is uniform throughout the cleft volume. A quadratic polynomial gave the best fit for the data, shown as Equation (5.10):

$$[I](r) = ar^2 + br + c \quad (5.10)$$

$$a = 8.8700 \cdot 10^{-4} \quad b = 0.0000 \quad c = 0.0006$$

The polynomial coefficients a , b , and c shown in Equation (5.10) were arithmetically averaged over the coefficient values of all the regressed polynomial distribution curves.

Even though the distribution curves appear flat with no significant gradients, such a qualitative judgment is of course not sufficient. A numerical description of the concentration gradients in the cleft during this injection process should be analyzed. Figure 5.13 shows the concentration gradients of the same process in time and space, and better illustrates the magnitude of the concentration differences along the radius. These gradient curves were determined from the derivative of each of the quadratic concentration distribution curves shown in Figure 5.12, and the surface in Figure 5.13 has been rotated to a different perspective from that of Figure 5.12 to provide a better intuitive grasp of the space and time relationship of the gradients. The axes in both figures occupy the same relative positions and represent the same information. Figure 5.13 shows a series of gradient curves plotted over the same 10 second period and sampled at approximately 200 millisecond intervals in the domain where the gradient was changing rapidly. The curves show a concentration gradient process which is initially zero across the entire radius, then shows linear relations which increase in slope to a maximum value over time, and then the slopes of the linear relations decrease with time

back to a zero value for the gradient across the radius. The maximum gradient value is $15.0 \cdot 10^{-3}$ mM/cm and located at the radius end-point where the cleft interfaces with the bloodstream. These results mesh with the process shown in Figure 5.12, as the quadratic concentration distribution curves will have concentration gradient curves which are linear. Initially, the distribution of inhibitor in the cleft is zero, and so it has a gradient of zero as well. As the inhibitor enters the cleft, there should be some time when the differences of inhibitor concentration along the radius in the cleft should be the greatest, and this corresponds to a maximum value for the gradient at that time and location. Finally, when the cleft is saturated with inhibitor, the concentration distribution will be uniform, and at this same time the concentration gradient in the cleft will be zero.

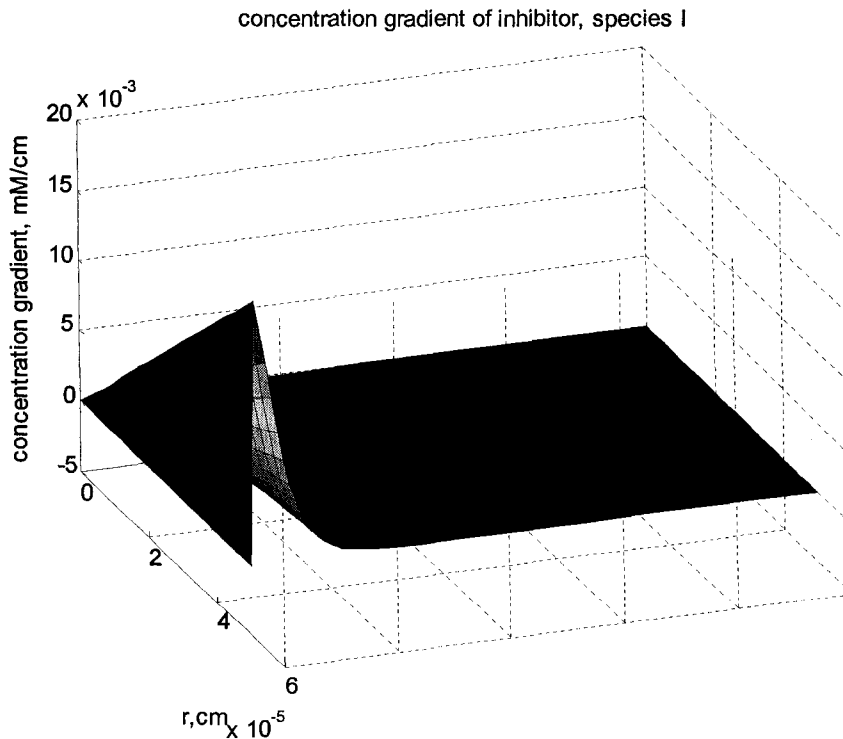


Figure 5.13. The simulated concentration gradient of inhibitor during diffusion into the neuromuscular junction.

Surface plots show the complete time and space relationships of the inhibitor concentration in the cleft, but this can be more information than is needed to interpret the relevant essential points in this analysis. Once the reader has an intuitive understanding of the general shape of the time, space, and concentration function in the cleft provided by the surface plots, it might be easier to interpret the salient characteristics of the inhibitor diffusion process with ordinary concentration vs. radius graphs where time dimension is presented as a set of level curves for different time values. Figure 5.14 shows the inhibitor concentration distributions of Figure 5.12 projected onto the concentration vs. radius plane, where the initial distribution is plotted with the symbol “x” and the final distribution uses the symbol “o”.

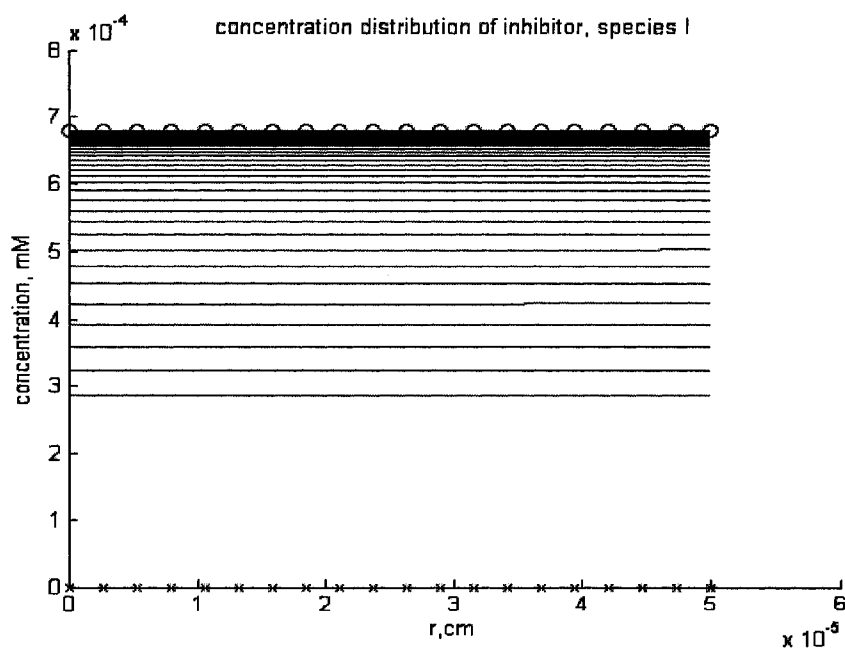


Figure 5.14. The inhibitor concentration distributions in the cleft, where $D_1 = 9.0 \cdot 10^{-10} \text{ cm}^2/\text{ms}$, over a time period of 10 seconds.

The distribution level curves are seen rising rapidly from zero and subsequently crowding around the final cleft saturation value as time increases. Figure 5.15 shows the inhibitor concentration gradients of Figure 5.13 projected onto the concentration vs. radius plane, where the initial gradient is plotted with the symbol “x” and the final gradient uses the symbol “o”. The gradient level curves rise from zero to a maximum value and decrease back to zero as time increases. The linear nature of these gradients is easily seen in this type of graph. In both graphs the level curves were sampled frequently where the concentration was changing rapidly, and sampled sparsely where the concentration changed slowly. Because of this, the different level curves do not represent a constant time interval between them.

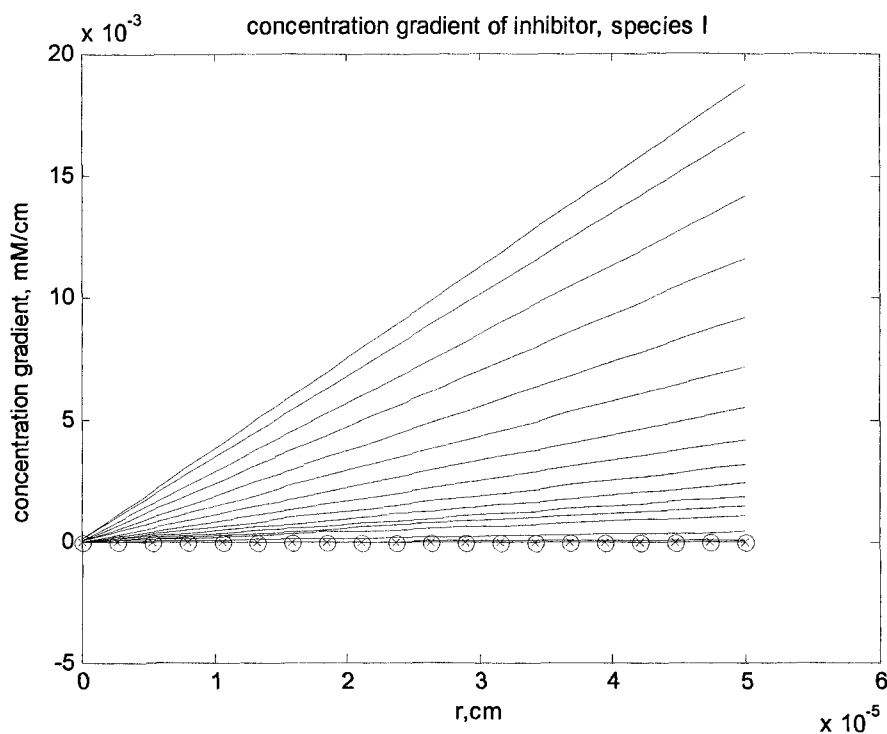


Figure 5.15. The inhibitor concentration gradients in the cleft, where $D_1 = 9.0 \cdot 10^{-10} \text{ cm}^2/\text{ms}$, over a time period of 10 seconds.

In Figures 5.12 and 5.14, the concentration distributions seem very flat across the cleft radius, yet the representation of the gradients in Figures 5.13 and 5.15 suggest that at certain times the gradients might be large. For this reason we shall now compare the analysis in the previous paragraphs with the analysis which follows using the relative concentration data. Normalizing the simulation data used to generate Figures 5.12 and 5.14 to their relative scales results in the graph depicted in Figure 5.16.

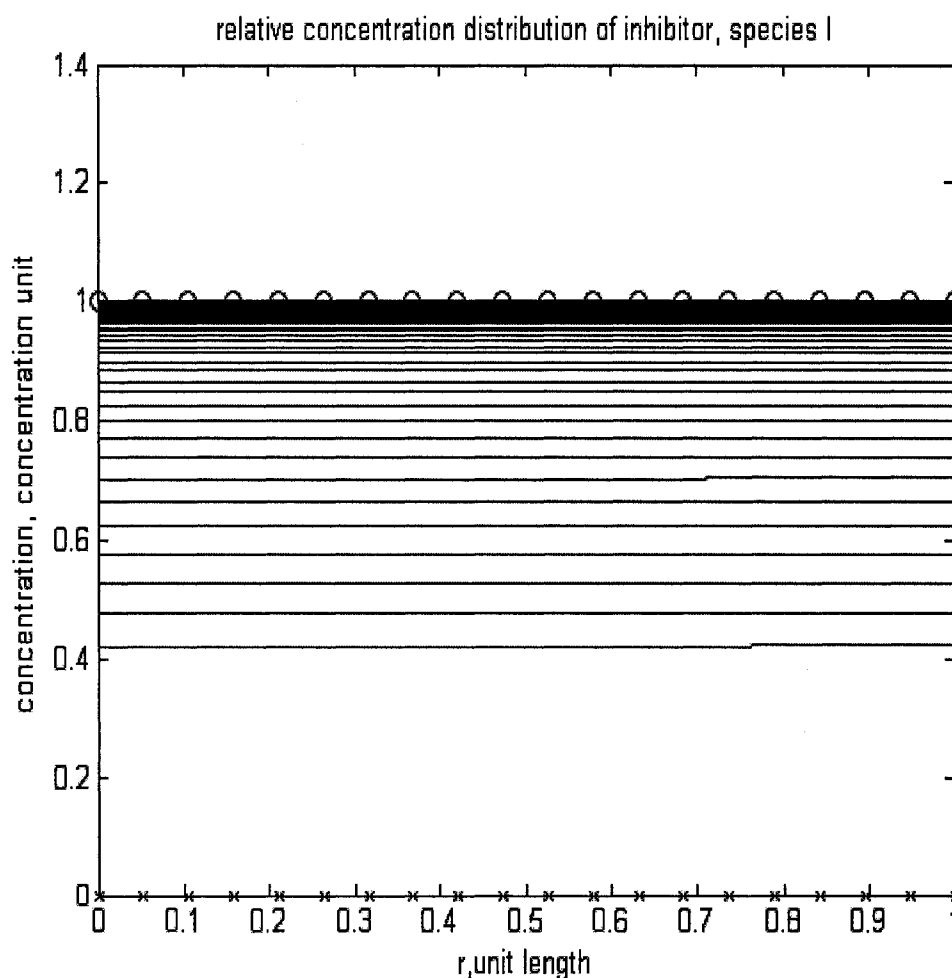


Figure 5.16. The normalized inhibitor concentration distributions in the cleft, where $D_I = 9.0 \cdot 10^{-10} \text{ cm}^2/\text{ms}$, over a time period of 10 seconds.

Figure 5.16 shows the inhibitor concentration distributions of Figure 5.12 normalized and projected onto the concentration vs. radius plane, where once again the initial distribution is plotted with the symbol “x” and the final distribution uses the symbol “o”. The distribution level curves rise rapidly from zero and subsequently crowd around the final cleft saturation value as time increases. However, in this case it is also seen that the level curves have a negligible slope (gradient) over time, which terminates at a zero value as the concentration of inhibitor in the cleft reaches saturation. Because it is known from the relative idealized step gradient (Figure 5.10) that a valid concentration interface needs at least 10 concentration units per length unit over a continuous distance that is less than 0.05 fraction of the total radius, we can easily conclude that no concentration gradients significant enough to produce a concentration boundary exist in the cleft under the conditions of this simulation. After 500 milliseconds no gradients large enough to be considered as possible concentration boundaries exist anywhere in the cleft. It would be useful to find the neurotoxin diffusion constant magnitude at which the Jenkins-Szlavik model predicts concentration boundaries might resolve in the neuromuscular junction.

In Figure 5.17 the level curves of normalized concentration distribution are shown for a neurotoxin diffusion constant decreased by a factor of 10, sampled at 100 millisecond intervals over a period of 20 seconds. The gradients of the level curves are seen to be negligible over the entire time domain.

Figure 5.18 shows the normalized concentration distribution curves for a neurotoxin diffusion constant decreased by a factor of 100, and the same sample interval

and time duration. The first few level curves show a small gradient that rapidly decays to zero in a period of twenty seconds.

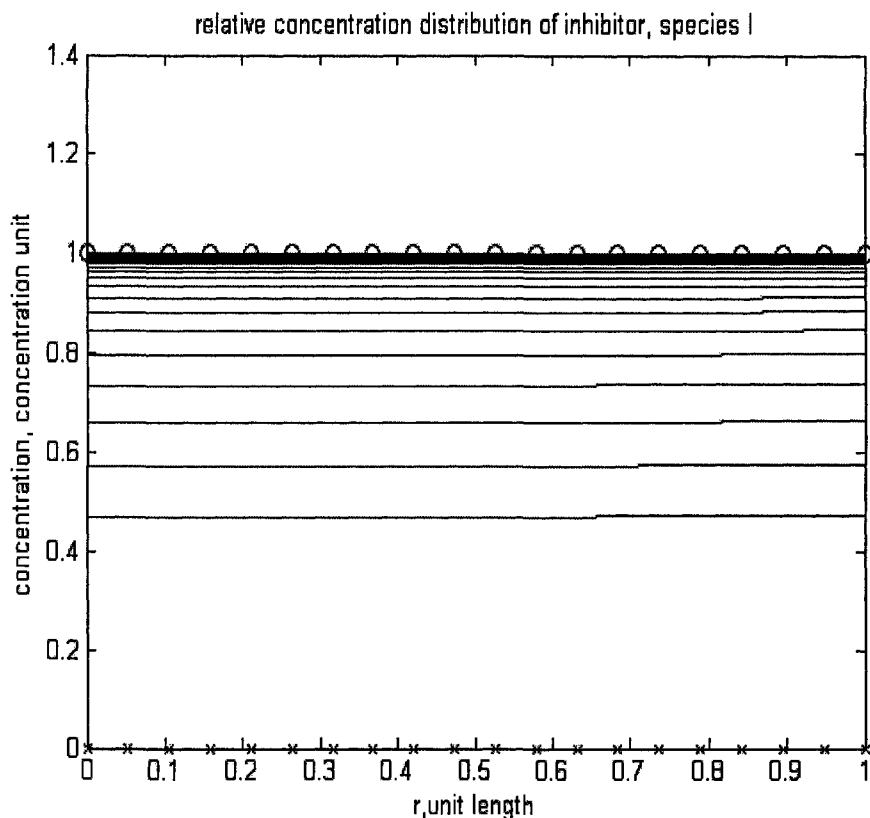


Figure 5.17. The normalized inhibitor concentration distributions in the cleft, where $D_I = 9.0 \cdot 10^{-11} \text{ cm}^2/\text{ms}$, over a time period of 20 seconds.

In Figure 5.19 the neurotoxin diffusion constant is decreased by a factor of 1000, and the level curves are sampled at 150 millisecond intervals over a period of 30 seconds. It is seen that significant concentration gradients are predicted to exist in the cleft for approximately 1.5 seconds. However, these gradients are not large enough to resolve a boundary between concentrations over a distance less than 0.05 fraction of the total radius. A diffusion constant approaching the magnitude of $10^{-13} \text{ cm}^2/\text{ms}$ is not physically

realizable in a biologically functioning neuromuscular junction for molecules the size of the known organophosphorus neurotoxins.

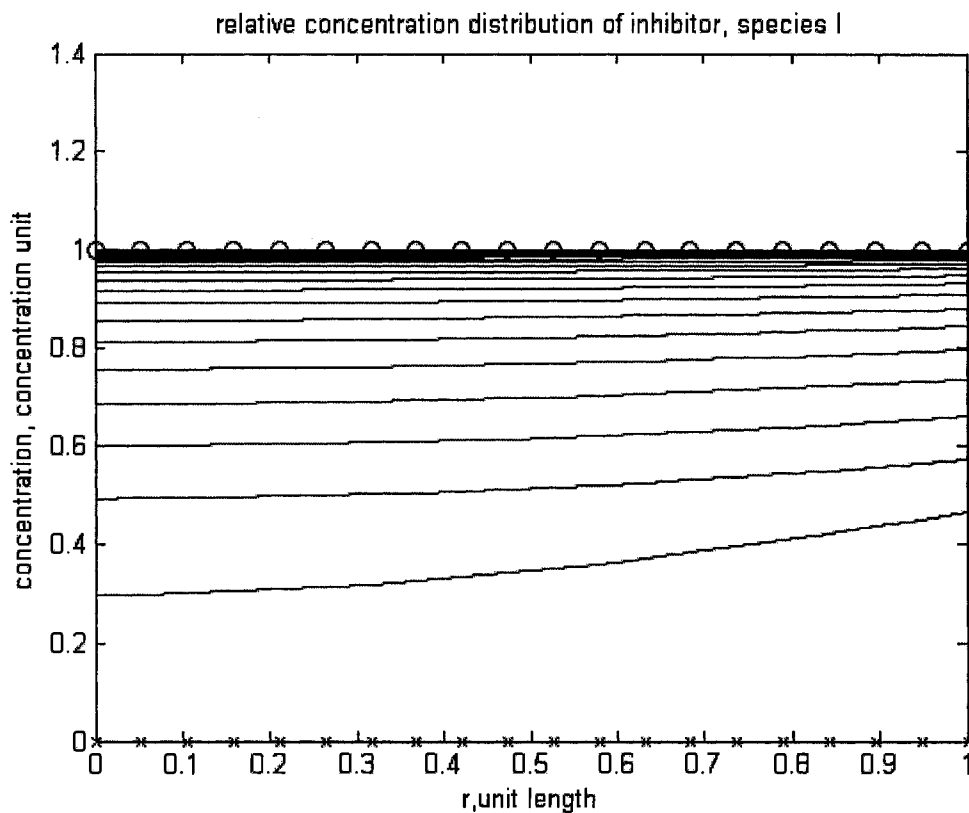


Figure 5.18. The normalized inhibitor concentration distributions in the cleft, where $D_I = 9.0 \cdot 10^{-12} \text{ cm}^2/\text{ms}$, over a time period of 20 seconds.

The data from this simulation shows that the concentration gradients of a neurotoxin in the cleft are never very large at the values for the diffusion coefficients, blood concentration, and length of time conditions which exist for typical biological processes. The concentration of inhibitor in the neuromuscular junction and in the blood are essentially always in equilibrium because the inhibitor transports throughout the cleft essentially as fast as it enters the blood. The optimal conditions to create a concentration

interface (for example between inhibited and normal acetylcholinesterase) inside the cleft would be a very rapid, and preferably high, concentration increase of inhibitor in the blood, coupled with a very small diffusion coefficient for the inhibitor within the cleft. A much longer radial diffusion length would also increase the likelihood of an interface being able to resolve.

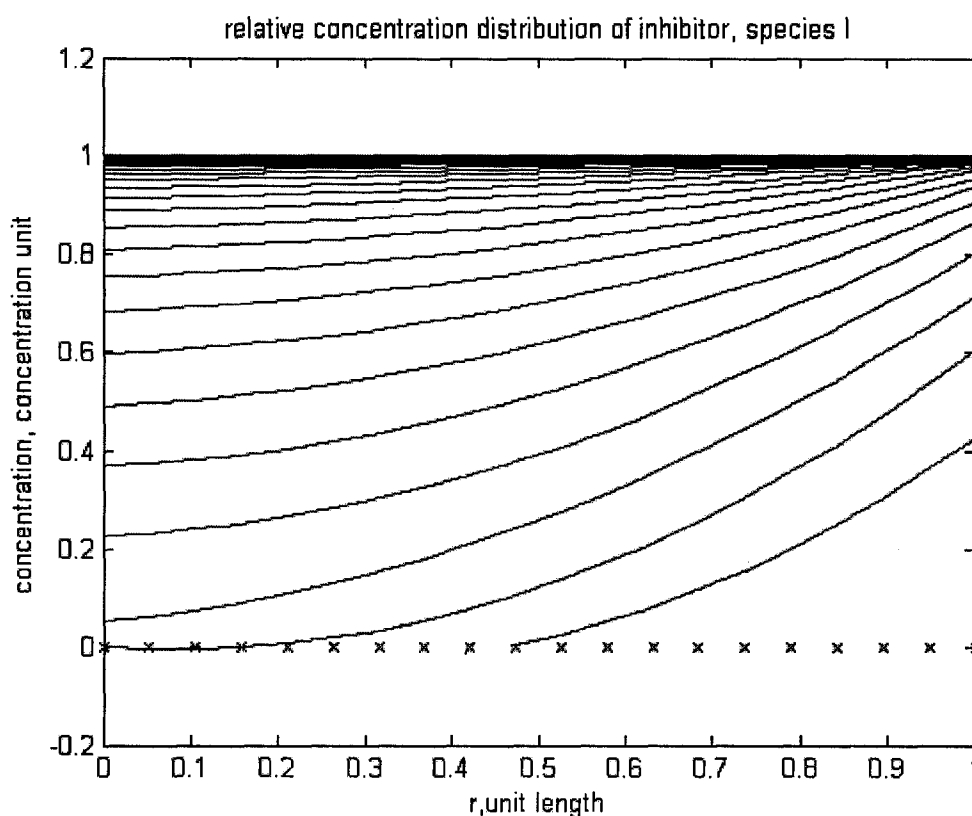


Figure 5.19. The normalized inhibitor concentration distributions in the cleft, where $D_1 = 9.0 \cdot 10^{-13} \text{ cm}^2/\text{ms}$, over a time period of 30 seconds.

Most humans will quickly begin dying at VX blood concentrations higher than 0.68 mM [72], [48], [49], so the modeling of larger concentrations does not seem useful. Faster methods to administer a lethal dose of toxin certainly exist, but most exposure

events involving military neurotoxins will likely produce infiltration rates on the order of minutes, or slower. Simulations with different diffusion coefficients produced data showing that significant radial concentration gradients do not appear in the cleft until the diffusion coefficient of the inhibitor is on the order of 10^{-12} cm²/ms or smaller. In summary, this simulation shows that the volume of the neuromuscular junction will not contain sharp concentration interfaces of inhibitor, enzyme, or significantly different receptor states along its radius, and the assumption of a uniformly mixed inhibitor concentration in the neuromuscular junction is valid. The kinetic events can be adequately modeled by summation of the discrete radial inhibitor concentration values and averaging them over the whole volume of the cleft.

It is well known that acetylcholinesterase is concentrated in the neuromuscular junction. This enzyme is also embedded in the membranes of erythrocytes, where it is thought to affect the functional life-span of red blood cells [78], [79], and occurs in other tissues with a non-quantified distribution. It has also been established that in the military or terrorist event context, the levels of exposure to military-grade neurotoxins can lead to severe incapacitation and lethality within minutes [50], [72]. These conditions, along with other factors such as the severe ethical barriers, combine to make the quantifiable time course of the total degree of acetylcholinesterase inhibition throughout the human body a non-trivial problem. Determining the parameters and exposure conditions needed to establish such a relationship could become the core of a future research project.

It is possible to reactivate organophosphorus (OP) poisoned acetylcholinesterase *in vitro* [12], [51], [80] - [84]. Therapeutic regimens using oxime compounds to rehabilitate acetylcholinesterase have been developed as part of the clinical treatment for

OP toxin exposure as well [50], [85], [86]. At this time, the standard treatment of poisoning by OP-type toxin includes the administration of atropine (an antimuscarinic agent) and obidoxime or pralidoxime as the enzyme reactivators.

Nerve agents act by inhibiting the hydrolysis of acetylcholine by acetylcholinesterase. They bind to the active site of acetylcholinesterase, rendering it incapable of deactivating acetylcholine. Acetylcholine that is not hydrolyzed can continue to interact with the postsynaptic receptor, which results in persistent and uncontrolled stimulation of that receptor. After persistent activation of the receptor, *fatigue* results. This is the same principle exhibited by the depolarizing neuromuscular blocker succinylcholine. The clinical effects of nerve agents are the result of this persistent stimulation and subsequent fatigue at the acetylcholine receptor. In an initial step, the enzyme becomes inactivated, but not permanently. Some degree of reactivation of the acetylcholinesterase enzyme occurs in this initial phase, but the process is slow. An additional reaction between acetylcholinesterase and the nerve agent makes their interaction irreversible, a phenomenon known as *aging*. The aging kinetics of VX is completed after a period of approximately 48 hours [80]. For the clinical effect to be reversed after aging occurs, new enzyme must be produced. This irreversible bond is one difference between the reactive chemistry of organophosphate compounds (including nerve agents) and carbamates, which bind reversibly to acetylcholinesterase. This concept is also used for pretreatment of military personnel with the carbamate pyridostigmine [87]. The qualitative kinetics of these reactions are becoming better understood, and computational models for these reactions in vitro have been developed and published [88]. Removal of the phosphyl moiety from the serine in the enzyme's active site is the

primary mechanism of oxime action, and the Jenkins-Szlavik model is the first attempt to computationally describe the kinetics of OP inhibited acetylcholinesterase reactivation with oxime compounds *in vivo*. If the kinetic parameters are known, it is of course no more difficult to compute the chemical dynamics of the reactivation reactions than it was for the inhibition reactions. The adult OP-therapy dosage is 1-2 grams of pralidoxime (137.16 g/mole) given intravenously over a period of 20-30 minutes [86]. The heart pumps about 5 liters per minute and the human body holds about 5 liters, so within about a minute most of the blood has made one circuit and can be modeled as uniformly mixed [70], [79]. After 2 minutes, most of the blood has circulated twice through the vasculature, and anything that did not mix the first time would be further equilibrated throughout the blood medium during subsequent laps through the circulatory system. Given this rapid blood mixing time relative to the period of pralidoxime administration, then the rate of molar pralidoxime delivery to the blood can be treated as constant at $1.46 \text{ nmole}\cdot\text{cm}^{-3}\cdot\text{ms}^{-1}$. The Jenkins-Szlavik simulation was used to model the process of clinical acetylcholinesterase reactivation in one typical neuromuscular junction under the following conditions: initially zero active enzyme, the diffusion constant of pralidoxime was the same as that of acetylcholine, and the therapy began after the amount of neurotoxin (VX) remaining in the blood became negligible.

Figure 5.20 below shows the average amount of inhibited enzyme in the cleft decreasing with time from the initial value of $7.4\cdot 10^{-5} \text{ mmole}/\text{cm}^3$ to zero in a five minute time period. Figure 5.21 depicts the regeneration of acetylcholinesterase as the average amount in the cleft rises from an initial value of zero to $7.4\cdot 10^{-5} \text{ mmole}/\text{cm}^3$ (the amount of enzyme in a normal junction) in the same time period.

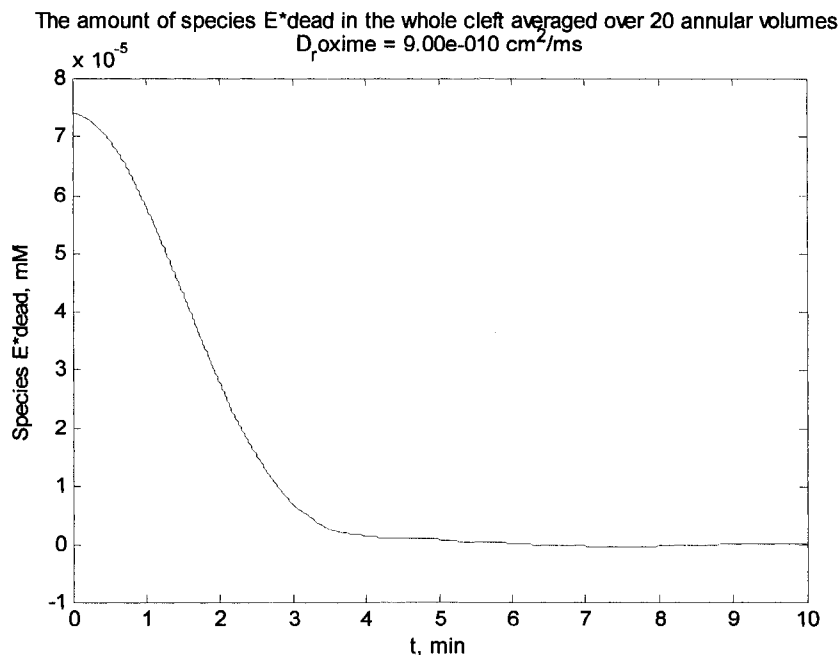


Figure 5.20. The average amount of inactive acetylcholinesterase in the cleft during oxime therapy.

Figure 5.22 shows the assumed linear rate of therapeutic pralidoxime entering the junction via the method of injection. Keep in mind that this simulation models the reactivation of enzyme which is occurring in one typical neuromuscular junction. In a genuine therapy situation, the neuromuscular junction population would have differing amounts of enzyme inhibition; the oxime kinetics would also reactivate the acetylcholinesterase throughout the body, not just the neuromuscular cleft. Those conditions, and other metabolic factors, suggest that recovery from a serious OP neurotoxin event would (of course) require more time and resources than five or ten minutes of chemical therapy. At this stage, these simulation results have been presented as a proof-of-concept which has a high degree ability to assist the development of feasible therapies to counter organophosphorus poisoning.

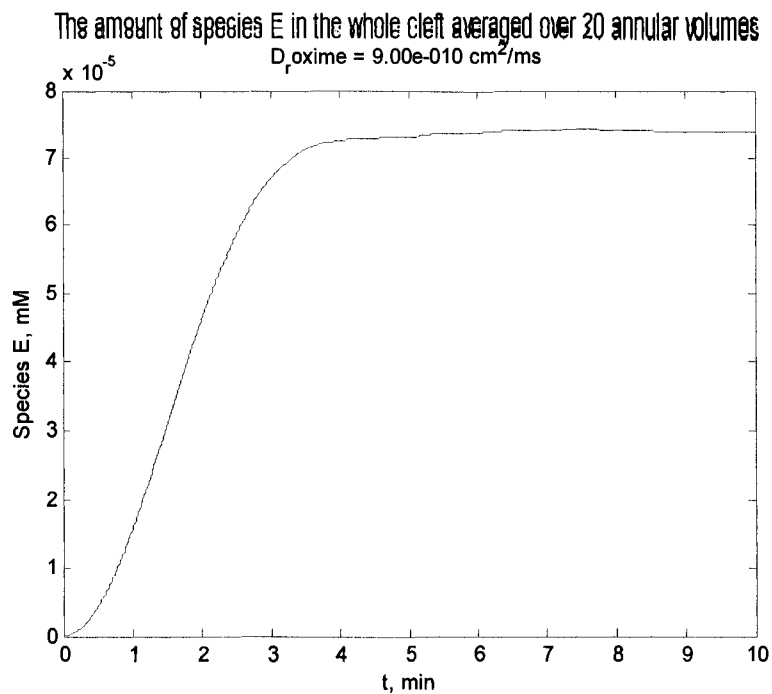


Figure 5.21. The average amount of active acetylcholinesterase in the cleft during oxime therapy.

This concludes the results portion of the dissertation. It has been shown that this model can duplicate the experimental and simulation results of prior published research concerning the normal and inhibited kinetics of the chemical species in the neuromuscular junction during an action potential event. Further, it was shown that this model is the first to simulate those kinetic events *in vivo* as a neurotoxin is simultaneously diffusing into the neuromuscular junction, rather than first artificially setting the degree of acetylcholinesterase inhibition to some value, then starting the simulation. The model demonstrated the potential to detect and resolve moving boundaries between concentration interfaces or different chemical species, and it was also shown that these boundaries do not exist in the normal biological environment of the

neuromuscular junction. Finally, this model is the first to simulate the regeneration of organophosphate inhibited acetylcholinesterase in the neuromuscular junction in the presence of an oxime compound diffusing into the cleft. It was shown that, in principle, this enzyme regeneration process is no more difficult to simulate than the enzyme inhibition process. The caveat of “in principle” is mentioned because coupling the enzyme regeneration results with quantifying the efficacy of therapeutic oxime infusion is another complex issue.

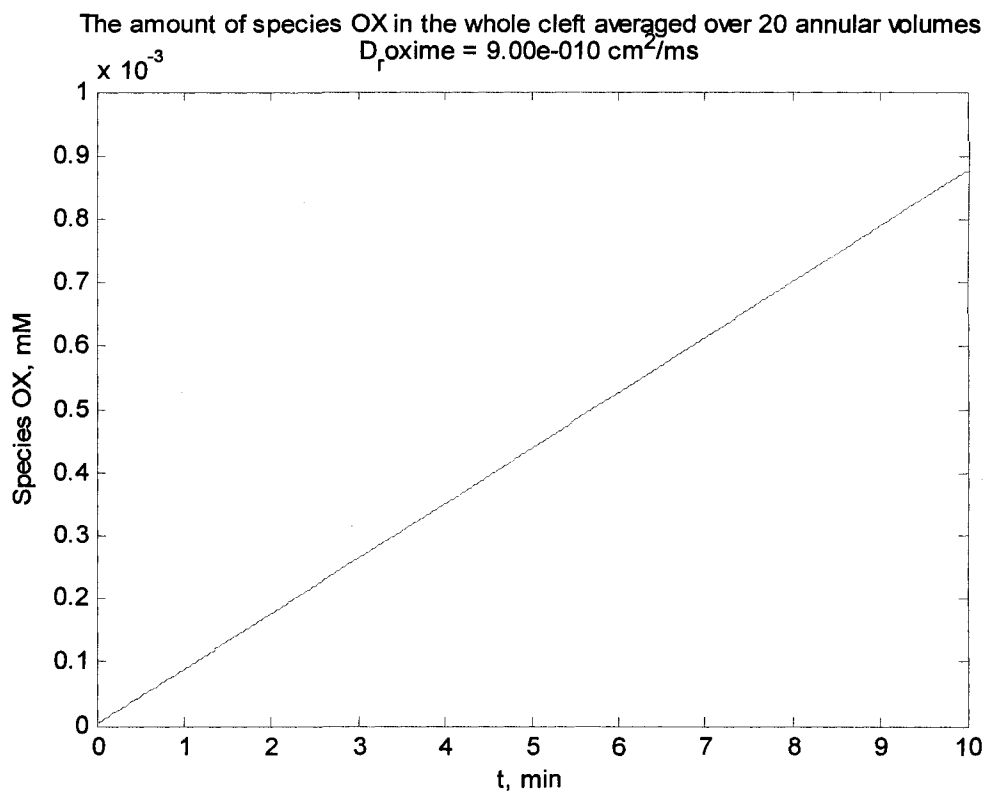


Figure 5.22. The average concentration of oxime in the cleft during oxime therapy.

CHAPTER 6

FUTURE WORK

Jenkins and Szlavik used a one dimensional diffusion model which took advantage of geometric symmetry to focus on the dominant transport effects. It was shown that the Jenkins-Szlavik simulation can reproduce the work of earlier research in depicting the time and spatial course of a normal action potential, and the time and spatial course of action potentials influenced by different degrees of acetylcholinesterase inhibition. This is the first simulation to achieve a model of acetylcholinesterase inhibition during the diffusion of a neurotoxic inhibitor into the neuromuscular junction, and show the altered subsequent action potentials. Jenkins and Szlavik illustrated how this simulation could detect the time and space dynamics of moving concentration gradients in the neuromuscular junction under suitable conditions. In addition, this model showed an in vivo simulation of inhibited acetylcholinesterase being returned to the active state through the kinetics of pralidoxime therapy.

The mathematical method used in these simulations easily generalizes to a complete three dimensional transport model of the diffusion-reaction processes occurring in the neuromuscular junction. In most previous cleft models, the model was constructed such that the injection of acetylcholine molecules is assumed to be a single quanta entering at the center of the presynaptic membrane. However, freeze-fracture images, and electron micrograph images, suggest that several quanta can simultaneously enter

the cleft at different locations on the presynaptic membrane surface. Figure 6.1 shows an electron micrograph of acetylcholine vesicles in the presynaptic membrane, prior to release of acetylcholine into the gap of the neuromuscular junction. The vesicles can be seen distributed along the boundary of the gap. With a complete 3D transport-reaction model (in cylindrical coordinates), the Jenkins-Szlavik model could address any valid criticisms of centered-membrane-quanta models, and investigate the effects of acetylcholine entering the cleft in different sectors.

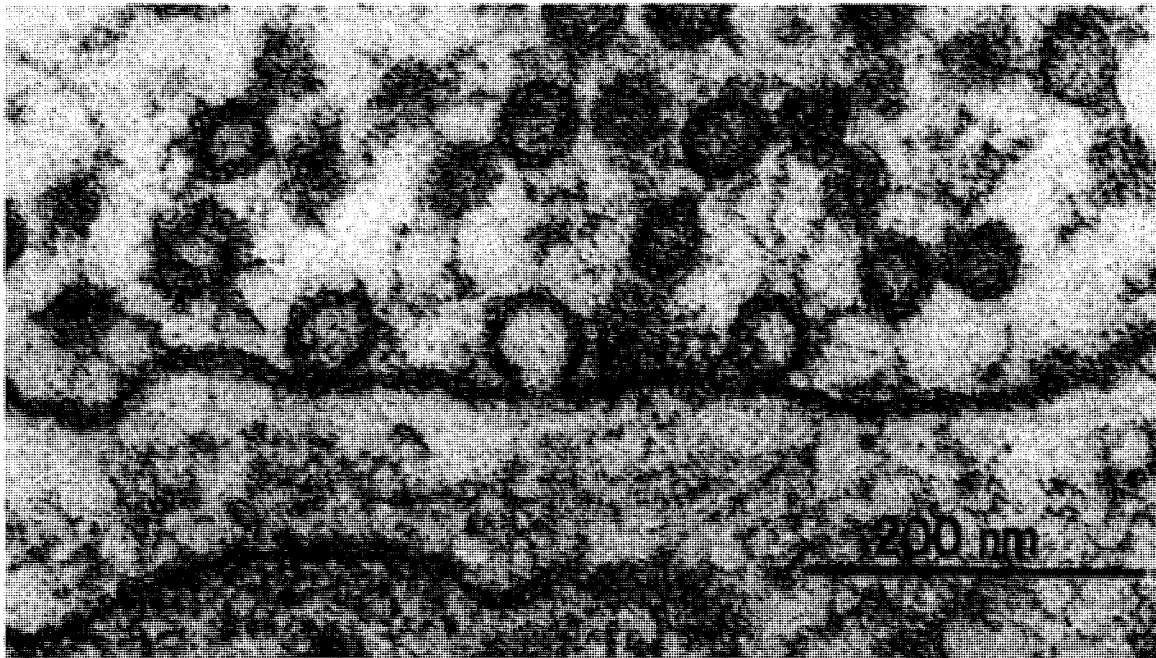


Figure 6.1. An electron micrograph image of transmitter vesicle release at the neuromuscular junction [30].

Figure 6.2 shows an example of this type of three dimensional model and the structure of the coordinates. The detail resolved by the number of levels, annuli, and sectors would, in principle, be limited only by the available computing power.

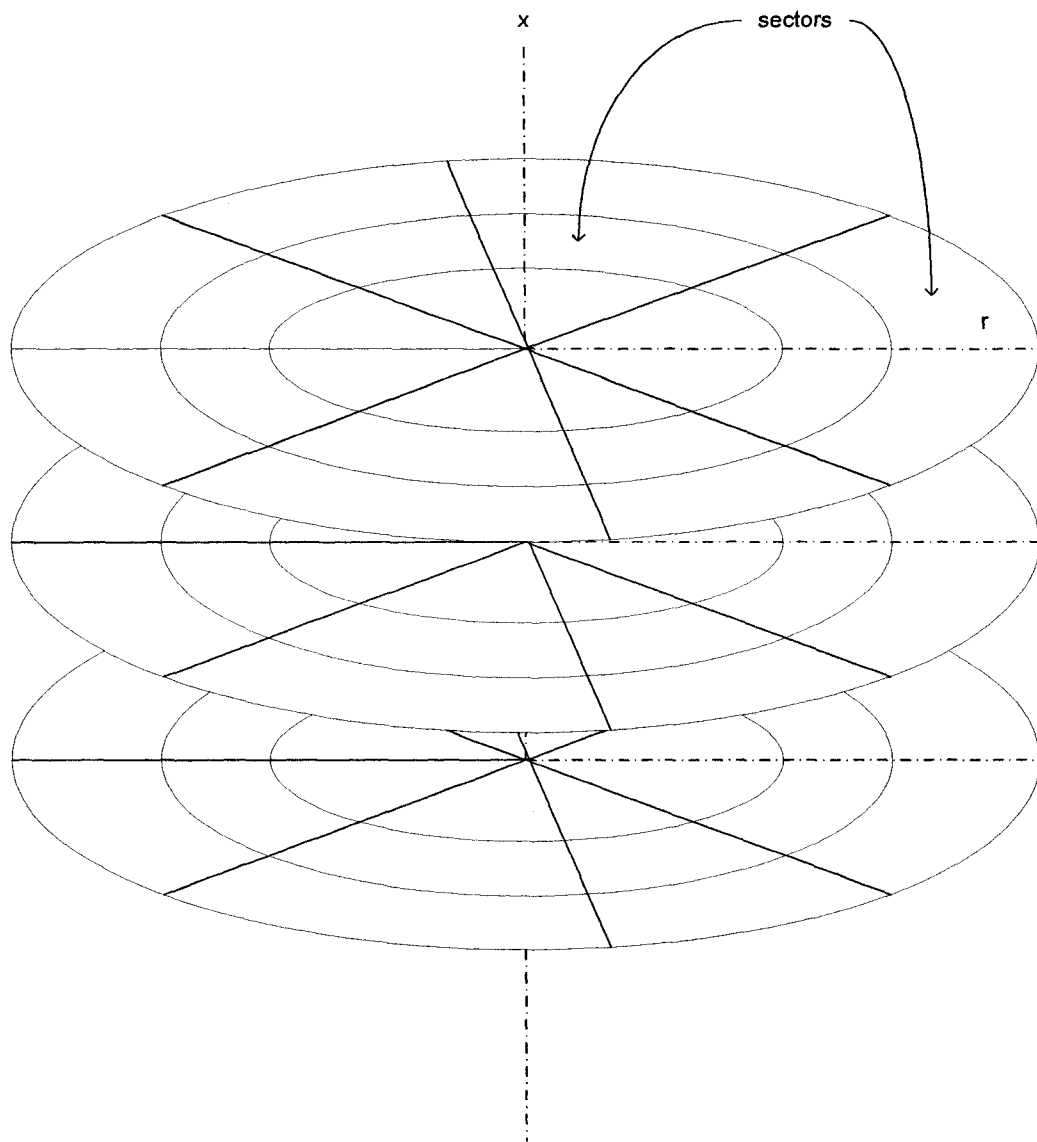


Figure 6.2. An example of a three dimensional discretization of the neuromuscular junction composed of three levels, nine annuli, and seventy-two sectors.

The Jenkins-Szlavik model has a large potential to advance the therapeutic methods of regenerating organophosphorus damaged acetylcholinesterase. The *in vitro* kinetic models of this therapy are well established, but effective therapy for living systems will require investigation of models that reflect a structure closer to that of the

living systems. A model of the regeneration kinetics of acetylcholinesterase in the cleft is a step closer to that goal.

This model can also provide a framework to develop models of prevention of organophosphorus trauma, and prevention is a better countermove than therapy. The core of this prevention process is human butylcholinesterase, and it is used something like a “vaccine” to the organophosphorus “infection”. This enzyme is closely related to acetylcholinesterase, but it is not crucial to neuronal signaling. Butylcholinesterase is found in glial cells and plasma; however, the detailed distribution of butylcholinesterase in the human body is not known [37]. Because its structure is close to acetylcholinesterase and it is a component of plasma, butylcholinesterase can be used as a method to protect against organophosphorus poisoning in an animal model. The basic strategy is to pretreat the blood with an infusion of butylcholinesterase before the encounter with neurotoxin, whereupon it can “soak up” the toxin before the toxin can enter the neuromuscular junction. This strategy of protection is an active area of research and significant progress has been made with kinetic models and experimental measurements [89]-[91]. Certainly the development of therapies and pharmacological preventions to neurotoxin trauma is never trivial, but a big advantage of working with butylcholinesterase is that it occurs in the body naturally, so toxicity issues are minimized. The kinetic model of the reactions in the cleft used in the Jenkins-Szlavik model can be readily adapted to address the chemistry of neurotoxicity prevention. It would be a simple matter to couple the kinetics of butylcholinesterase reacting with neurotoxin in the blood (well mixed) with the diffusion-reaction kinetic events in the

neuromuscular junction in time and space. It would even be possible to examine the effectiveness of butylcholinesterase combined with pyridostigmine, or other therapeutics.

This method-of-lines algorithm has a level of detail that is simple to scale up, and is easily “tuned” to many kinds of physical models. Any number of mobile or immobile chemical species can be implemented, along with their respective kinetic and diffusion constants. Source and sink terms can be applied as a function of any of the system variables, and at any location. In a real sense, the only practical limit is the degree of computing power available. The Jenkins-Szlavik simulation provides an opportunity to recursively couple a highly flexible model to data from experiments supported by state-of-the-art instruments, and this recursive coupling is an excellent way to quantify and advance our knowledge of the processes that occur during neuromuscular transmission.

APPENDIX A

MATLAB SOURCE CODES

```

% THIS PROGRAM QUALITATIVELY WORKS
% Models the complete normal and inhibited chemistry in the neuromuscular junction;
% the model consists of a series of instantly and uniformly mixed
% volumes which share transport of Acetylcholine via 1D diffusion at
% each adjacent border
%
% VOLUME 1
% f(t) ----> A
%
%
% VOLUME 2 - 40
% kD
% A ----> @
%
% U1 U2 kE1 U3 kE2 U4 kE3 U2
% A + E <----> AE ----> acE ----> E + ChP
% kE_1
%
% U2 U9 kI1 U10
% E + I <----> EI
%
% U10 k_dead U11
% EI -----> E_dead

%
% VOLUME 41 - 50
% U1 U5 2*kR1 U6
% A + R <-----> AR
% kR_1
%
% U1 U5 kR2 U7
% A + AR <-----> A2R
% 2*kR_2
%
% U7 oR U8
% A2R <-----> A2R*
% cR

% five CSTR uniform volumes,
%function MOL_50
clc;
clear;
clear;
A_inf = 0.0; % mM
I_inf = 1.65e-7; % mM
% total volume in the cleft
V_cleft = 3.93e-17; % ( L )

```

```

% the length of the cleft (width, or height) (L^1/3)
L_cleft = 5.0e-7;

% the radius of the cleft (L^1/3)
R_cleft = 5.0e-6;

% the number of equal axial disks
P = 1;
x_cleft = zeros(1,P)

% the number of annular rings per disk
Q = 20;

% number of coupled sub-volumes
S = P*Q

%thickness of each radial annulus
dr = R_cleft/Q;

%thickness of each axial disk
dx = L_cleft/P;

% area of the cleft edge
Area_edge = 2*pi*R_cleft*L_cleft;

% axial direction vector
x = linspace(0.0, L_cleft, P+1);

%radial direction vector
r = linspace(0.0, R_cleft, Q);

% This loop assigns an x-value coordinate to the center of each well mixed
% axial disk
for j = 1:P
    x_cleft(j) = 0.5*( x(j) + x(j+1) );
end
x_cleft;

% create the "space", a 1-dimension vector that all the axial and radial volume points are mapped
% into
s = [1:S];

% axial diffusion constant (cm^2/ms)
D_x = 2.0e-9;

% radial diffusion constant for Ach (L^2/3*ms^-1)
D_r = 3.50e-11; % 3.50e-11

% radial diffusion constant for the inhibitor
D_r_tox = 3.5e-11;

%number of time points

```



```

N=2000;

%number of time samples
n_sample = 15;

N_grad =floor(linspace(1, N, n_sample))%these values need to be integers because they will be
vector indices

%time interval vector for the normal and inhibited reactions (ms, 1e-3 s)
t_0 = 0.0; t_f = 5.0; % ms
t = linspace(t_0, t_f, N);
tspan = [t];

%time interval vector for the diffusing toxin reaction
t_tox_0 = 0.0; t_tox_f = 4.0e+7; % ms
t_tox = linspace(t_tox_0, t_tox_f, N);
tspan_tox = [t_tox];

% pulse parameters
t_on = 3.0; t_off = 4.50; %*THIS IS NOT THE TIME INTERVAL*

n_on = round((((t_on - t_0)/(t_f - t_0))*(length(t)-1) + 1);
n_off = round(((t_off - t_0)*(length(t) - 1)/( t_f - t_0) + 1);
peak = round(0.5*(n_on + n_off));
spread = 20.0;
magnitude = 0.50;

% calculate the volume of each annulus
volume = zeros(1,Q); % ( L )
vol_frac = volume;
for i=1:Q
    volume(i) = ((2*i-1)/Q^2)*pi*L_cleft*R_cleft^2;
    vol_frac(i) = volume(i)/V_cleft;
end
sum(volume(1:Q)); % a check of the annuli sum should equal the V_cleft
sum(vol_frac(1:Q));
V_cleft;

% forward and backwards difference vectors
r_grad_b = r(2:length(r));
r_grad_f = r(1:length(r)-1);

% defining the initial value vectors of the diffusing toxin reaction reactants
A_0_tox = zeros(1,S);
E_0_tox = zeros(1,S);
AE_0_tox = zeros(1,S);
acE_0_tox = zeros(1,S);
R_0_tox = zeros(1,S);
AR_0_tox = zeros(1,S);

```

```

A2R_0_tox = zeros(1,S);
A2Ro_0_tox = zeros(1,S);
I_0_tox = zeros(1,S);
EI_0_tox = zeros(1,S);
E_dead_0_tox = zeros(1,S);
ChP_0_tox = zeros(1,S);

% defining the initial value vectors of the normal AP reaction reactants
A_0_n = zeros(1,S);
E_0_n = zeros(1,S);
AE_0_n = zeros(1,S);
acE_0_n = zeros(1,S);
R_0_n = zeros(1,S);
AR_0_n = zeros(1,S);
A2R_0_n = zeros(1,S);
A2Ro_0_n = zeros(1,S);
ChP_0_n = zeros(1,S);

% defining the initial value vectors of the inhibited AP reaction
% reactants,
A_0_i = zeros(1,S);
E_0_i = zeros(1,S);
AE_0_i = zeros(1,S);
acE_0_i = zeros(1,S);
R_0_i = zeros(1,S);
AR_0_i = zeros(1,S);
A2R_0_i = zeros(1,S);
A2Ro_0_i = zeros(1,S);
I_0_i = zeros(1,S);
EI_0_i = zeros(1,S);
E_dead_0_i = zeros(1,S);
ChP_0_i = zeros(1,S);

factor_R= 1.0;
standard_R = 0.664;

% Toxin diffusion reaction initial cleft values of A, E, R in mM
A_0_tox(1,1) = 0.0; % in mM (10 annuli is used as the control reference)
E_0_tox(1,:) = 0.0277; % in mM
R_0_tox(1,:) = factor_R*standard_R; % in mM

% Toxin diffusion reaction initial value vector
W0 = [A_0_tox ... A ( V(1)-V(Q) )
      E_0_tox ... E ( V(Q+1) - V(2Q) )
      AE_0_tox ... AE ( V(2Q+1) - V(3Q) )
      acE_0_tox ... acE ( V(3Q+1) - V(4Q0) )
      R_0_tox ... R ( V(4Q+1) - V(5Q) )
      AR_0_tox ... AR ( V(5Q+1) - V(6Q) )
      A2R_0_tox ... A2R ( V(6Q+1) - V(7Q) )
      A2Ro_0_tox ... A2R* ( V(7Q+1) - V(8Q) )
      I_0_tox ... I ( V(8Q+1) - V(9Q) )
      EI_0_tox ... EI ( V(9Q+1) - V(10Q) )

```

```

E_dead_0_tox ...E_dead ( V(10Q+1) - V(11Q) )
ChP_0_tox ... ChP ( V(11Q+1) - V(12Q) )

];

E_tox = zeros(length(t), length(r)); % toxin diffusion enzyme reaction matrix
R_tox = zeros(length(t), length(r)); % toxin diffusion receptor reaction matrix
I_tox = zeros(length(t), length(r)); % toxin diffusion inhibitor of esterase
EI_tox = zeros(length(t), length(r)); % toxin diffusion enzyme-toxin reaction matrix
E_dead_tox = zeros(length(t), length(r)); %toxin diffusion poisoned enzyme reaction matrix

E_cleft_tox = zeros(N,1); % toxin diffusion reaction species
R_cleft_tox = zeros(N,1);
I_cleft_tox = zeros(N,1);
EI_cleft_tox = zeros(N,1);
E_dead_cleft_tox = zeros(N,1);

molecule_E_cleft_tox = zeros(N,1); % toxin diffusion reaction species
molecule_R_cleft_tox = zeros(N,1);
molecule_I_cleft_tox = zeros(N,1);
molecule_EI_cleft_tox = zeros(N,1);
molecule_E_dead_cleft_tox = zeros(N,1);

% run the diffusing toxin reaction function
[t_tox, W]= ode15s(@Func_Radial_toxin_kinetics, tspan_tox, W0, [], D_x, D_r, D_r_tox, r, dx, dr,
t_on, t_off );

for i = 1:length(t) % time length vector
    for j = 1:length(r) % radius length vector

        E_tox(i,j) = W(i,j+Q); % toxic diffusion reaction species
        R_tox(i,j) = W(i,j+4*Q);
        I_tox(i,j) = W(i,j+8*Q);
        EI_tox(i,j) = W(i,j+9*Q);
        E_dead_tox(i,j) = W(i,j+10*Q);
    end
end

% calculate the total amounts of these species in the cleft
for i = 1:N
    for j = 1:Q

        E_cleft_tox(i) = E_cleft_tox(i) +(volume(j)*E_tox(i,j))/V_cleft; % toxin diffusion molar
        species
        R_cleft_tox(i) = R_cleft_tox(i) +(volume(j)*R_tox(i,j))/V_cleft;
        I_cleft_tox(i) = I_cleft_tox(i) +(volume(j)*I_tox(i,j))/V_cleft;
    end
end

```

```

EI_cleft_tox(i) = EI_cleft_tox(i) +(volume(j)*EI_tox(i,j))/V_cleft;
E_dead_cleft_tox(i) = E_dead_cleft_tox(i) +(volume(j)*E_dead_tox(i,j))/V_cleft;

    molecule_E_cleft_tox(i) = E_cleft_tox(i)*V_cleft*(6.02e+20); % toxin diffusion molecule
species
    molecule_R_cleft_tox(i) = R_cleft_tox(i)*V_cleft*(6.02e+20);
    molecule_I_cleft_tox(i) = I_cleft_tox(i)*V_cleft*(6.02e+20);
    molecule_EI_cleft_tox(i) = EI_cleft_tox(i)*V_cleft*(6.02e+20);
    molecule_E_dead_cleft_tox(i) = E_dead_cleft_tox(i)*V_cleft*(6.02e+20);
end
end
t_min = t_tox./(1000*60);
%{
figure(1)
plot(t_min, E_dead_cleft_tox)
title(sprintf('Concentration of poisoned enzyme vs time \n soman kinetics and blood concentration
of %i mM\n initial active enzyme %i mM', I_inf, E_cleft_tox(1,1)));
xlabel('time, min'); ylabel('Poisoned Enzyme, mM');
%}
figure(2)
E_tox_active_frac = 100*((E_0_tox(1,1)-E_dead_cleft_tox)/E_0_tox(1,1));
plot(t_min, E_tox_active_frac)
title(sprintf('Percent enzyme active in cleft vs. time,\n with soman kinetics and blood concentration
of %i mM ', (I_inf)));
xlabel('time, min'); ylabel('Percent active enzyme');

% tolerance value
tol = 0.0001;
loop_count = 0;
choice = 1;

while(choice == 1)

E_i_active_percent = input('What percent active enzyme will be in the cleft during the inhibited
action potential reaction?\n');

E_initial_inhibited = (E_i_active_percent/100)*E_0_tox(1,1); % in mM
disp(sprintf('\n The initial amount of active enzyme in the cleft \n during the inhibited reaction is
%i mM ', E_initial_inhibited));

tox_index = find((E_cleft_tox >= E_initial_inhibited - tol) & (E_cleft_tox <= E_initial_inhibited +
tol), 1);
disp(sprintf('\n The location of the time point index is %i ', tox_index));

disp(sprintf('\n This is equivalent to starting the action potential after %i minutes have passed
since exposure to the toxic inhibitor \n ', t_tox(tox_index)/(60000)));

%E_cleft_tox'

```

```

factor_A = 1.0;
standard_A = 42.3*((Q/10)^2);
factor_E = 1.0;
standard_E = 0.0277;
% Normal AP reaction initial cleft values of A, E, R in mM
A_0_n(1,1) = factor_A*standard_A; % in mM (10 annuli is used as the control reference)
E_0_n(1,:) = factor_E*standard_E; % in mM
R_0_n(1,:) = factor_R*standard_R; % in mM

```

```

%normal AP reaction initial value vector
U0 = [ A_0_n ... A ( U(1) - U(Q) )
      E_0_n ... E ( U(Q+1) - U(2Q) )
      AE_0_n ... AE ( U(2Q+1) - U(3Q) )
      acE_0_n ... acE ( U(3Q+1) - U(4Q) )
      R_0_n ... R ( U(4Q+1) - U(5Q) )
      AR_0_n ... AR ( U(5Q+1) - U(6Q) )
      A2R_0_n ... A2R ( U(6Q+1) - U(7Q) )
      A2Ro_0_n ... A2R* ( U(7Q+1) - U(8Q) )
      ChP_0_n ... ChP ( U(8Q+1) - U(9Q) )
      ];

```

```

% Inhibited AP reaction initial cleft values of A, E, R in mM
A_0_i(1,1) = factor_A*standard_A; % in mM (10 annuli is used as the control reference)
E_0_i(1,:) = E_tox(tox_index,:); % in mM
R_0_i(1,:) = R_tox(tox_index,:); % in mM
I_0_i(1,:) = I_tox(tox_index,:); % in mM
EI_0_i(1,:) = EI_tox(tox_index,:); % in mM
E_dead_0_i = E_dead_tox(tox_index,:); % in mM

```

```

% Inhibited AP reaction initial value vector
V0 = [ A_0_i ... A ( V(1)-V(Q) )
      E_0_i ... E ( V(Q+1) - V(2Q) )
      AE_0_i ... AE ( V(2Q+1) - V(3Q) )
      acE_0_i ... acE ( V(3Q+1) - V(4Q0) )
      R_0_i ... R ( V(4Q+1) - V(5Q) )
      AR_0_i ... AR ( V(5Q+1) - V(6Q) )
      A2R_0_i ... A2R ( V(6Q+1) - V(7Q) )
      A2Ro_0_i ... A2R* ( V(7Q+1) - V(8Q) )
      I_0_i ... I ( V(8Q+1) - V(9Q) )
      EI_0_i ... EI ( V(9Q+1) - V(10Q) )
      E_dead_0_i ... E_dead ( V(10Q+1) - V(11Q) )
      ChP_0_i ... ChP ( V(11Q+1) - V(12Q) )
      ];

```

```

% run the normal enzyme reaction function
[t,U] = ode15s(@Func_Radial_normal_kinetics, tspan, U0, [], D_x, D_r, r, dx, dr, t_on, t_off);

```

```

% run the inhibited enzyme reaction function

```

```
[t,V]=ode15s(@Func_Radial_inhibited_kinetics, tspan, V0, [], D_x, D_r, D_r_tox, r, dx, dr, t_on,
t_off);
```

```
% create the normal and inhibited reaction species concentration matrices as functions of r and t
A_n = zeros(length(t),length(r)); % normal acetylcholine reaction matrix
E_n = zeros(length(t), length(r)); % normal enzyme reaction matrix
AE_n = zeros(length(t), length(r));% normal enzyme-complex reaction matrix
acE_n = zeros(length(t), length(r));% normal acylated-enzyme reaction matrix
R_n = zeros(length(t), length(r));% normal receptor reaction matrix
AR_n = zeros(length(t), length(r));% normal single bound receptor reaction matrix
A2R_n = zeros(length(t), length(r));% normal double bound receptor reaction matrix
A2Ro_n = zeros(length(t), length(r));% normal open receptor reaction matrix
ChP_n = zeros(length(t), length(r));% normal choline/product reaction matrix
```

```
A_i = zeros(length(t), length(r)); % inhibited acetylcholine reaction matrix
E_i = zeros(length(t), length(r)); % inhibited enzyme reaction matrix
AE_i = zeros(length(t), length(r)); % inhibited enzyme-complex reaction matrix
acE_i = zeros(length(t), length(r)); % inhibited acylated-enzyme reaction matrix
R_i = zeros(length(t), length(r));% inhibited receptor reaction matrix
AR_i = zeros(length(t), length(r));% inhibited single bound receptor reaction matrix
A2R_i = zeros(length(t), length(r));% inhibited double bound receptor reaction matrix
A2Ro_i = zeros(length(t), length(r));% inhibited open receptor reaction matrix
I_i = zeros(length(t), length(r)); % inhibitor of esterase
EI_i = zeros(length(t), length(r)); % enzyme-toxin reaction matrix
E_dead_i = zeros(length(t), length(r)); % poisoned enzyme reaction matrix
ChP_i = zeros(length(t), length(r)); % inhibited choline/product reaction matrix
```

```
for q = 1:length(N_grad) %represents the distributed time points in N, accessed through
N_grad(q)
```

```
for i = 1:length(t) % time length vector
for j = 1:length(r) % radius length vector
```

```
A_n(i,j) = U(i,j); % normal reaction species
E_n(i,j) = U(i,j+Q);
AE_n(i,j) = U(i,j+2*Q);
acE_n(i,j) = U(i,j+3*Q);
R_n(i,j) = U(i,j+4*Q);
AR_n(i,j) = U(i,j+5*Q);
A2R_n(i,j) = U(i,j+6*Q);
A2Ro_n(i,j) = U(i,j+7*Q);
ChP_n(i,j) = U(i,j+8*Q);
```

```
A_i(i,j) = V(i,j); % inhibited reaction species
E_i(i,j) = V(i,j+Q);
AE_i(i,j) = V(i,j+2*Q);
acE_i(i,j) = V(i,j+3*Q);
R_i(i,j) = V(i,j+4*Q);
AR_i(i,j) = V(i,j+5*Q);
A2R_i(i,j) = V(i,j+6*Q);
A2Ro_i(i,j) = V(i,j+7*Q);
```

```

    I_i(i,j) = V(i,j+8*Q);
    EI_i(i,j) = V(i,j+9*Q);
    E_dead_i(i,j) = V(i,j+10*Q);
    ChP_i(i,j) = V(i,j+11*Q);
end
end

% calculate the concentration gradients of these species
cocn_grad_A_n = diff(A_n(N_grad(q,:))./diff(r);
cocn_grad_I = diff(I_i(N_grad(q,:))./diff(r);
cocn_grad_E = diff(E_i(N_grad(q,:))./diff(r);

%plot(r, A_n(N_grad(q,:))); hold on;
figure(1)
title('[A] gradient')
plot(r_grad_b, cocn_grad_A_n); hold on;

figure (2)
title('[I] gradient')
plot(r_grad_b, cocn_grad_I); hold on;

figure (3)
title('[E] gradient')
plot(r_grad_b, cocn_grad_E); hold on;

end
hold off;

%2*pi*R_cleft*L_cleft*D_r/dr

% calculate the normal and inhibited Ach lost from the last annulus via diffusion
%[t, A_lost] = ode15s(@Acetylcholine_lost, tspan, A_n(1,14), [], D_r, dr, r);

%A_n_lost = (D_r/(2*r(15)*dr))*(A_inf - A_n(:,14))%cumtrapz(t,(2*pi*R_cleft*L_cleft*D_r/1e-
18)*A_n(:,Q));
%A_i_lost = cumtrapz(t,(2*pi*R_cleft*L_cleft*D_r/1e-18)*A_i(:,Q));

% initialize the total concentration/molecules in the cleft vectors

A_cleft_n = zeros(N,1);% normal reaction species
E_cleft_n = zeros(N,1);
AĒ_cleft_n = zeros(N,1);

```

```

acE_cleft_n = zeros(N,1);
R_cleft_n = zeros(N,1);
AR_cleft_n = zeros(N,1);
A2R_cleft_n = zeros(N,1);
A2Ro_cleft_n = zeros(N,1);
ChP_cleft_n = zeros(N,1);

molecule_A_cleft_n = zeros(N,1);% normal reaction species
molecule_E_cleft_n = zeros(N,1);
molecule_AE_cleft_n = zeros(N,1);
molecule_acE_cleft_n = zeros(N,1);
molecule_R_cleft_n = zeros(N,1);
molecule_AR_cleft_n = zeros(N,1);
molecule_A2R_cleft_n = zeros(N,1);
molecule_A2Ro_cleft_n = zeros(N,1);
molecule_ChP_cleft_n = zeros(N,1);

A_cleft_i = zeros(N,1); % inhibited reaction species
E_cleft_i = zeros(N,1);
AE_cleft_i = zeros(N,1);
acE_cleft_i = zeros(N,1);
R_cleft_i = zeros(N,1);
AR_cleft_i = zeros(N,1);
A2R_cleft_i = zeros(N,1);
A2Ro_cleft_i = zeros(N,1);
I_cleft_i = zeros(N,1);
EI_cleft_i = zeros(N,1);
E_dead_cleft_i = zeros(N,1);
ChP_cleft_i = zeros(N,1);

molecule_A_cleft_i = zeros(N,1);% inhibited reaction species
molecule_E_cleft_i = zeros(N,1);
molecule_AE_cleft_i = zeros(N,1);
molecule_acE_cleft_i = zeros(N,1);
molecule_R_cleft_i = zeros(N,1);
molecule_AR_cleft_i = zeros(N,1);
molecule_A2R_cleft_i = zeros(N,1);
molecule_A2Ro_cleft_i = zeros(N,1);
molecule_I_cleft_i = zeros(N,1);
molecule_EI_cleft_i = zeros(N,1);
molecule_E_dead_cleft_i = zeros(N,1);
molecule_ChP_cleft_i = zeros(N,1);

%{
%Species names
species_names = ['A','E','AE','acE','R','AR','A2R','A2R*','I','EI','E_dead','ChP','A_lost'];
species_names(1)
species_names(2)
%}

% calculate the total amounts of these species in the cleft
for i = 1:N
    for j = 1:Q

        A_cleft_n(i) = A_cleft_n(i) +(volume(j)*A_n(i,j))/V_cleft; %normal molar species
    
```



```

E_cleft_n(i) = E_cleft_n(i) +(volume(j)*E_n(i,j))/V_cleft;
AE_cleft_n(i) = AE_cleft_n(i) +(volume(j)*AE_n(i,j))/V_cleft;
acE_cleft_n(i) = acE_cleft_n(i) +(volume(j)*acE_n(i,j))/V_cleft;
R_cleft_n(i) = R_cleft_n(i) +(volume(j)*R_n(i,j))/V_cleft;
AR_cleft_n(i) = AR_cleft_n(i) +(volume(j)*AR_n(i,j))/V_cleft;
A2R_cleft_n(i) = A2R_cleft_n(i) +(volume(j)*A2R_n(i,j))/V_cleft;
A2Ro_cleft_n(i) = A2Ro_cleft_n(i) +(volume(j)*A2Ro_n(i,j))/V_cleft;
ChP_cleft_n(i) = ChP_cleft_n(i) +(volume(j)*ChP_n(i,j))/V_cleft;

A_cleft_i(i) = A_cleft_i(i) +(volume(j)*A_i(i,j))/V_cleft;    % inhibited molar species
E_cleft_i(i) = E_cleft_i(i) +(volume(j)*E_i(i,j))/V_cleft;
AE_cleft_i(i) = AE_cleft_i(i) +(volume(j)*AE_i(i,j))/V_cleft;
acE_cleft_i(i) = acE_cleft_i(i) +(volume(j)*acE_i(i,j))/V_cleft;
R_cleft_i(i) = R_cleft_i(i) +(volume(j)*R_i(i,j))/V_cleft;
AR_cleft_i(i) = AR_cleft_i(i) +(volume(j)*AR_i(i,j))/V_cleft;
A2R_cleft_i(i) = A2R_cleft_i(i) +(volume(j)*A2R_i(i,j))/V_cleft;
A2Ro_cleft_i(i) = A2Ro_cleft_i(i) +(volume(j)*A2Ro_i(i,j))/V_cleft;
I_cleft_i(i) = I_cleft_i(i) +(volume(j)*I_i(i,j))/V_cleft;
EI_cleft_i(i) = EI_cleft_i(i) +(volume(j)*EI_i(i,j))/V_cleft;
E_dead_cleft_i(i) = E_dead_cleft_i(i) +(volume(j)*E_dead_i(i,j))/V_cleft;
ChP_cleft_i(i) = ChP_cleft_i(i) +(volume(j)*ChP_i(i,j))/V_cleft;

molecule_A_cleft_n(i) = A_cleft_n(i)*V_cleft*(6.02e+20);    %normal molecule species
molecule_E_cleft_n(i) = E_cleft_n(i)*V_cleft*(6.02e+20);
molecule_AE_cleft_n(i) = AE_cleft_n(i)*V_cleft*(6.02e+20);
molecule_acE_cleft_n(i) = acE_cleft_n(i)*V_cleft*(6.02e+20);
molecule_R_cleft_n(i) = R_cleft_n(i)*V_cleft*(6.02e+20);
molecule_AR_cleft_n(i) = AR_cleft_n(i)*V_cleft*(6.02e+20);
molecule_A2R_cleft_n(i) = A2R_cleft_n(i)*V_cleft*(6.02e+20);
molecule_A2Ro_cleft_n(i) = A2Ro_cleft_n(i)*V_cleft*(6.02e+20);
molecule_ChP_cleft_n(i) = ChP_cleft_n(i)*V_cleft*(6.02e+20);

molecule_A_cleft_i(i) = A_cleft_i(i)*V_cleft*(6.02e+20);    %inhibited molecule species
molecule_E_cleft_i(i) = E_cleft_i(i)*V_cleft*(6.02e+20);
molecule_AE_cleft_i(i) = AE_cleft_i(i)*V_cleft*(6.02e+20);
molecule_acE_cleft_i(i) = acE_cleft_i(i)*V_cleft*(6.02e+20);
molecule_R_cleft_i(i) = R_cleft_i(i)*V_cleft*(6.02e+20);
molecule_AR_cleft_i(i) = AR_cleft_i(i)*V_cleft*(6.02e+20);
molecule_A2R_cleft_i(i) = A2R_cleft_i(i)*V_cleft*(6.02e+20);
molecule_A2Ro_cleft_i(i) = A2Ro_cleft_i(i)*V_cleft*(6.02e+20);
molecule_I_cleft_i(i) = I_cleft_i(i)*V_cleft*(6.02e+20);
molecule_EI_cleft_i(i) = EI_cleft_i(i)*V_cleft*(6.02e+20);
molecule_E_dead_cleft_i(i) = E_dead_cleft_i(i)*V_cleft*(6.02e+20);
molecule_ChP_cleft_i(i) = ChP_cleft_i(i)*V_cleft*(6.02e+20);
end
end

%figure(loop_count + 3)

%plot( t, molecule_A2Ro_cleft_n(:),t,molecule_A2Ro_cleft_i(:));
%ylabel('molecules of open receptor');xlabel('t, ms');

```

```

%title(sprintf('Total molecules of open receptor species A2R* in the whole cleft,\n norm and
inhibited, averaged over %i annular volume elements,\n %i percent active enzyme; D_r = %i',Q,
E_i_active_percent,D_r));%

loop_count = loop_count+1;
choice = input('Do you want to run another inhibited reaction: 1(yes), 0(no)? \n');
end

% save the species concentration data to data files
save U U; save V V; save W W;

save A_0_n A_0_n; save A_0_i A_0_i; save E_0_i E_0_i;
save E_0_tox E_0_tox;

save A_n A_n; save E_n E_n; save AE_n AE_n; save acE_n acE_n; save R_n R_n; save AR_n
AR_n; save A2R_n A2R_n;
save A2Ro_n A2Ro_n; save ChP_n ChP_n; %save A_n_lost A_n_lost;

save A_i A_i; save E_i E_i; save AE_i AE_i; save acE_i acE_i; save EI_i EI_i; save E_dead_i
E_dead_i; save R_i R_i;
save AR_i AR_i; save A2R_i A2R_i; save A2Ro_i A2Ro_i; save I_i I_i; save ChP_i ChP_i; %save
A_i_lost A_i_lost;

save A_cleft_n A_cleft_n; save E_cleft_n E_cleft_n;
save AE_cleft_n AE_cleft_n; save acE_cleft_n acE_cleft_n; save R_cleft_n R_cleft_n;
save AR_cleft_n AR_cleft_n; save A2R_cleft_n A2R_cleft_n;
save A2Ro_cleft_n A2Ro_cleft_n; save ChP_cleft_n ChP_cleft_n;

save A_cleft_i A_cleft_i; save E_cleft_i E_cleft_i; save AE_cleft_i AE_cleft_i;
save acE_cleft_i acE_cleft_i; save R_cleft_i R_cleft_i; save AR_cleft_i AR_cleft_i;
save A2R_cleft_i A2R_cleft_i; save A2Ro_cleft_i A2Ro_cleft_i; save I_cleft_i I_cleft_i;
save EI_cleft_i EI_cleft_i; save E_dead_cleft_i E_dead_cleft_i;
save ChP_cleft_i ChP_cleft_i;

save molecule_A_cleft_n molecule_A_cleft_n;
save molecule_E_cleft_n molecule_E_cleft_n;
save molecule_AE_cleft_n molecule_AE_cleft_n;
save molecule_acE_cleft_n molecule_acE_cleft_n;
save molecule_R_cleft_n molecule_R_cleft_n;
save molecule_AR_cleft_n molecule_AR_cleft_n;
save molecule_A2R_cleft_n molecule_A2R_cleft_n;
save molecule_A2Ro_cleft_n molecule_A2Ro_cleft_n;
save molecule_ChP_cleft_n molecule_ChP_cleft_n;

save molecule_A_cleft_i molecule_A_cleft_i;
save molecule_E_cleft_i molecule_E_cleft_i;
save molecule_AE_cleft_i molecule_AE_cleft_i;
save molecule_acE_cleft_i molecule_acE_cleft_i;
save molecule_R_cleft_i molecule_R_cleft_i;
save molecule_AR_cleft_i molecule_AR_cleft_i;
save molecule_A2R_cleft_i molecule_A2R_cleft_i;
save molecule_A2Ro_cleft_i molecule_A2Ro_cleft_i;
save molecule_I_cleft_i molecule_I_cleft_i;

```

```

save molecule_EI_cleft_i molecule_EI_cleft_j;
save molecule_E_dead_cleft_i molecule_E_dead_cleft_j;
save molecule_ChP_cleft_i molecule_ChP_cleft_j;

save E_cleft_tox E_cleft_tox;
save R_cleft_tox R_cleft_tox;
save I_cleft_tox I_cleft_tox;
save EI_cleft_tox EI_cleft_tox;
save E_dead_cleft_tox E_dead_cleft_tox;

save molecule_E_cleft_tox molecule_E_cleft_tox;
save molecule_R_cleft_tox molecule_R_cleft_tox;
save molecule_I_cleft_tox molecule_I_cleft_tox;
save molecule_EI_cleft_tox molecule_EI_cleft_tox;
save molecule_E_dead_cleft_tox molecule_E_dead_cleft_tox;

save r r; save D_r D_r; save dr dr;
save t t; save t_tox t_tox;
save N N; save Q Q;
save volume volume;
save I_inf I_inf;

disp('latest data saved, program finished');

%{
figure(2)
plot(t,A_lost);
ylabel('normal Ach, mM');xlabel('t, ms');
title(sprintf('Molar normal Ach lost via diffusion, in the whole cleft\n averaged over %i annular
volume elements',Q));%

figure(1)
surf(t, r, A_n')
shading flat
title(sprintf('Species A in pure radial diffusion and reaction through %i volume elements', Q));
xlabel('time, ms'); ylabel('radius, cm'); zlabel(' concentration, mmole/cm^3');
A_lost
%A_balance =
sum(U(:,1:10))+sum(U(:,21:30))+sum(U(:,51:60))+sum(U(:,61:70))+sum(U(:,71:80))

%}

```

```

% THIS PROGRAM QUALITATIVELY WORKS
% This program simulates the regeneration of acetylcholinesterase in the
% cleft

%***** CHECKED FOR UNIT/DIMENSION CONSISTENCY ON 4/15/07, 17:00
*****
%

clc;
clear;
% if the diffusion constant has dimensions of cm^3/ms then the following
% units apply
A_inf = 0.0; % mmole/cm^3 = M
save A_inf A_inf;
I_inf = 2.65e-2; % mmole/cm^3 = M
save I_inf I_inf;
OX_inf = 7.30e-5; % mmole/cm^3 = M
save OX_inf OX_inf;

% total volume in the cleft
V_cleft = 3.93e-14; % ( cm^3 )

% the length of the cleft (width, or height) (L^1/3)
L_cleft = 5.0e-6; % cm

% the radius of the cleft
R_cleft = 5.0e-5; % cm

% the number of equal axial disks
P = 1;
x_cleft = zeros(1,P)

% the number of annular rings per disk
Q = 20;

% number of coupled sub-volumes
S = P*Q

%thickness of each radial annulus
dr = R_cleft/Q; % cm

%thickness of each axial disk
dx = L_cleft/P; %cm

% area of the cleft edge
Area_edge = 2*pi*R_cleft*L_cleft; %cm^2

% axial direction vector
x = linspace(0.0, L_cleft, P+1);

%radial direction vector

```

```

r = linspace(0.0, R_cleft, Q);
save r r;

% This loop assigns an x-value coordinate to the center of each well mixed
% axial disk
for j = 1:P
    x_cleft(j) = 0.5*( x(j) + x(j+1) );
end
x_cleft;
save x_cleft x_cleft;

% create the "space", a 1-dimension vector that all the axial and radial volume points are mapped
% into
s = [1:S];

% axial diffusion constantfor Ach (cm^2/ms)
D_x = 2.0e-9;

% radial diffusion constant for Ach (cm^2/ms)
D_r_Ach = 0.90e-9; % 3.50e-9 cm^2/ms
save D_r_Ach D_r_Ach;

% radial diffusion constant for the inhibitor
D_r_tox = 0.90e-9 %cm^2/ms ; %logspace(-6,-12,10)
save D_r_tox D_r_tox;

% radial diffusion constant for the oxime
D_r_oxime = 0.9e-9 %cm^2/ms; %logspace(-6,-12,10) %
save D_r_oxime D_r_oxime;

%number of time points
N=7000;

%time interval vector for the normal and inhibited reactions (ms, 1e-3 s)
t_0 = 0.0; t_f = 5.0; % ms
t = linspace(t_0, t_f, N);
tspan = [t];

%time interval vector for the diffusing oxime reaction
t_regen_0 = 0.0; t_regen_f = 2.50e+5; % ms
t_regen = linspace(t_regen_0, t_regen_f, N);
tspan_regen = [t_regen];

% pulse parameters
t_on = 3.0; t_off = 4.50; % ms    %*THIS IS NOT THE TIME INTERVAL*

n_on = round((((t_on - t_0)/(t_f - t_0))*(length(t)-1)) + 1);
n_off = round(((t_off - t_0)*(length(t) - 1)/( t_f - t_0) + 1);
peak = round(0.5*(n_on + n_off));
spread = 20.0;
magnitude = 0.50;

```

```

% calculate the volume of each annulus
volume = zeros(1,Q); % ( cm^3 )
vol_frac = volume;
for i=1:Q
    volume(i) = ((2*i-1)/Q^2)*pi*L_cleft*R_cleft^2;
    vol_frac(i) = volume(i)/V_cleft;
end
sum(volume(1:Q)); % a check of the annuli sum should equal the V_cleft
sum(vol_frac(1:Q));
V_cleft;

```

```

% defining the initial value vectors of the diffusing toxin reaction reactants
A_0_tox = zeros(1,S);
E_0_tox = zeros(1,S);
AE_0_tox = zeros(1,S);
acE_0_tox = zeros(1,S);
R_0_tox = zeros(1,S);
AR_0_tox = zeros(1,S);
A2R_0_tox = zeros(1,S);
A2Ro_0_tox = zeros(1,S);
I_0_tox = zeros(1,S);
EI_0_tox = zeros(1,S);
E_dead_0_tox = zeros(1,S);
ChP_0_tox = zeros(1,S);

```

```

% defining the initial value vectors of the normal AP reaction reactants
A_0_n = zeros(1,S);
E_0_n = zeros(1,S);
AE_0_n = zeros(1,S);
acE_0_n = zeros(1,S);
R_0_n = zeros(1,S);
AR_0_n = zeros(1,S);
A2R_0_n = zeros(1,S);
A2Ro_0_n = zeros(1,S);
ChP_0_n = zeros(1,S);

```

```

% defining the initial value vectors of the inhibited AP reaction
% reactants,
A_0_i = zeros(1,S);
E_0_i = zeros(1,S);
AE_0_i = zeros(1,S);
acE_0_i = zeros(1,S);
R_0_i = zeros(1,S);
AR_0_i = zeros(1,S);
A2R_0_i = zeros(1,S);
A2Ro_0_i = zeros(1,S);
I_0_i = zeros(1,S);
EI_0_i = zeros(1,S);
E_dead_0_i = zeros(1,S);
ChP_0_i = zeros(1,S);

```

```

% defining the initial value vectors of the oxime regeneration reaction
% reactants,
A_0_regen = zeros(1,S);
E_0_regen = zeros(1,S);
AE_0_regen = zeros(1,S);
acE_0_regen = zeros(1,S);
R_0_regen = zeros(1,S);
AR_0_regen = zeros(1,S);
A2R_0_regen = zeros(1,S);
A2Ro_0_regen = zeros(1,S);
E_dead_0_regen = zeros(1,S);
OX_0_regen = zeros(1,S);
EIOX_0_regen = zeros(1,S);
IOX_0_regen = zeros(1,S);

%*****

% This runs the program for 10 values of the oxime diffusion constant
for loop = 1:1

factor_R= 1.0;
standard_R = 6.64e-4; %mmole/cm^3 = M
factor_E_dead = 0.5;
standard_E_dead = 7.4e-5; %mmole/cm^3 = M (Naka, et al)
% oxime diffusion reaction initial cleft values of A, E, R in mM
A_0_regen(1,1) = 0.0; % in mM (10 annuli is used as the control reference)
E_0_regen(1,:) = (1 - factor_E_dead)*standard_E_dead;
E_dead_0_regen(1,:) = factor_E_dead*standard_E_dead; % in mM
R_0_regen(1,:) = factor_R*standard_R; % in mM

% Toxin diffusion reaction initial value vector
Z0 = [A_0_regen ... A ( Z(1)-Z(Q) )
      E_0_regen ... E ( Z(Q+1) - Z(2Q) )
      AE_0_regen ... AE ( Z(2Q+1) - Z(3Q) )
      acE_0_regen ... acE ( Z(3Q+1) - Z(4Q) )
      R_0_regen ... R ( Z(4Q+1) - Z(5Q) )
      AR_0_regen ... AR ( Z(5Q+1) - Z(6Q) )
      A2R_0_regen ... A2R ( Z(6Q+1) - Z(7Q) )
      A2Ro_0_regen ... A2R* ( Z(7Q+1) - Z(8Q) )
      E_dead_0_regen ... E_dead ( Z(8Q+1) - Z(9Q) )
      OX_0_regen ...OX ( Z(9Q+1) - Z(10Q) )
      EIOX_0_regen ...EIOX ( Z(10Q+1) - Z(11Q) )
      %IOX_0_regen ... IOX ( Z(11Q+1) - Z(12Q) )

];

E_regen = zeros(length(t), length(r)); % oxime diffusion enzyme reaction matrix
R_regen = zeros(length(t), length(r)); % oxime diffusion receptor reaction matrix
OX_regen = zeros(length(t), length(r)); % oxime diffusion reaction matrix
EIOX_regen = zeros(length(t), length(r)); % oxime diffusion enzyme-toxin-oxime reaction matrix
E_dead_regen = zeros(length(t), length(r)); %oxime diffusion poisoned enzyme reaction matrix

```

```

E_cleft_regen = zeros(N,1); % toxin diffusion reaction species
R_cleft_regen = zeros(N,1);
OX_cleft_regen = zeros(N,1);
EIOX_cleft_regen = zeros(N,1);
E_dead_cleft_regen = zeros(N,1);

molecule_E_cleft_regen = zeros(N,1); % toxin diffusion reaction species
molecule_R_cleft_regen = zeros(N,1);
molecule_OX_cleft_regen = zeros(N,1);
molecule_EIOX_cleft_regen = zeros(N,1);
molecule_E_dead_cleft_regen = zeros(N,1);

% run the diffusing toxin reaction function
[t_regen, Z]= ode15s(@Func_regen_parameters, tspan_regen, Z0, [], D_x, D_r_Ach,
D_r_oxime(loop), r, dx, dr, t_on, t_off, OX_inf ) ;

for i = 1:length(t) % time length vector
    for j = 1:length(r) % radius length vector
        E_regen(i,j) = Z(i,j+Q); % toxic diffusion reaction species
        R_regen(i,j) = Z(i,j+4*Q);
        OX_regen(i,j) = Z(i,j+9*Q);
        EIOX_regen(i,j) = Z(i,j+10*Q);
        E_dead_regen(i,j) = Z(i,j+8*Q);
    end
end
switch loop
case(1)
    E_regen_1 = E_regen;
    save E_regen_1 E_regen_1;
    R_regen_1 = R_regen;
    save R_regen_1 R_regen_1;
    OX_regen_1 = OX_regen;
    save OX_regen_1 OX_regen_1;
    EIOX_regen_1 = EIOX_regen;
    save EIOX_regen_1 EIOX_regen_1;
    E_dead_regen_1 = E_dead_regen;
    save E_dead_regen_1 E_dead_regen_1;
case(2)
    E_regen_2 = E_regen;
    save E_regen_2 E_regen_2;
    R_regen_2 = R_regen;
    save R_regen_2 R_regen_2;
    OX_regen_2 = OX_regen;
    save OX_regen_2 OX_regen_2;
    EIOX_regen_2 = EIOX_regen;
    save EIOX_regen_2 EIOX_regen_2;
    E_dead_regen_2 = E_dead_regen;
    save E_dead_regen_2 E_dead_regen_2;

```



```
case(3)
  E_regen_3 = E_regen;
  save E_regen_3 E_regen_3;
  R_regen_3 = R_regen;
  save R_regen_3 R_regen_3;
  OX_regen_3 = OX_regen;
  save OX_regen_3 OX_regen_3;
  EIOX_regen_3 = EIOX_regen;
  save EIOX_regen_3 EIOX_regen_3;
  E_dead_regen_3 = E_dead_regen;
  save E_dead_regen_3 E_dead_regen_3;
case(4)
  E_regen_4 = E_regen;
  save E_regen_4 E_regen_4;
  R_regen_4 = R_regen;
  save R_regen_4 R_regen_4;
  OX_regen_4 = OX_regen;
  save OX_regen_4 OX_regen_4;
  EIOX_regen_4 = EIOX_regen;
  save EIOX_regen_4 EIOX_regen_4;
  E_dead_regen_4 = E_dead_regen;
  save E_dead_regen_4 E_dead_regen_4;
case(5)
  E_regen_5 = E_regen;
  save E_regen_5 E_regen_5;
  R_regen_5 = R_regen;
  save R_regen_5 R_regen_5;
  OX_regen_5 = OX_regen;
  save OX_regen_5 OX_regen_5;
  EIOX_regen_5 = EIOX_regen;
  save EIOX_regen_5 EIOX_regen_5;
  E_dead_regen_5 = E_dead_regen;
  save E_dead_regen_5 E_dead_regen_5;
case(6)
  E_regen_6 = E_regen;
  save E_regen_6 E_regen_6;
  R_regen_6 = R_regen;
  save R_regen_6 R_regen_6;
  OX_regen_6 = OX_regen;
  save OX_regen_6 OX_regen_6;
  EIOX_regen_6 = EIOX_regen;
  save EIOX_regen_6 EIOX_regen_6;
  E_dead_regen_6 = E_dead_regen;
  save E_dead_regen_6 E_dead_regen_6;
case(7)
  E_regen_7 = E_regen;
  save E_regen_7 E_regen_7;
  R_regen_7 = R_regen;
  save R_regen_7 R_regen_7;
  OX_regen_7 = OX_regen;
  save OX_regen_7 OX_regen_7;
  EIOX_regen_7 = EIOX_regen;
  save EIOX_regen_7 EIOX_regen_7;
  E_dead_regen_7 = E_dead_regen;
  save E_dead_regen_7 E_dead_regen_7;
case(8)
```

```

E_regen_8 = E_regen;
save E_regen_8 E_regen_8;
R_regen_8 = R_regen;
save R_regen_8 R_regen_8;
OX_regen_8 = OX_regen;
save OX_regen_8 OX_regen_8;
EIOX_regen_8 = EIOX_regen;
save EIOX_regen_8 EIOX_regen_8;
E_dead_regen_8 = E_dead_regen;
save E_dead_regen_8 E_dead_regen_8;
case(9)
E_regen_9 = E_regen;
save E_regen_9 E_regen_9;
R_regen_9 = R_regen;
save R_regen_9 R_regen_9;
OX_regen_9 = OX_regen;
save OX_regen_9 OX_regen_9;
EIOX_regen_9 = EIOX_regen;
save EIOX_regen_9 EIOX_regen_9;
E_dead_regen_9 = E_dead_regen;
save E_dead_regen_9 E_dead_regen_9;
case(10)
E_regen_10 = E_regen;
save E_regen_10 E_regen_10;
R_regen_10 = R_regen;
save R_regen_10 R_regen_10;
OX_regen_10 = OX_regen;
save OX_regen_10 OX_regen_10;
EIOX_regen_10 = EIOX_regen;
save EIOX_regen_10 EIOX_regen_10;
E_dead_regen_10 = E_dead_regen;
save E_dead_regen_10 E_dead_regen_10;
end

% calculate the total amounts of these species in the cleft
for i = 1:N
    for j = 1:Q

        E_cleft_regen(i) = E_cleft_regen(i) +(volume(j)*E_regen(i,j))/V_cleft;    % toxin diffusion
        molar species
        R_cleft_regen(i) = R_cleft_regen(i) +(volume(j)*R_regen(i,j))/V_cleft;
        OX_cleft_regen(i) = OX_cleft_regen(i) +(volume(j)*OX_regen(i,j))/V_cleft;
        EIOX_cleft_regen(i) = EIOX_cleft_regen(i) +(volume(j)*EIOX_regen(i,j))/V_cleft;
        E_dead_cleft_regen(i) = E_dead_cleft_regen(i) +(volume(j)*E_dead_regen(i,j))/V_cleft;

        molecule_E_cleft_regen(i) = E_cleft_regen(i)*V_cleft*(6.02e+20);    % toxin diffusion
        molecule species
        molecule_R_cleft_regen(i) = R_cleft_regen(i)*V_cleft*(6.02e+20);
        molecule_OX_cleft_regen(i) = OX_cleft_regen(i)*V_cleft*(6.02e+20);
        molecule_EIOX_cleft_regen(i) = EIOX_cleft_regen(i)*V_cleft*(6.02e+20);
        molecule_E_dead_cleft_regen(i) = E_dead_cleft_regen(i)*V_cleft*(6.02e+20);
    end
end
t_min = t_regen./(1000*60);

```

```

%
figure(5*loop+1);
plot(t_min(:), E_cleft_regen(:)/standard_E_dead);
title(sprintf('The amount of species %s in the whole cleft averaged over %i annular
volumes\nD_roxime = %-.5.2e cm^2/ms', 'E', Q, D_r_oxime(loop)));
xlabel(sprintf('t, minutes')); ylabel(sprintf('Species %s, fraction', 'E'));

figure(5*loop+2);
plot(t_regen(:), OX_cleft_regen(:));
title(sprintf('The amount of species %s in the whole cleft averaged over %i annular
volumes\nD_roxime = %-.5.2e cm^2/ms', 'OX', Q, D_r_oxime(loop)));
xlabel(sprintf('t, ms')); ylabel(sprintf('Species %s, mM', 'OX'));

figure(5*loop+3);
plot(t_regen(:), EIOX_cleft_regen(:));
title(sprintf('The amount of species %s in the whole cleft averaged over %i annular
volumes\nD_roxime = %-.5.2e cm^2/ms', 'EIOX', Q, D_r_oxime(loop)));
xlabel(sprintf('t, ms')); ylabel(sprintf('Species %s, mM', 'EIOX'));

figure(5*loop+4);
plot(t_regen(:), E_dead_cleft_regen(:));
title(sprintf('The amount of species %s in the whole cleft averaged over %i annular volumes\n
D_roxime = %-.5.2e cm^2/ms', 'E*dead', Q, D_r_oxime(loop)));
xlabel(sprintf('t, ms')); ylabel(sprintf('Species %s, mM', 'E*dead'));

figure(5*loop+5);
plot(t_regen(:), molecule_R_cleft_regen(:));
title(sprintf('The amount of species %s in the whole cleft averaged over %i annular volumes\n
D_roxime = %-.5.2e cm^2/ms', 'R', Q, D_r_oxime(loop)));
xlabel(sprintf('t, ms')); ylabel(sprintf('Species %s, molecules', 'R'));
%
switch loop
case(1)
    molecule_E_cleft_regen_1 = molecule_E_cleft_regen;
    save molecule_E_cleft_regen_1 molecule_E_cleft_regen_1;
    molecule_R_cleft_regen_1 = molecule_R_cleft_regen;
    save molecule_R_cleft_regen_1 molecule_R_cleft_regen_1;
    molecule_OX_cleft_regen_1 = molecule_OX_cleft_regen;
    save molecule_OX_cleft_regen_1 molecule_OX_cleft_regen_1;
    molecule_EIOX_cleft_regen_1 = molecule_EIOX_cleft_regen;
    save molecule_EIOX_cleft_regen_1 molecule_EIOX_cleft_regen_1;
    molecule_E_dead_cleft_regen_1 = molecule_E_dead_cleft_regen;
    save molecule_E_dead_cleft_regen_1 molecule_E_dead_cleft_regen_1;
case(2)
    molecule_E_cleft_regen_2 = molecule_E_cleft_regen;
    save molecule_E_cleft_regen_2 molecule_E_cleft_regen_2;
    molecule_R_cleft_regen_2 = molecule_R_cleft_regen;
    save molecule_R_cleft_regen_2 molecule_R_cleft_regen_2;
    molecule_OX_cleft_regen_2 = molecule_OX_cleft_regen;
    save molecule_OX_cleft_regen_2 molecule_OX_cleft_regen_2;
    molecule_EIOX_cleft_regen_2 = molecule_EIOX_cleft_regen;
    save molecule_EIOX_cleft_regen_2 molecule_EIOX_cleft_regen_2;
    molecule_E_dead_cleft_regen_2 = molecule_E_dead_cleft_regen;

```

```
save molecule_E_dead_cleft_regen_2 molecule_E_dead_cleft_regen_2;
case(3)
molecule_E_cleft_regen_3 = molecule_E_cleft_regen;
save molecule_E_cleft_regen_3 molecule_E_cleft_regen_3;
molecule_R_cleft_regen_3 = molecule_R_cleft_regen;
save molecule_R_cleft_regen_3 molecule_R_cleft_regen_3;
molecule_OX_cleft_regen_3 = molecule_OX_cleft_regen;
save molecule_OX_cleft_regen_3 molecule_OX_cleft_regen_3;
molecule_EIOX_cleft_regen_3 = molecule_EIOX_cleft_regen;
save molecule_EIOX_cleft_regen_3 molecule_EIOX_cleft_regen_3;
molecule_E_dead_cleft_regen_3 = molecule_E_dead_cleft_regen;
save molecule_E_dead_cleft_regen_3 molecule_E_dead_cleft_regen_3;
case(4)
molecule_E_cleft_regen_4 = molecule_E_cleft_regen;
save molecule_E_cleft_regen_4 molecule_E_cleft_regen_4;
molecule_R_cleft_regen_4 = molecule_R_cleft_regen;
save molecule_R_cleft_regen_4 molecule_R_cleft_regen_4;
molecule_OX_cleft_regen_4 = molecule_OX_cleft_regen;
save molecule_OX_cleft_regen_4 molecule_OX_cleft_regen_4;
molecule_EIOX_cleft_regen_4 = molecule_EIOX_cleft_regen;
save molecule_EIOX_cleft_regen_4 molecule_EIOX_cleft_regen_4;
molecule_E_dead_cleft_regen_4 = molecule_E_dead_cleft_regen;
save molecule_E_dead_cleft_regen_4 molecule_E_dead_cleft_regen_4;
case(5)
molecule_E_cleft_regen_5 = molecule_E_cleft_regen;
save molecule_E_cleft_regen_5 molecule_E_cleft_regen_5;
molecule_R_cleft_regen_5 = molecule_R_cleft_regen;
save molecule_R_cleft_regen_5 molecule_R_cleft_regen_5;
molecule_OX_cleft_regen_5 = molecule_OX_cleft_regen;
save molecule_OX_cleft_regen_5 molecule_OX_cleft_regen_5;
molecule_EIOX_cleft_regen_5 = molecule_EIOX_cleft_regen;
save molecule_EIOX_cleft_regen_5 molecule_EIOX_cleft_regen_5;
molecule_E_dead_cleft_regen_5 = molecule_E_dead_cleft_regen;
save molecule_E_dead_cleft_regen_5 molecule_E_dead_cleft_regen_5;
case(6)
molecule_E_cleft_regen_6 = molecule_E_cleft_regen;
save molecule_E_cleft_regen_6 molecule_E_cleft_regen_6;
molecule_R_cleft_regen_6 = molecule_R_cleft_regen;
save molecule_R_cleft_regen_6 molecule_R_cleft_regen_6;
molecule_OX_cleft_regen_6 = molecule_OX_cleft_regen;
save molecule_OX_cleft_regen_6 molecule_OX_cleft_regen_6;
molecule_EIOX_cleft_regen_6 = molecule_EIOX_cleft_regen;
save molecule_EIOX_cleft_regen_6 molecule_EIOX_cleft_regen_6;
molecule_E_dead_cleft_regen_6 = molecule_E_dead_cleft_regen;
save molecule_E_dead_cleft_regen_6 molecule_E_dead_cleft_regen_6;
case(7)
molecule_E_cleft_regen_7 = molecule_E_cleft_regen;
save molecule_E_cleft_regen_7 molecule_E_cleft_regen_7;
molecule_R_cleft_regen_7 = molecule_R_cleft_regen;
save molecule_R_cleft_regen_7 molecule_R_cleft_regen_7;
molecule_OX_cleft_regen_7 = molecule_OX_cleft_regen;
save molecule_OX_cleft_regen_7 molecule_OX_cleft_regen_7;
molecule_EIOX_cleft_regen_7 = molecule_EIOX_cleft_regen;
save molecule_EIOX_cleft_regen_7 molecule_EIOX_cleft_regen_7;
molecule_E_dead_cleft_regen_7 = molecule_E_dead_cleft_regen;
save molecule_E_dead_cleft_regen_7 molecule_E_dead_cleft_regen_7;
```

```

case(8)
    molecule_E_cleft_regen_8 = molecule_E_cleft_regen;
    save molecule_E_cleft_regen_8 molecule_E_cleft_regen_8;
    molecule_R_cleft_regen_8 = molecule_R_cleft_regen;
    save molecule_R_cleft_regen_8 molecule_R_cleft_regen_8;
    molecule_OX_cleft_regen_8 = molecule_OX_cleft_regen;
    save molecule_OX_cleft_regen_8 molecule_OX_cleft_regen_8;
    molecule_EIOX_cleft_regen_8 = molecule_EIOX_cleft_regen;
    save molecule_EIOX_cleft_regen_8 molecule_EIOX_cleft_regen_8;
    molecule_E_dead_cleft_regen_8 = molecule_E_dead_cleft_regen;
    save molecule_E_dead_cleft_regen_8 molecule_E_dead_cleft_regen_8;
case(9)
    molecule_E_cleft_regen_9 = molecule_E_cleft_regen;
    save molecule_E_cleft_regen_9 molecule_E_cleft_regen_9;
    molecule_R_cleft_regen_9 = molecule_R_cleft_regen;
    save molecule_R_cleft_regen_9 molecule_R_cleft_regen_9;
    molecule_OX_cleft_regen_9 = molecule_OX_cleft_regen;
    save molecule_OX_cleft_regen_9 molecule_OX_cleft_regen_9;
    molecule_EIOX_cleft_regen_9 = molecule_EIOX_cleft_regen;
    save molecule_EIOX_cleft_regen_9 molecule_EIOX_cleft_regen_9;
    molecule_E_dead_cleft_regen_9 = molecule_E_dead_cleft_regen;
    save molecule_E_dead_cleft_regen_9 molecule_E_dead_cleft_regen_9;
case(10)
    molecule_E_cleft_regen_10 = molecule_E_cleft_regen;
    save molecule_E_cleft_regen_10 molecule_E_cleft_regen_10;
    molecule_R_cleft_regen_10 = molecule_R_cleft_regen;
    save molecule_R_cleft_regen_10 molecule_R_cleft_regen_10;
    molecule_OX_cleft_regen_10 = molecule_OX_cleft_regen;
    save molecule_OX_cleft_regen_10 molecule_OX_cleft_regen_10;
    molecule_EIOX_cleft_regen_10 = molecule_EIOX_cleft_regen;
    save molecule_EIOX_cleft_regen_10 molecule_EIOX_cleft_regen_10;
    molecule_E_dead_cleft_regen_10 = molecule_E_dead_cleft_regen;
    save molecule_E_dead_cleft_regen_10 molecule_E_dead_cleft_regen_10;

end
%{
disp(sprintf('Stop when loop count is 10, the present loop count is %i', loop_count+1));
loop_count = loop_count+1;
choice = input('Do you want to run another inhibited reaction: 1(yes), 0(no)? \n');
if choice == 1
    D_r_oxime = input(sprintf('What is the new radial diffusion constant for the inhibitor? The last
value was (%-5.2e) \n',D_r_oxime));
end
%}
loop %keeps track of where the program is computationally
end

save loop loop; save Q Q;
save t t; save t_regen t_regen; save t_min t_min;
disp('data saved, program finished');

%{
loop_count = 0;
choice = 1;

```

```

while(choice == 1)

E_i_active_percent = input('What percent active enzyme will be in the cleft during the inhibited
action potential reaction?\n');

E_initial_inhibited = (E_i_active_percent/100)*E_0_tox(1,1); % in mM
disp(sprintf('\n The initial amount of active enzyme in the cleft \n during the inhibited reaction is
%-5.2e mM ', E_initial_inhibited));

tox_index = find((E_cleft_tox >= E_initial_inhibited - tol) & (E_cleft_tox <= E_initial_inhibited +
tol), 1);
disp(sprintf('\n The location of the time point index is %i ', tox_index));

disp(sprintf('\n This is equivalent to starting the action potential after %-5.2f minutes have passed
since exposure to the toxic inhibitor \n ', t_tox(tox_index)/(60000)));

E_cleft_tox';

%*****
*****
% species string array
species = ['A ' ;'E ' ;'AE ' ;'acE ' ;'R ' ;'AR ' ;'A2R ' ;'A2R* ' ;'I ' ;'EI ' ;'E_dead';'ChP ' ]%

loop_count = loop_count+1;
choice = input('Do you want to run another inhibited reaction: 1(yes), 0(no)? \n');

end

save (sprintf('E_cleft_tox_%i',loop_count+1), 'E_cleft_tox' );
save (sprintf('I_cleft_tox_%i',loop_count+1), 'I_cleft_tox' );
save (sprintf('EI_cleft_tox_%i',loop_count+1), 'EI_cleft_tox' );
save (sprintf('E_dead_cleft_tox_%i',loop_count+1), 'E_dead_cleft_tox' );

save (sprintf('molecule_E_cleft_tox_%i',loop_count+1), 'molecule_E_cleft_tox');
save (sprintf('molecule_I_cleft_tox_%i',loop_count+1), 'molecule_I_cleft_tox');
save (sprintf('molecule_EI_cleft_tox_%i',loop_count+1), 'molecule_EI_cleft_tox');
save (sprintf('molecule_E_dead_cleft_tox_%i',loop_count+1), 'molecule_E_dead_cleft_tox');

%}

```

```

%
% Models the complete normal and inhibited chemistry in the neuromuscular junction;
% the model consists of a series of instantly and uniformly mixed
% volumes which share transport of Acetylcholine via 1D diffusion at
% each adjacent border
%
%The user inputs the degree of enzyme inhibition at which to run the
%simulation

% VOLUME 1
% f(t) ----> A
%
%
% VOLUME 2 - 40
% kD
% A ----> @
%
% U1 U2 kE1 U3 kE2 U4 kE3 U2
% A + E <----> AE ----> acE ----> E + ChP
% kE_1
%
% U2 U9 kI1 U10
% E + I <----> EI
%
% U10 k_dead U11
% EI -----> E_dead

%
% VOLUME 41 - 50
% U1 U5 2*kR1 U6
% A + R <-----> AR
% kR_1
%
% U1 U5 kR2 U7
% A + AR <-----> A2R
% 2*kR_2
%
% U7 oR U8
% A2R <-----> A2R*
% cR

%***** CHECKED FOR UNIT/DIMENSION CONSISTENCY ON 3/25/07, 17:45
%*****

%

clc;

clear;

A_inf = 0.0; % mmole/cm^3 = M
I_inf = 0.1*5.68e-4; % mmole/cm^3 = M (the same concentration in blood as nitrogen at STP)

```

```

% total volume in the cleft
V_cleft = 3.93e-14; % ( cm^3 )

% the length of the cleft (width, or height)
L_cleft = 5.0e-6; % cm

% the radius of the cleft
R_cleft = 5.0e-5; % cm

% the number of equal axial disks
P = 1;
x_cleft = zeros(1,P)

% the number of annular rings per disk
Q = 20;

% number of coupled sub-volumes
S = P*Q

%thickness of each radial annulus
dr = R_cleft/Q; % cm

%thickness of each axial disk
dx = L_cleft/P; % cm

% area of the cleft edge
Area_edge = 2*pi*R_cleft*L_cleft; % cm^2

% axial direction vector
x = linspace(0.0, L_cleft, P+1);

%radial direction vector
r = linspace(0.0, R_cleft, Q);

% This loop assigns an x-value coordinate to the center of each well mixed
% axial disk
for j = 1:P
    x_cleft(j) = 0.5*( x(j) + x(j+1) );
end
x_cleft;

% create the "space", a 1-dimension vector that all the axial and radial volume points are mapped
% into
s = [1:S];

% axial diffusion constant (cm^2/ms)
D_x = 2.0e-6;

% radial diffusion constant for Ach (cm^2/ms)
D_r = 0.90e-9; % 3.50e-9 cm^2/ms

```



```

% radial diffusion constant for the inhibitor
D_r_tox = D_r; %3.5e-9;

%number of time points
N=5000;

%time interval vector for the normal and inhibited reactions (ms, 1e-3 s)
t_0 = 0.0; t_f = 5.0; % ms
t = linspace(t_0, t_f, N);
tspan = [t];

%time interval vector for the diffusing toxin reaction
t_tox_0 = 0.0; t_tox_f = (3.0e+5); % ms, 5 minutes
t_tox = linspace(t_tox_0, t_tox_f, N);
tspan_tox = [t_tox];

% pulse parameters
t_on = 3.0; t_off = 4.50; %*THIS IS NOT THE TIME INTERVAL*

n_on = round((((t_on - t_0)/(t_f - t_0))*(length(t)-1) + 1);
n_off = round(((t_off - t_0)*(length(t) - 1)/(t_f - t_0) + 1);
peak = round(0.5*(n_on + n_off));
spread = 20.0;
magnitude = 0.50;

% calculate the volume of each annulus
volume = zeros(1,Q); % ( cm^3 )
vol_frac = volume;
for i=1:Q
    volume(i) = ((2*i-1)/Q^2)*pi*L_cleft*R_cleft^2;
    vol_frac(i) = volume(i)/V_cleft;
end
sum(volume(1:Q)); % a check of the annuli sum should equal the V_cleft
sum(vol_frac(1:Q));
V_cleft;

% creation of function handle
I_blood = @Func_I_blood_cocn ;

% this computes the concentration of the inhibitor in the blood as a
% function of time
I_cocn = Func_I_blood_cocn( tspan_tox, I_inf );

% defining the initial value vectors of the diffusing toxin reaction reactants
A_0_tox = zeros(1,S);
E_0_tox = zeros(1,S);
AE_0_tox = zeros(1,S);
acE_0_tox = zeros(1,S);
R_0_tox = zeros(1,S);

```

```

AR_0_tox = zeros(1,S);
A2R_0_tox = zeros(1,S);
A2Ro_0_tox = zeros(1,S);
I_0_tox = zeros(1,S);
EI_0_tox = zeros(1,S);
E_dead_0_tox = zeros(1,S);
ChP_0_tox = zeros(1,S);

% defining the initial value vectors of the normal AP reaction reactants
A_0_n = zeros(1,S);
E_0_n = zeros(1,S);
AE_0_n = zeros(1,S);
acE_0_n = zeros(1,S);
R_0_n = zeros(1,S);
AR_0_n = zeros(1,S);
A2R_0_n = zeros(1,S);
A2Ro_0_n = zeros(1,S);
ChP_0_n = zeros(1,S);

% defining the initial value vectors of the inhibited AP reaction
% reactants,
A_0_i = zeros(1,S);
E_0_i = zeros(1,S);
AE_0_i = zeros(1,S);
acE_0_i = zeros(1,S);
R_0_i = zeros(1,S);
AR_0_i = zeros(1,S);
A2R_0_i = zeros(1,S);
A2Ro_0_i = zeros(1,S);
I_0_i = zeros(1,S);
EI_0_i = zeros(1,S);
E_dead_0_i = zeros(1,S);
ChP_0_i = zeros(1,S);

factor_R= 1.0;
standard_R = 6.64e-4; %mmole/cm^3 Friboulet, Wathey (2.0e-3, Naka, et al)
factor_E_tox = 1.0;
standard_E_tox = 7.4e-5; %mmole/cm^3 (Naka, et al)
% Toxin diffusion reaction initial cleft values of A, E, R in mM
A_0_tox(1,1) = 0.0; % in mM (10 annuli is used as the control reference)
E_0_tox(1,:) = factor_E_tox*standard_E_tox; % in mM
R_0_tox(1,:) = factor_R*standard_R; % in mM

% Toxin diffusion reaction initial value vector
W0 = [A_0_tox ... A ( V(1)-V(Q) )
      E_0_tox ... E ( V(Q+1) - V(2Q) )
      AE_0_tox ... AE ( V(2Q+1) - V(3Q) )
      acE_0_tox ... acE ( V(3Q+1) - V(4Q) )
      R_0_tox ... R ( V(4Q+1) - V(5Q) )
      AR_0_tox ... AR ( V(5Q+1) - V(6Q) )
      A2R_0_tox ... A2R ( V(6Q+1) - V(7Q) )
      A2Ro_0_tox ... A2R* ( V(7Q+1) - V(8Q) )
      I_0_tox ... I ( V(8Q+1) - V(9Q) )

```

```

EI_0_tox ...EI ( V(9Q+1) = V(10Q) )
E_dead_0_tox ...E_dead ( V(10Q+1) - V(11Q) )
ChP_0_tox ... ChP ( V(11Q+1) - V(12Q) )

```

```

];

```

```

E_tox = zeros(length(t), length(r)); % toxin diffusion enzyme reaction matrix
R_tox = zeros(length(t), length(r)); % toxin diffusion receptor reaction matrix
I_tox = zeros(length(t), length(r)); % toxin diffusion inhibitor of esterase
EI_tox = zeros(length(t), length(r)); % toxin diffusion enzyme-toxin reaction matrix
E_dead_tox = zeros(length(t), length(r)); %toxin diffusion poisoned enzyme reaction matrix

```

```

E_cleft_tox = zeros(N,1); % toxin diffusion reaction species
R_cleft_tox = zeros(N,1);
I_cleft_tox = zeros(N,1);
EI_cleft_tox = zeros(N,1);
E_dead_cleft_tox = zeros(N,1);

```

```

molecule_E_cleft_tox = zeros(N,1); % toxin diffusion reaction species
molecule_R_cleft_tox = zeros(N,1);
molecule_I_cleft_tox = zeros(N,1);
molecule_EI_cleft_tox = zeros(N,1);
molecule_E_dead_cleft_tox = zeros(N,1);

```

```

% run the diffusing toxin reaction function
[t_tox, W]= ode15s(@Func_Radial_toxin_kinetics_test, tspan_tox, W0, [], D_x, D_r, D_r_tox, r,
dx, dr, t_on, t_off, I_blood, I_inf );

```

```

for i = 1:length(t) % time length vector
    for j = 1:length(r) % radius length vector

```

```

        E_tox(i,j) = W(i,j+Q); % toxic diffusion reaction species
        R_tox(i,j) = W(i,j+4*Q);
        I_tox(i,j) = W(i,j+8*Q);
        EI_tox(i,j) = W(i,j+9*Q);
        E_dead_tox(i,j) = W(i,j+10*Q);

```

```

    end
end

```

```

% calculate the total amounts of these species in the cleft

```

```

for i = 1:N
    for j = 1:Q

```

```

        E_cleft_tox(i) = E_cleft_tox(i) +(volume(j)*E_tox(i,j))/V_cleft; % toxin diffusion molar
species
        R_cleft_tox(i) = R_cleft_tox(i) +(volume(j)*R_tox(i,j))/V_cleft;

```

```

I_cleft_tox(i) = I_cleft_tox(i) +(volume(j)*I_tox(i,j))/V_cleft;
EI_cleft_tox(i) = EI_cleft_tox(i) +(volume(j)*EI_tox(i,j))/V_cleft;
E_dead_cleft_tox(i) = E_dead_cleft_tox(i) +(volume(j)*E_dead_tox(i,j))/V_cleft;

molecule_E_cleft_tox(i) = E_cleft_tox(i)*V_cleft*(6.02e+20); % toxin diffusion molecule
species
molecule_R_cleft_tox(i) = R_cleft_tox(i)*V_cleft*(6.02e+20);
molecule_I_cleft_tox(i) = I_cleft_tox(i)*V_cleft*(6.02e+20);
molecule_EI_cleft_tox(i) = EI_cleft_tox(i)*V_cleft*(6.02e+20);
molecule_E_dead_cleft_tox(i) = E_dead_cleft_tox(i)*V_cleft*(6.02e+20);
end
end
t_min = t_tox./(1000*60);

figure(1)
plot(t_min, E_dead_cleft_tox)
title(sprintf('Concentration of poisoned enzyme vs time \n VX kinetics and blood concentration of
%i mM\n initial active enzyme %i mM', I_inf, E_cleft_tox(1,1)));
xlabel('time, min'); ylabel('Poisoned Enzyme, mM');

figure(2)
E_tox_active_frac = 100*((E_0_tox(1,1)-E_dead_cleft_tox)/E_0_tox(1,1));
plot(t_min, E_tox_active_frac)
title(sprintf('Percent enzyme active in cleft vs. time,\n with VX kinetics and blood concentration of
%-5.2e mM ', (I_inf)));
xlabel('time, min'); ylabel('Percent active enzyme');

figure(1)
plot(tspan_tox./60000,I_cocn);
title('Blood concentration of nerve agent')
xlabel('time, min'); ylabel('Inhibitor blood concentration, mmole/cm^3');

% tolerance value
tol = 1.0e-7;
loop_count = 0;
choice = 1;

while(choice == 1)

E_i_active_percent = input('What percent active enzyme will be in the cleft during the inhibited
action potential reaction?\n');

E_initial_inhibited = (E_i_active_percent/100)*E_0_tox(1,1); % in mM
disp(sprintf('\n The initial amount of active enzyme in the cleft \n during the inhibited reaction is
%-5.2e mM ', E_initial_inhibited));

tox_index = find((E_cleft_tox >= E_initial_inhibited - tol) & (E_cleft_tox <= E_initial_inhibited +
tol), 1);
disp(sprintf('\n The location of the time point index is %i ', tox_index));

```

```
disp(sprintf('\n This is equivalent to starting the action potential after %-5.2f minutes have passed
since exposure to the toxic inhibitor \n ', t_tox(tox_index)/(60000)));
```

```
E_cleft_tox';
```

```
factor_A = 1.5;
standard_A = 0.0423*((Q/10)^2); %( mmole/cm^3)
factor_E = 1.0;
standard_E = 7.4e-5; %( mmole/cm^3) (Naka, et al )
% Normal AP reaction initial cleft values of A, E, R in mM
A_0_n(1,1) = factor_A*standard_A; % in mM (10 annuli is used as the control reference)
E_0_n(1,:) = factor_E*standard_E; % in mM
R_0_n(1,:) = factor_R*standard_R; % in mM
```

```
%normal AP reaction initial value vector
U0 = [ A_0_n ... A ( U(1) - U(Q) )
      E_0_n ... E ( U(Q+1) - U(2Q) )
      AE_0_n ... AE ( U(2Q+1) - U(3Q) )
      acE_0_n ... acE ( U(3Q+1) - U(4Q) )
      R_0_n ... R ( U(4Q+1) - U(5Q) )
      AR_0_n ... AR ( U(5Q+1) - U(6Q) )
      A2R_0_n ... A2R ( U(6Q+1) - U(7Q) )
      A2Ro_0_n ... A2R* ( U(7Q+1) - U(8Q) )
      ChP_0_n ... ChP ( U(8Q+1) - U(9Q) )
      ];
```

```
% Inhibited AP reaction initial cleft values of A, E, R in mM
A_0_i(1,1) = factor_A*standard_A; % in mM (10 annuli is used as the control reference)
E_0_i(1,:) = E_tox(tox_index,:); % in mM
R_0_i(1,:) = R_tox(tox_index,:); % in mM
I_0_i(1,:) = I_tox(tox_index,:); % in mM
EI_0_i(1,:) = EI_tox(tox_index,:); % in mM
E_dead_0_i = E_dead_tox(tox_index,:); % in mM
```

```
% Inhibited AP reaction initial value vector
V0 = [A_0_i ... A ( V(1)-V(Q) )
      E_0_i ... E ( V(Q+1) - V(2Q) )
      AE_0_i ... AE ( V(2Q+1) - V(3Q) )
      acE_0_i ... acE ( V(3Q+1) - V(4Q) )
      R_0_i ... R ( V(4Q+1) - V(5Q) )
      AR_0_i ... AR ( V(5Q+1) - V(6Q) )
      A2R_0_i ... A2R ( V(6Q+1) - V(7Q) )
      A2Ro_0_i ... A2R* ( V(7Q+1) - V(8Q) )
      I_0_i ... I ( V(8Q+1) - V(9Q) )
      EI_0_i ... EI ( V(9Q+1) - V(10Q) )
      E_dead_0_i ... E_dead ( V(10Q+1) - V(11Q) )
      ChP_0_i ... ChP ( V(11Q+1) - V(12Q) )
      ];
```

```
% run the normal enzyme reaction function
[t,U] = ode15s(@Func_Radial_normal_kinetics_test, tspan, U0, [], D_x, D_r, r, dx, dr, t_on, t_off);
```

```
% run the inhibited enzyme reaction function
[t,V] = ode15s(@Func_Radial_inhibited_kinetics_test, tspan, V0, [], D_x, D_r, D_r_tox, r, dx, dr, t_on, t_off);
```

```
% create the normal and inhibited reaction species concentration matrices as functions of r and t
A_n = zeros(length(t),length(r)); % normal acetylcholine reaction matrix
E_n = zeros(length(t), length(r)); % normal enzyme reaction matrix
AE_n = zeros(length(t), length(r));% normal enzyme-complex reaction matrix
acE_n = zeros(length(t), length(r));% normal acylated-enzyme reaction matrix
R_n = zeros(length(t), length(r));% normal receptor reaction matrix
AR_n = zeros(length(t), length(r));% normal single bound receptor reaction matrix
A2R_n = zeros(length(t), length(r));% normal double bound receptor reaction matrix
A2Ro_n = zeros(length(t), length(r));% normal open receptor reaction matrix
ChP_n = zeros(length(t), length(r));% normal choline/product reaction matrix
```

```
A_i = zeros(length(t), length(r)); % inhibited acetylcholine reaction matrix
E_i = zeros(length(t), length(r)); % inhibited enzyme reaction matrix
AE_i = zeros(length(t), length(r)); % inhibited enzyme-complex reaction matrix
acE_i = zeros(length(t), length(r)); % inhibited acylated-enzyme reaction matrix
R_i = zeros(length(t), length(r));% inhibited receptor reaction matrix
AR_i = zeros(length(t), length(r));% inhibited single bound receptor reaction matrix
A2R_i = zeros(length(t), length(r));% inhibited double bound receptor reaction matrix
A2Ro_i = zeros(length(t), length(r));% inhibited open receptor reaction matrix
I_i = zeros(length(t), length(r)); % inhibitor of esterase
EI_i = zeros(length(t), length(r)); % enzyme-toxin reaction matrix
E_dead_i = zeros(length(t), length(r)); % poisoned enzyme reaction matrix
ChP_i = zeros(length(t), length(r)); % inhibited choline/product reaction matrix
```

```
for i = 1:length(t) % time length vector
    for j = 1:length(r) % radius length vector
```

```
        A_n(i,j) = U(i,j); % normal reaction species
        E_n(i,j) = U(i,j+Q);
        AE_n(i,j) = U(i,j+2*Q);
        acE_n(i,j) = U(i,j+3*Q);
        R_n(i,j) = U(i,j+4*Q);
        AR_n(i,j) = U(i,j+5*Q);
        A2R_n(i,j) = U(i,j+6*Q);
        A2Ro_n(i,j) = U(i,j+7*Q);
        ChP_n(i,j) = U(i,j+8*Q);
```

```
        A_i(i,j) = V(i,j); % inhibited reaction species
        E_i(i,j) = V(i,j+Q);
        AE_i(i,j) = V(i,j+2*Q);
```

```

    acE_i(i,j) = V(i,j+3*Q);
    R_i(i,j) = V(i,j+4*Q);
    AR_i(i,j) = V(i,j+5*Q);
    A2R_i(i,j) = V(i,j+6*Q);
    A2Ro_i(i,j) = V(i,j+7*Q);
    I_i(i,j) = V(i,j+8*Q);
    EI_i(i,j) = V(i,j+9*Q);
    E_dead_i(i,j) = V(i,j+10*Q);
    ChP_i(i,j) = V(i,j+11*Q);
end
end

%2*pi*R_cleft*L_cleft*D_r/dr

% calculate the normal and inhibited Ach lost from the last annulus via diffusion
%[t, A_lost] = ode15s(@Acetylcholine_lost, tspan, A_n(1,14), [], D_r, dr, r);

%A_n_lost = (D_r/(2*r(15)*dr))*(A_inf - A_n(:,14))%cumtrapz(t,(2*pi*R_cleft*L_cleft*D_r/1e-
18)*A_n(:,Q));
%A_i_lost = cumtrapz(t,(2*pi*R_cleft*L_cleft*D_r/1e-18)*A_i(:,Q));

% initialize the total concentration/molecules in the cleft vectors

A_cleft_n = zeros(N,1);% normal reaction species
E_cleft_n = zeros(N,1);
AE_cleft_n = zeros(N,1);
acE_cleft_n = zeros(N,1);
R_cleft_n = zeros(N,1);
AR_cleft_n = zeros(N,1);
A2R_cleft_n = zeros(N,1);
A2Ro_cleft_n = zeros(N,1);
ChP_cleft_n = zeros(N,1);

molecule_A_cleft_n = zeros(N,1);% normal reaction species
molecule_E_cleft_n = zeros(N,1);
molecule_AE_cleft_n = zeros(N,1);
molecule_acE_cleft_n = zeros(N,1);
molecule_R_cleft_n = zeros(N,1);
molecule_AR_cleft_n = zeros(N,1);
molecule_A2R_cleft_n = zeros(N,1);

```

```

molecule_A2Ro_cleft_n = zeros(N,1);
molecule_ChP_cleft_n = zeros(N,1);

A_cleft_i = zeros(N,1); % inhibited reaction species
E_cleft_i = zeros(N,1);
AE_cleft_i = zeros(N,1);
acE_cleft_i = zeros(N,1);
R_cleft_i = zeros(N,1);
AR_cleft_i = zeros(N,1);
A2R_cleft_i = zeros(N,1);
A2Ro_cleft_i = zeros(N,1);
I_cleft_i = zeros(N,1);
EI_cleft_i = zeros(N,1);
E_dead_cleft_i = zeros(N,1);
ChP_cleft_i = zeros(N,1);

molecule_A_cleft_i = zeros(N,1);% inhibited reaction species
molecule_E_cleft_i = zeros(N,1);
molecule_AE_cleft_i = zeros(N,1);
molecule_acE_cleft_i = zeros(N,1);
molecule_R_cleft_i = zeros(N,1);
molecule_AR_cleft_i = zeros(N,1);
molecule_A2R_cleft_i = zeros(N,1);
molecule_A2Ro_cleft_i = zeros(N,1);
molecule_I_cleft_i = zeros(N,1);
molecule_EI_cleft_i = zeros(N,1);
molecule_E_dead_cleft_i = zeros(N,1);
molecule_ChP_cleft_i = zeros(N,1);

%{
%Species names
species_names = ['A','E','AE','acE','R','AR','A2R','A2R*','I','EI','E_dead','ChP','A_lost'];
species_names(1)
species_names(2)
%}

% calculate the total amounts of these species in the cleft
for i = 1:N
    for j = 1:Q
        A_cleft_n(i) = A_cleft_n(i) +(volume(j)*A_n(i,j))/V_cleft; %normal molar species
        E_cleft_n(i) = E_cleft_n(i) +(volume(j)*E_n(i,j))/V_cleft;
        AE_cleft_n(i) = AE_cleft_n(i) +(volume(j)*AE_n(i,j))/V_cleft;
        acE_cleft_n(i) = acE_cleft_n(i) +(volume(j)*acE_n(i,j))/V_cleft;
        R_cleft_n(i) = R_cleft_n(i) +(volume(j)*R_n(i,j))/V_cleft;
        AR_cleft_n(i) = AR_cleft_n(i) +(volume(j)*AR_n(i,j))/V_cleft;
        A2R_cleft_n(i) = A2R_cleft_n(i) +(volume(j)*A2R_n(i,j))/V_cleft;
        A2Ro_cleft_n(i) = A2Ro_cleft_n(i) +(volume(j)*A2Ro_n(i,j))/V_cleft;
        ChP_cleft_n(i) = ChP_cleft_n(i) +(volume(j)*ChP_n(i,j))/V_cleft;

        A_cleft_i(i) = A_cleft_i(i) +(volume(j)*A_i(i,j))/V_cleft; % inhibited molar species
        E_cleft_i(i) = E_cleft_i(i) +(volume(j)*E_i(i,j))/V_cleft;
        AE_cleft_i(i) = AE_cleft_i(i) +(volume(j)*AE_i(i,j))/V_cleft;
        acE_cleft_i(i) = acE_cleft_i(i) +(volume(j)*acE_i(i,j))/V_cleft;
        R_cleft_i(i) = R_cleft_i(i) +(volume(j)*R_i(i,j))/V_cleft;
    end
end

```



```

AR_cleft_i(i) = AR_cleft_i(i) +(volume(j)*AR_i(i,j))/V_cleft;
A2R_cleft_i(i) = A2R_cleft_i(i) +(volume(j)*A2R_i(i,j))/V_cleft;
A2Ro_cleft_i(i) = A2Ro_cleft_i(i) +(volume(j)*A2Ro_i(i,j))/V_cleft;
I_cleft_i(i) = I_cleft_i(i) +(volume(j)*I_i(i,j))/V_cleft;
EI_cleft_i(i) = EI_cleft_i(i) +(volume(j)*EI_i(i,j))/V_cleft;
E_dead_cleft_i(i) = E_dead_cleft_i(i) +(volume(j)*E_dead_i(i,j))/V_cleft;
ChP_cleft_i(i) = ChP_cleft_i(i) +(volume(j)*ChP_i(i,j))/V_cleft;

molecule_A_cleft_n(i) = A_cleft_n(i)*V_cleft*(6.02e+20);    %normal molecule species
molecule_E_cleft_n(i) = E_cleft_n(i)*V_cleft*(6.02e+20);
molecule_AE_cleft_n(i) = AE_cleft_n(i)*V_cleft*(6.02e+20);
molecule_acE_cleft_n(i) = acE_cleft_n(i)*V_cleft*(6.02e+20);
molecule_R_cleft_n(i) = R_cleft_n(i)*V_cleft*(6.02e+20);
molecule_AR_cleft_n(i) = AR_cleft_n(i)*V_cleft*(6.02e+20);
molecule_A2R_cleft_n(i) = A2R_cleft_n(i)*V_cleft*(6.02e+20);
molecule_A2Ro_cleft_n(i) = A2Ro_cleft_n(i)*V_cleft*(6.02e+20);
molecule_ChP_cleft_n(i) = ChP_cleft_n(i)*V_cleft*(6.02e+20);

molecule_A_cleft_i(i) = A_cleft_i(i)*V_cleft*(6.02e+20);    %inhibited molecule species
molecule_E_cleft_i(i) = E_cleft_i(i)*V_cleft*(6.02e+20);
molecule_AE_cleft_i(i) = AE_cleft_i(i)*V_cleft*(6.02e+20);
molecule_acE_cleft_i(i) = acE_cleft_i(i)*V_cleft*(6.02e+20);
molecule_R_cleft_i(i) = R_cleft_i(i)*V_cleft*(6.02e+20);
molecule_AR_cleft_i(i) = AR_cleft_i(i)*V_cleft*(6.02e+20);
molecule_A2R_cleft_i(i) = A2R_cleft_i(i)*V_cleft*(6.02e+20);
molecule_A2Ro_cleft_i(i) = A2Ro_cleft_i(i)*V_cleft*(6.02e+20);
molecule_I_cleft_i(i) = I_cleft_i(i)*V_cleft*(6.02e+20);
molecule_EI_cleft_i(i) = EI_cleft_i(i)*V_cleft*(6.02e+20);
molecule_E_dead_cleft_i(i) = E_dead_cleft_i(i)*V_cleft*(6.02e+20);
molecule_ChP_cleft_i(i) = ChP_cleft_i(i)*V_cleft*(6.02e+20);
end
end

figure(3)
plot( t, molecule_A2Ro_cleft_n(:,t),molecule_A2Ro_cleft_i(:)); hold on;
ylabel('molecules of open receptor');xlabel('t, ms');
title(sprintf('Total molecules of open receptor species A2R* in the whole cleft,\n at 0, 25, 50, 75, and 100 percent enzyme inhibition,\n averaged over %i annular volume elements,\n D_r = %-5.2e cm^2/ms, %-5.2f X quantum A',Q, D_r, factor_A));%
%{
figure(4*loop_count + 2)
plot( t(:), molecule_A_cleft_n(:,t(:),molecule_A_cleft_i(:));
ylabel('molecules of Acetylcholine');xlabel('t, ms');
title(sprintf('Total molecules of acetylcholine species A in the whole cleft,\n norm and inhibited, averaged over %i annular volume elements,\n %-5.2f percent active enzyme; D_r = %-5.2e cm^2/ms\n %-5.2f X quantum A',Q, E_i_active_percent,D_r,factor_A));%

figure(4*loop_count + 3)
plot( t, molecule_E_cleft_n(:,t),molecule_E_cleft_i(:));
ylabel('molecules of Acetylcholinesterase');xlabel('t, ms');

```

```
title(sprintf('Total molecules of acetylcholinesterase species E in the whole cleft,\n norm and
inhibited, averaged over %i annular volume elements,\n %-5.2f percent active enzyme; D_r = %-
5.2e cm^2/ms\n %-5.2f X quantum A',Q, E_i_active_percent,D_r,factor_A));%
```

```
figure(4*loop_count + 4)
plot( t_tox, molecule_E_cleft_tox(:));
ylabel('molecules of Acetylcholinesterase');xlabel('t, ms');
title(sprintf('Total molecules of acetylcholinesterase species E in the whole cleft,\n averaged over
%i annular volume elements,\n %-5.2f percent active enzyme; D_r = %-5.2e cm^2/ms\n %-5.2f X
quantum A',Q, E_i_active_percent,D_r,factor_A));%
%}
loop_count = loop_count+1;
choice = input('Do you want to run another inhibited reaction: 1(yes), 0(no)? \n');
end
```

```
% save the species concentration data to data files
save U U; save V V; save W W;
```

```
save A_0_n A_0_n; save A_0_i A_0_i; save E_0_i E_0_i;
save E_0_tox E_0_tox;
```

```
save A_n A_n; save E_n E_n; save AE_n AE_n; save acE_n acE_n; save R_n R_n; save AR_n
AR_n; save A2R_n A2R_n;
save A2Ro_n A2Ro_n; save ChP_n ChP_n; %save A_n_lost A_n_lost;
```

```
save A_i A_i; save E_i E_i; save AE_i AE_i; save acE_i acE_i; save EI_i EI_i; save E_dead_i
E_dead_i; save R_i R_i;
save AR_i AR_i; save A2R_i A2R_i; save A2Ro_i A2Ro_i; save I_i I_i; save ChP_i ChP_i; %save
A_i_lost A_i_lost;
```

```
save A_cleft_n A_cleft_n; save E_cleft_n E_cleft_n;
save AE_cleft_n AE_cleft_n; save acE_cleft_n acE_cleft_n; save R_cleft_n R_cleft_n;
save AR_cleft_n AR_cleft_n; save A2R_cleft_n A2R_cleft_n;
save A2Ro_cleft_n A2Ro_cleft_n; save ChP_cleft_n ChP_cleft_n;
```

```
save A_cleft_i A_cleft_i; save E_cleft_i E_cleft_i; save AE_cleft_i AE_cleft_i;
save acE_cleft_i acE_cleft_i; save R_cleft_i R_cleft_i; save AR_cleft_i AR_cleft_i;
save A2R_cleft_i A2R_cleft_i; save A2Ro_cleft_i A2Ro_cleft_i; save I_cleft_i I_cleft_i;
save EI_cleft_i EI_cleft_i; save E_dead_cleft_i E_dead_cleft_i;
save ChP_cleft_i ChP_cleft_i;
```

```
save molecule_A_cleft_n molecule_A_cleft_n;
save molecule_E_cleft_n molecule_E_cleft_n;
save molecule_AE_cleft_n molecule_AE_cleft_n;
save molecule_acE_cleft_n molecule_acE_cleft_n;
save molecule_R_cleft_n molecule_R_cleft_n;
save molecule_AR_cleft_n molecule_AR_cleft_n;
save molecule_A2R_cleft_n molecule_A2R_cleft_n;
save molecule_A2Ro_cleft_n molecule_A2Ro_cleft_n;
save molecule_ChP_cleft_n molecule_ChP_cleft_n;
```

```
save molecule_A_cleft_i molecule_A_cleft_i;
save molecule_E_cleft_i molecule_E_cleft_i;
```

```

save molecule_AE_cleft_i molecule_AE_cleft_i;
save molecule_acE_cleft_i molecule_acE_cleft_i;
save molecule_R_cleft_i molecule_R_cleft_i;
save molecule_AR_cleft_i molecule_AR_cleft_i;
save molecule_A2R_cleft_i molecule_A2R_cleft_i;
save molecule_A2Ro_cleft_i molecule_A2Ro_cleft_i;
save molecule_I_cleft_i molecule_I_cleft_i;
save molecule_EI_cleft_i molecule_EI_cleft_i;
save molecule_E_dead_cleft_i molecule_E_dead_cleft_i;
save molecule_ChP_cleft_i molecule_ChP_cleft_i;

save E_cleft_tox E_cleft_tox;
save R_cleft_tox R_cleft_tox;
save I_cleft_tox I_cleft_tox;
save EI_cleft_tox EI_cleft_tox;
save E_dead_cleft_tox E_dead_cleft_tox;

save molecule_E_cleft_tox molecule_E_cleft_tox;
save molecule_R_cleft_tox molecule_R_cleft_tox;
save molecule_I_cleft_tox molecule_I_cleft_tox;
save molecule_EI_cleft_tox molecule_EI_cleft_tox;
save molecule_E_dead_cleft_tox molecule_E_dead_cleft_tox;

save r r; save D_r D_r; save dr dr;
save t t; save t_tox t_tox;
save N N; save Q Q;
save volume volume;
save I_inf I_inf;

disp('latest data saved, program finished');

%{
figure(2)
plot(t,A_lost);
ylabel('normal Ach, mM');xlabel('t, ms');
title(sprintf('Molar normal Ach lost via diffusion, in the whole cleft\n averaged over %i annular
volume elements',Q));%

figure(1)
surf(t, r, A_n')
shading flat
title(sprintf('Species A in pure radial diffusion and reaction through %i volume elements', Q));
xlabel('time, ms'); ylabel('radius, cm'); zlabel(' concentration, mmole/cm^3');
A_lost
%A_balance =
sum(U(:,1:10))+sum(U(:,21:30))+sum(U(:,51:60))+sum(U(:,61:70))+sum(U(:,71:80))

%}

```

APPENDIX B

The parameters for the exponential decay approximations used in the error comparison

Naka					$y = a_1 \cdot \exp(-a_2 \cdot t)$	
	t	R	ln t	ln R	$a_1 \cdot 10^{-3}$	$a_2 \cdot 10^{-3}$
#1	2	118	0.693	4.77	4.3699	0.00018
	1.2	500	0.182	6.215		
#2	0.64	1250	-0.446	7.131	3.1621	0.0015
	2	174	0.693	5.159		
#3	2.5	153	0.916	5.03	2.8553	0.0012
	0.55	1500	-0.598	7.313		
#4	0.75	1500	-0.288	7.313	2.9534	0.0009
	3.5	125	1.194	4.828		
#5	0.85	1759	-0.162	7.472	2.5884	0.0005
	4.5	334	1.504	5.811		
Fribulet						
#1	0.5	1257	-0.693	7.136	3.046	0.0018
	3.0	15	1.10	2.708		

#2	0.5	1529	-0.693	7.332	3.029	0.0014
	3.0	50	1.10	3.912		
#3	0.5	1676	-0.693	7.424	2.9771	0.0011
	4.0	30	1.386	3.401		
#4	0.5	1853	-0.693	7.524	2.5982	0.0007
	5.0	88	1.609	4.477		
#5	1.0	1800	-0.693	7.495	2.4333	0.0003
	6.5	345	1.872	5.843		

REFERENCES

- [1] Kordas, M., and Brzin, M., "A comparison of the effect of cholinesterase inhibitors on end-plate current and on cholinesterase activity in frog muscle", *Neuropharmacology*, vol. 14, pp. 791-800, 1975.
- [2] Maxwell, Donald, and Brecht, Karen, "Acetylcholinesterase inhibition: does it explain the toxicity of organophosphorus compounds?", *Archives of toxicology*, vol. 80, pp. 756-760, 2006.
- [3] Magleby, K. L., Stevens, C. F., "A quantitative description of endplate currents", *Journal of Physiology*, vol. 223, pp. 173-197, 1972.
- [4] Magleby, K. L., Stevens, C. F., "The effect of voltage on the time course of endplate currents", *Journal of Physiology*, vol. 223, pp. 151-171, 1972.
- [5] Rosenberry, Terrone L., "Quantitative simulation of endplate currents at neuromuscular junctions based on the reaction of acetylcholine with acetylcholine receptor and acetylcholinesterase", *Biophysical Journal*, vol. 26, pp. 263-290, May, 1979.
- [6] Kordas, M., "On the role of junctional cholinesterase in determining the time course of the endplate current", *Journal of Physiology*, vol. 270, pp. 133-150, 1977.
- [7] Kordas, M., "An attempt at an analysis of the factors determining the time course of the end-plate current", *Journal of Physiology*, vol. 224, pp. 333-348, 1972.

- [8] Hartzell, H. Criss, and Kuffler, Stephen W., "Post-synaptic potentiation: interaction between quanta of acetylcholine at the skeletal neuromuscular synapse", *Journal of Physiology*, vol. 251, pp. 427-463, 1975.
- [9] Miledi, R, et al., "Acetylcholinesterase activity in intact and homogenized skeletal muscle of the frog", *Journal of Physiology*, vol. 349, pp. 663-686, 1984.
- [10] Forsberg, Ake, and Puu, Gertrud, "Kinetics of inhibition of acetylcholinesterase from the electric eel by some organophosphates and carbamates", *European Journal of Biochemistry*, vol. 140, pp. 153-156, 1984.
- [11] Eckert, Saskia, et al., "Development of a dynamic model for real-time determination of membrane-bound acetylcholinesterase activity upon perfusion with inhibitors and reactivators", *Biochemical Pharmacology*, vol. 72, pp. 358-365, 2006.
- [12] Gage, Peter W, and McBurney, Robert, "Effects of membrane potential, temperature, and neostigmine on the conductance change caused by a quantum of acetylcholine at the toad neuromuscular junction", *Journal of Physiology*, vol. 244, pp. 385-407, 1975.
- [13] Aidley, David, *The Physiology of Excitable Cells*, 4th Ed., Cambridge, 1998.
- [14] Matthews, Gary, *Cellular Physiology of Nerve and Muscle*, 2nd Ed., Blackwell Scientific Publications, 1991.
- [15] Weiss, Thomas, *Cellular Biophysics*, The MIT Press, 1996.
- [16] Johnston, Daniel, and Mao-Sin Wu, Samuel, *Foundations of Cellular Neurophysiology*, The MIT Press, 1995.

- [17] Wathey, John C., and Nass, Menasche M., "Numerical reconstruction of the quantal event at nicotinic synapses", *Biophysical Journal*, vol. 27, pp. 145-164, July, 1979.
- [18] Madsen, B. W., Edeson, R. O., Lam, H. S., and Milne, R. K., "Numerical simulation of miniature endplate currents", *Neuroscience Letters*, vol. 48, pp. 67-74, 1984.
- [19] Schild, J. H., et al., "Afferent synaptic drive of rat medial nucleus tractus solitarius neurons: dynamic simulation of graded vesicular mobilization, release, and non-NMDA receptor kinetics", *Journal of Neurophysiology*, vol. 74, no. 4, October, 1995.
- [20] Carr, Russell L., and Chambers, Howard, "Modelling the interactions of mixtures of organophosphorus insecticides with cholinesterase", *Electronic Journal of Differential Equations*, Conference 10, pp. 89-99, 2003.
- [21] Lester, Henry, "The response to acetylcholine", *Scientific American*, vol. 236, no. 2, pp. 106-117, 1977.
- [22] Katz, B., Miledi, R., "The binding of acetylcholine to receptors and its removal from the synaptic cleft", *Journal of Physiology*, vol. 231, pp. 549-574, 1973.
- [23] Rosenfeld, Clint, and Sultatos, Lester, "Concentration dependent kinetics of acetylcholinesterase inhibition by the organophosphate paraxon", *Toxicological Sciences*, vol. 90, no. 2, pp. 460-469, 2006.
- [24] Kleinle, J., "Transmitter concentration profiles in the synaptic cleft: an analytical model of release and diffusion", *Biophysical Journal*, vol. 71, pp. 2413-2426, 1996.
- [25] Thomas Gillingwater, Center for Integrative Physiology, www.cip.ed.ac.uk/images/GillingwaterElectronMicrograph.jpg.
- [26] www.wysiwicked.com/encyclopedia/?title=Neuromuscular_junction
- [27] www.wysiwicked.com/encyclopedia/?title=Image:Synapse_diag4.png

- [28] Junge, Douglas, *Nerve and Muscle Excitation*, Sinauer Associates Inc., 1992.
- [29] Hall, Zach W., *An Introduction to Molecular Neurobiology*, Sinauer Associates Inc., 1992.
- [30] Levitan, Irwin, *The Neuron: Cell and Molecular Biology*, Oxford University Press, 1997.
- [31] Beers, W. H., and Reich, E., "Structure and activity of acetylcholine", *Nature*, vol. 228, pp. 917-921, 1970.
- [32] Barry, Peter, and Lynch, Joseph, "Ligand-gated channels", *IEEE Transactions on Nanobioscience*, vol. 4, no.1, March, 2005.
- [33] Encyclopedia Britanica, Inc., 2002.
- [34] Hess, George, and Andrews, John, "Functional acetylcholine receptor-electroplax membrane microsacs: Purification and characterization", *Proceedings of the National Academy of Sciences*, vol. 74, no. 2, pp 482-486, February, 1977.
- [35] Dudai, Yadin, "Molecular structures of acetylcholinesterase from electric organ tissue of the electric eel", *Proceedings of the National Academy of Sciences*, vol. 70, no. 9, pp 2473-2476, September, 1973.
- [36] Cooper, Jack R., *The Biochemical Basis of Neuropharmacology*, Oxford University Press, 1996.
- [37] Rosenberry, Terrone L., "Purification of acetylcholinesterase by affinity chromatography and determination of active site stoichiometry", *Journal of Biological Chemistry*, vol. 247, no. 5, March, 1972.
- [38] Krohn, Kenneth, "Interpreting enzyme and receptor kinetics: keeping it simple, but not too simple", *Nuclear Medicine and Biology*, vol. 30, pp. 819-826, 2003.

- [39] Chen Yu Zong, National University of Singapore, http://bidd.nus.edu.sg/group/images/full_acetylcholinesterase.gif.
- [40] Grunhagen, Hans-Heinrich, "Fast Kinetic studies on the interaction of cholinergic agonists with membrane-bound acetylcholine receptor from *Torpedo marmorata* as revealed by quinacrine fluorescence", *European Journal of Biochemistry*, vol. 80, pp. 225-242, 1977.
- [41] Cornish-Bowden, Athel, *Fundamentals of Enzyme Kinetics*, Portland Press, 2004.
- [42] Schulz, G. E., *Principles of Protein Structure*, Springer-Verlag, 1979.
- [43] www.hi.com.au/heinemannfiles/586/3f3_4s.gif.
- [44] Koshland, Daniel, "Application of a theory of enzyme specificity to protein synthesis", *Proceedings of the National Academy of Sciences*, vol. 44, no. 2, pp. 98-104, 1958.
- [45] Murray, J. D., *Mathematical Biology*, Springer-Verlag, 1989.
- [46] Banks, H. T., *Lecture Notes in Biomathematics: Modeling and Control in the Biomedical Sciences*, Springer-Verlag, 1975.
- [47] Walker, Bailus, "Current concepts: organophosphate toxicity", *Inhalation Toxicology*, vol. 14, pp. 975-990, 2002.
- [48] Krupesh, N., "Organophosphorus poisoning - still a challenging proposition", *Indian Journal of Anesthesia*, vol. 46, no. 1, pp. 40-43, 2002.
- [49] Polhuijs, Martine, and Langenberg, Jan P., "New method for retrospective detection of exposure to organophosphorus anticholinesterases: application to alleged sarin victims of Japanese terrorists", *Toxicology and Applied Pharmacology*, vol. 146, pp. 156-161, 1997.

- [50] Worek, Franz, et al., "Evaluation of oxime efficacy in nerve agent poisoning: development of a kinetic-based dynamic model", *Toxicology and Applied Pharmacology*, vol. 209, pp. 193-202, 2005.
- [51] Chang, Raymond, Chemistry 6th Ed., McGraw-Hill, 1998.
- [52] McQuarrie, Donald, General Chemistry, W. H. Freeman and Company, New York, 1984.
- [53] Schnell, S., and Turner, T. E., "Reaction kinetics in intracellular environments with macromolecular crowding: simulations and rate laws", *Progress in Biophysics & Molecular Biology*, Vol. 85, pp. 235-260, 2004.
- [54] McQuarrie, Donald, Physical Chemistry: A Molecular Approach, University Science Books, 1997.
- [55] Konopka, Andrzej, Systems Biology, CRC Press, 2007.
- [56] Friboulet, Alain and Thomas, Daniel, "Reaction-diffusion coupling in a structured system: application to the quantitative simulation of endplate currents", *Journal of Theoretical Biology*, vol. 160, pp. 441-455, 1993.
- [57] Naka, Takashi and Shiba, Kosuke, "A two-dimensional compartment model for the reaction-diffusion system of acetylcholine in the synaptic cleft at the neuromuscular junction," *BioSystems*, vol. 41, pp. 17-27, 1997.
- [58] Schiesser, W. E., The Numerical Method of lines: integration of partial differential equations, Academic Press, San Diego, 1991.
- [59] Nowycky, M. C., and Pinter, M. J., "Time courses of calcium and calcium-bound buffers following calcium influx in a model cell", *Biophysical Journal*, vol. 64, pp. 77-91, 1993.

- [60] Sala, F., and Hernandez-Cruz, A., "Calcium diffusion modeling in a spherical neuron: relevance of buffering properties", *Biophysical Journal*, vol. 57, pp. 313-324, 1990.
- [61] Vijayendran, R., "A computational reaction-diffusion model for the analysis of transport-limited kinetics", *Analytical Chemistry*, vol. 71, pp. 5405-5412, 1999.
- [62] Holmes, W., "Modeling the effects of glutamate diffusion and uptake on NMDA and non-NMDA receptor saturation", *Biophysical Journal*, vol. 69, pp. 1734-1747, 1995.
- [63] Nakasaki, K., "Dynamic modeling of immobilized cell reactor: application to ethanol fermentation", *Biotechnology and Bioengineering*, vol. 33, pp. 1317-1323, 1989.
- [64] Cortassa, S., "Pattern formation in an immobilized bienzyme system", *Biochemical Journal*, vol. 269, pp. 115-122, 1990.
- [65] Vieth, Wolf R., "Transport models of the neurotransmitter-receptor interaction", *Biochemical Engineering II*, New York Academy of Sciences, Vol. 369, 1982.
- [66] Magleby, K. L., Terrar, D. A., "Factors affecting the time course of decay of end-plate currents: A possible cooperative action of acetylcholine on receptors at the neuromuscular junction", *Journal of Physiology*, vol. 244, pp. 467-495, 1975.
- [67] Anderson, C. R., and Stevens, C. F., "Voltage clamp analysis of acetylcholine produced end-plate current fluctuations at frog neuromuscular junction", *Journal of Physiology*, vol. 235, pp. 655-691, 1973.

- [68] Tsoukias, Nikolaos, and Popel, Aleksander, "Erythrocyte consumption of nitric oxide in presence and absence of plasma-based hemoglobin", *American Journal of Physiology: Heart and Circulatory Physiology*, vol. 282, pp. H2265-H2277, June, 2002.
- [69] Jones, Steve; Louisiana Tech University, Personal communication.
- [70] Truskey, George A., *Transport Phenomena in Biological Systems*, Prentice Hall, 2004.
- [71] VX, MSDS CAS Registry No.
- [72] Lide, David (Ed.), *CRC Handbook of Chemistry and Physics 86th Ed.*, CRC Press, 2006.
- [73] Long, Cyril (Ed.), *Biochemist's Handbook*, D. Van Nostrand Company, 1961.
- [74] Patnaik, Pradyot (Ed.), *Handbook of Inorganic Chemicals*, McGraw-Hill, 2002.
- [75] Barton, Allan, *CRC Handbook of Solubility Parameters and Other Cohesion Parameters 2nd Ed.*, CRC Press, 1991.
- [76] Lide, David (Ed.), *CRC Handbook of Data on Organic Compounds 3rd Ed.*, CRC Press, 1993.
- [77] Magnotti, Ralph, "Measurement of acetylcholinesterase in erythrocytes in the field", *Clinical Chemistry*, vol. 33, no. 10, pp. 1731-1735, 1987.
- [78] Burton, Alan C., *Physiology and Biophysics of the Circulation 2nd Ed.*, Year Book Medical Publishers, 1972.
- [79] Aurbek, N., et al., "Analysis of inhibition, reactivation, and aging kinetics of highly toxic organophosphorus compounds with human and pig acetylcholinesterase", *Toxicology*, vol. 224, pp. 91-99, 2006.

- [80] Worek, Franz, and Thiermann, Horst, "Kinetic analysis of interactions between human acetylcholinesterase, structurally different organophosphorus compounds and oximes", *Biochemical Pharmacology*, vol. 68, pp. 2237-2248, 2004.
- [81] Aurbek, N., and Thiermann, H., "Application of kinetic-based computer modeling to evaluate the efficacy of HI 6 in percutaneous VX poisoning", *Toxicology*, vol. 224, pp. 74-80, 2006.
- [82] Fossier, P., and Baux, G., "Direct and indirect effects of an organophosphorus acetylcholinesterase inhibitor and of an oxime on a neuro-neuronal synapse", *Pflügers Archive*, vol. 396, pp. 15-22, 1983
- [83] Kuča, Kamil, "Reactivation of organophosphate inhibited acetylcholinesterase activity by α,β -bis-(4-hydroxyiminomethylpyridinium) alkanes *in vitro*", *Journal of Applied Biomedicine*, Vol. 1, pp. 207-211, 2003.
- [84] Prevention and treatment of Chemical Warfare Agents, *The Medical Letter*, vol. 44, No. 1121, pp. 1-3, 2002.
- [85] Sidell, F. R., and Borak, J., "Chemical warfare agents: II. Nerve agents", *Annals of Emergency Medicine*, vol. 21, pp. 865-871, 1992.
- [86] Lallement, Guy, and Foquin, Annie, "Subchronic administration of various pretreatments of nerve agent poisoning. II Compared efficacy against soman toxicity", *Drug and Chemical Toxicology*, vol. 24, no. 2, pp. 165-180, 2001.
- [87] Yun-Bae, Kim, and Sungho, Shin, "Effectiveness of procyclidine in combination with carbamate prophylactics against diisopropylfluorophosphate poisoning", *Environmental Toxicology and Pharmacology*, vol. 5, no. 1, pp. 43-49, 1998.

- [88] Ashani, Yacov, and Pistinner, Shlomi, "Estimation of the upper limit of human butylcholinesterase dose required for protection against organophosphates toxicity: a mathematically based toxicokinetic model", *Toxicological Sciences*, vol. 77, pp. 358-367, 2004.
- [89] Masson, Patrick, and Nachon, Florian, "High activity of human butylcholinesterase at low pH in the presence of excess butyrylthiocholine", *European Journal of Biochemistry*, vol. 270, pp. 315-324, 2003.
- [90] Kato, Masato, and Hashimoto, Yasuhiko, "Inhibition of human plasma cholinesterase and erythrocyte acetylcholinesterase by nondepolarizing neuromuscular blocking agents", *Journal of Anesthesia*, vol. 14, pp. 30-34, 2000.